University of Kerbala
College of Science
Department of Physics

# Study of The Nuclear Properties of Some Light Nuclei Using Different Potentials

Thesis Submitted to the Council of the College of Science, University of Kerbala in Partial Fulfillment of the Requirements for the Master Degree Science Physics

by

**Bashair Hassan Jweed**

**BSc 2018**

Supervised by

**Prof. Dr. Adie D. Salman**

2022 A.D 1443 A.H

بسم الله الرحمن الرحيم

﴿وَعِندَهُ مَفَاتِحُ الْغَيْبِ لا يَعلمُها إلا هُو وَيَعْلَمُ
مَاْ فِي البَرِّ وَالبَحْرِ وَمَا تَسْقُطُ مِنْ وَرَقَةٍ
إلا يَعْلَمُها وَلا حَبَّةٍ فِي ظُلُماتِ الأَرْضِ
وَلا رَطْبٍ وَلا يَابِسٍ إلا فِي
كِتابٍ مُبِينْ﴾

صدق الله العلي العظيم

سورة الأنعام (الآية : ٥٩)

# Examination Committee Certification

We certify that we have read this thesis entitled " **Study of The Nuclear Properties of Some Light Nuclei Using Different Potentials**" as the examining committee, examined the student " " ***Bashair Hassan Jweed***" on its contents, and that in our opinion, it is adequate for the partial fulfillment of the requirements for the Degree of Master in Science of Physics.

Signature:

Name: **Dr. Khalid H. H. Attyiah**

Title: Professor

Address: Department of physics, college of science/ University of Babylon

Date: 15/5/2021

**(Chairman)**

Signature: A. K. Hashim

Name: **Dr. Abdalsattar K. Hashim**

Title: Professor

Address: Department of physics, college of science/ University of Kerbala

Date: 15/5/2021

**(Member)**

Signature:

Name: **Dr. Samah O. Al-Ramahi**

Title: Assist. Professor

Address: Department of physics, college of science/ University of Kufa

Date: 15/5/2021

**(Member)**

Signature:

Name: **Dr. Adie D. Salman**

Title:. Professor

Address: Department of physics, college of science/ University of Kerbala

Date: 15/5/2021

**(Supervisor)**

Signature:

Name: **Dr. Jasem Hanoon Hashim Al-Awadi**

Title: Assist. professor

Dean of the college of science / University of Kerbala

Date: 2 / 6 / 2021

# Supervisor Certificate

I certify that the preparation of this thesis, entitled "**Study of The Nuclear Properties of Some Light Nuclei Using Different Potentials"** was made under my supervision by **"Bashair Hassan Jweed"** at the College of Science, University of Kerbala in partial fulfillment of the requirements for the degree of **Master of Science in Physics.**

Signature:

Name: Dr. Adie D. Salman

Title: Professor

Data: / / 2022

In view of the available recommendations, I forward the thesis for debate by the examination committee.

Signature:

Name: Dr. Rajaa Abdul AL-Ameer

Title: Professor

Head of Physics Department, College of Science

Data: / / 2022

# *Acknowledgments*


Praise to **Allah**, Mercy and peace are to the Prophet Mohammed and his relatives and companions.

First and foremost I offer my sincerest gratitude to my supervisor

***Prof. Dr. Adie D. Salman***

for suggesting this project research point and for supporting me throughout my thesis with his patience and knowledge.

A word of thanks is due to staff members of the Physics Department in the College of Education for Pure Sciences for their help and kind assistance.

I wish I had a word better than thanks to express my feeling to my mother.

Lastly, I would like to thank my brother and sisters for their unconditional support, both financially and emotionally throughout my study. I thank everyone who asked God for my success.

# Abstract

The large-scale shell-model calculations have been officiated, including several cores, to study the structure and some physical properties for $^{10}$B, $^{12}$C, and $^{17}$O nuclei using Nushell code. The shell model calculation included three model p, psd, and spsdpf model space with the ckpot, psdmwk, and wbm interactions, respectively, for $^{10}$B, $^{12}$C nuclei, and zbme model space with the rewile interaction for the $^{17}$O nucleus. The calculation results that the inclusion of the core-polarization effects with a polarization charge contribution and choosing the appropriate model space gave better results to calculate inelastic and elastic form factors for the low-lying excited state of these nuclei. In this work, different potentials were adopted for single-particle radial wave function, namely Harmonic-Oscillator (HO), Wood-Saxon (WS), and Skyrme (Ska) potentials in our calculations. Calculations compared with experimental data have been performed by using the large-basis spsdpf model space which includes $1s_{1/2}$, $1p_{3/2}1p_{1/2}$, $1d_{5/2}2s_{1/2}1d_{3/2}$, $1f_{7/2}2p_{3/2}1f_{5/2}2p_{1/2}$ orbits these have been truncated to $2\hbar$□ because the expansion to 4 and $6\hbar$□ couldn't significantly improve the results, while the psd model space has included $1p_{3/2}1p_{1/2}$, $1d_{5/2}2s_{1/2}1d_{3/2}$ orbits without any restrictions imposing on the valence nucleons outside the core that gave acceptable results. The calculation results for both $^{10}$B and $^{12}$C nuclei with adopted the psd model space were in better agreement with experimental data compared to the theoretical calculation for previous work that used spsdpf expansions. For the $^{17}$O nucleus, the zbme model space used which included the $1p_{1/2}$, $1d_{5/2}2s_{1/2}1d_{3/2}$ orbits without any restrictions gave good agreement with experimental data for Skyrme (ska) potential compared with other (HO, WS) potentials.

# ***Contents***

# List of Figures

# ***Chapter One***

# ***General Introduction***

## 1.1 Introduction

In the history of nuclear structure research was one of the most important identifying developments and most prominent and successful nuclear models in which those nucleons occupy discrete orbitals, which attitudinize shells. A shell model helps us to better understand the physical properties of nuclei and is used in the study of the nuclear structure [1, 2]. The nucleon properties in this model can be described as properties and behavior of valance electrons that exist out of a closed shell in the atom, where valance nucleons (proton or neutron) in a nucleus are placed out of close shells [3]. Studying the nuclear structure through electron scattering, which is important because the nuclear matrix of the element depends on the momentum transfer that gives information about both the ground and the excited density states. The shell model can predict various observables systematically and precisely. The Cohen-Kurath and psdmwk interactions for the p and psd shells are “standard” effective interactions for light nuclei [4, 5].

In the p-shell model space, the $^4He$ is supposed to be an inert core, as the valence nucleons are distributed over the $1p_{3/2}$ $1p_{1/2}$ orbits within the limits of the Pauli principle. This model was unsuccessful to obtain results from factors in agreement with experimental data unless taking into consideration the higher configuration (core polarization) effects. Thus, adding the core polarization effect gives a better result compared with the experimental data. The expanded seed shell model has included two shells (1p, 1d-2s) [6].

## 1.2 Shell Model

The shell model entered nuclear physics more than fifty years ago. This model is the basic type for nuclear structure calculations in terms of nucleons [7]. This model describes how the quantum numbers change and how much energy to move nucleons is required in orbits (in the nucleus each nucleon moves separately in a potential explicate that average interaction a for the other nucleons in the nucleus). Also, that illustrates some nuclear properties such as nuclear spectra, parity assignments, spin, transition probabilities, and magnetic moment. The nucleons that unconnected motion can realize specifically from a federation of the weakness for the Pauli Exclusion Principle and the nuclear long-range attraction [8].

When all the protons or neutrons in a nucleus are infilled shells, the number of protons or neutrons is called a “magic number”, these nuclei have exceptional stability and total angular momentum J equal to zero. The J value of the new ground state is determined by adding valance nucleons. When proton or neutron (singly or in a couple), are excited out of the ground state its isospin projection quantum numbers and parity of the nucleus and the angular momentum are changed [9].

## 1.3 Electron Scattering

The electron scattering method has provided important information about the nuclear structure when the electron contains high energy (100 MeV greater than 100MeV) and interacts with the local charge and current density in the target. If not, a point is expected to be a dimension of the order of a few Fermis [10].

There are two kinds of electron scattering:

**a-Elastic electron scattering**

When the energy of the electron is unchanged it means that the electron scattering leaves the nucleus at its ground state [11], this way studies properties such as static distribution and magnetization of the ground state energy [12].

**b-Inelastic electron scattering**

When an electron is scattering the amount of energy taken up by the nucleus leaves the nucleus in a different excited state and has final energy decreases from the initial state [11], which allows for studying the cross-section of the electrical excitation (current densities and charge distributions) [12].

In the scattering of electrons, the form factor of the nucleus multiplying the Mott cross-section by a factor that depends on the current and charges distribution and magnetization of the target nucleus. The form factor as a function of the momentum transferred to the nucleus can be determined by the energy of the incident and scattered electron and the scattering angle [13]. The nucleus is inelastic with electrons described according to the first-Born approximation as the interaction of the electromagnetic field via its charge and current densities [14].

According to the first-Born approximation, the form factor is divided into two main types of form factors:

**1-Coulomb (longitudinal) form factors**

The interaction of the electron with the charge distributions of the nucleus is considered as an exchange of a virtual photon of angular momentum zero along the direction of q known as “Coulomb or Longitudinal form factors”, the electron, in this case, does not flip spin, due to the conservation of angular momentum. Longitudinal scattering gives information about the charge distribution of the nuclear system [14].

**2- Transverse form factors**

According to a first-Born approximation, in the nucleus interaction of the electron with the current distributions and spin is considered as an exchange of a virtual photon of angular momentum ±1 along the direction of q, this is known as “Transverse form factors”. Transverse scattering gives information about the magnetization and current distribution in nuclei. According to the angular momentum selection rules and parity the transverse form factors can be divided into magnetic (M) and electric (E) form factors [14].

## 1.4 Literature Review

Many attempts were made to explain the experimental data of electron scattering and to understand the nature of nuclear force and the structure of the nuclei in B, C, and O nuclei**.** Flanz et al. (1978) [15] measured the inelastic transverse form factors of 4.439 MeV at $2^+$ 0 and 16.17 MeV at $2^+$ 1 for $^{12}C$. Their results were with a contribution of convection current remarkably at low momentum transfer for energy 4.439 MeV. And the magnetizations' current contribution gave good results with experimental data to the transverse 16.17 MeV at high momentum transfer.

Ansaldo et al. (1979) [16] measured the elastic transverse electr0on scattering form factors at 1.74 $0^+$ and 5.17 $2^+$ MeV in $^{10}B$. Their results transverse form factors were in agreement based on Cohen-Kurath and the results of longitudinal form factors at 6.03 $4^+$ MeV state were in good accord with the Hartree-Fock wave functions.

Hynes M. V et al. (1979) [17] calculated the elastic transverse form factors of $^{17}O$. The shell model with core polarization and meson exchange calculations are not given good results but an enhancement of the high q of the M5.

Manley D. M et al. (1987) [18] measured the inelastic electron scattering form factors at 15 states with negative parity and positive parity of $^{17}O$. The results were observed clearly for momentum transfer between 0.8 and 2.6 $fm^{-1}$.

Peterson et al. (1988) [19] studied the transverse elastic form factors for $^{10}B$ and $^{11}B$. Where the radial shape of the $1p_{3/2}$ single-particle wave function is determined within a nuclear interior.

Amos and Steward (1990) [20] calculated the transverse and longitudinal form factors for ($^{12}C$, $^{20}Ne$, $^{24}Mg$) at $2_1^+$ and $4_1^+$ states. Their results using projected the Hartree-Fock wave functions were compared with (the shell model) to show that momentum transfer dependent corrections can be quite diverted.

Booten (1992) [21] studied the transverse form factors of nuclei ($^{6}Li$, $^{7}Li$, $^{10}B$, $^{11}B$, $^{14}N$, and $^{15}N$) at $2\hbar$ □ model space. The results inclusion of MEC in the first q-region was much better cloned in the $2\hbar$ □ model space and at high momentum transfer, MEC contribution enhancement the calculation of electromagnetic properties of p-shell nuclei.

Amaro et al. (1994) [22] studied the transverse elastic form factors with MEC for $^{12}C$ and $^{40}Ca$ nuclei. The results with the effect of meson exchange contribution in the 1p1h response were negative and the magnitude of the reduction of the peak increases with the momentum transfer.

The transverse form factors for nuclei ($^{6}Li$, $^{10}B$, $^{11}B$, $^{14}N$, and $^{15}N$) were calculated by Booten and van Hees (1994) [23]. Their shell model calculations at 1p-shell and extended (0+2) $\hbar$ □ model space and the inclusion of the meson exchange current improved the agreement of the transverse form factor with experimental results.

Karataglidis et al. (1995) [24] calculated the transverse E2 electron scattering form factors for ($^{12}C$, $^{20}N$, $^{24}Mg$, and $^{28}Si$). The results for all three operators (standard electric multipole operators, invoking current conservation and for arbitrary wavelength gave similar form factors in $q \leq 3\ fm^{-1}$.

Cichonki et al. (1995) [25] measured longitudinal and transverse form factors of $^{10}$B and compared their result with the calculated 1p-shell model including 1s, 2s1d, and 2p1f configurations. They found that only 10□ improvements were realized and found that the including of higher excited configuration employing core polarization calculation was essential to remove the remaining shortfall.

Radhi et al. (2001) [26] studied the Coulomb form factors of C2 transitions for p-shell nuclei, including the core-polarization effects excited up to $6\hbar$□. They found that the core-polarization effect is essential in both the momentum transfer and transition strengths and their results were in good agreement with no adjustable parameters.

The inelastic longitudinal C2 form factors for ($^{6}$Li, $^{7}$Li, $^{10}$B, and $^{12}$C) in the shell model were calculated by Zeina (2003) [27]. The calculation results using the Tassie model with contribution core-polarization gave an agreement result with the experimental data in momentum transfer $q \leq 3$ $fm^{-1}$.

The transverse and longitudinal form factors in some p-shell nuclei were studied by Adie (2005) [8]. The calculations inclusion of the second-order core-polarization effects enhancement the calculated results in a little amount of longitudinal and transverse strength form factors.

Majeed et al. (2006) [28] studied the electroexcitations of all possible T=1p-1h states of all allowed angular momenta for $^{12}$C. The results with1f-2p shell a major contribution gives a good fit to the experimental form factors.

The elastic and inelastic electron scattering form factors in p-shell nuclei ($^{6}$Li, $^{7}$Li, $^{9}$Be, $^{10}$B, $^{11}$B, $^{12}$C, $^{13}$C, and $^{15}$N) calculated by Khalid (2007) [29]. The core-polarization calculations with the higher energy excitations from 1s-shell core orbits and 1p-shell to higher allowed orbits up to $2\hbar$□. Their calculations using Cohen-Kurath interaction gave good agreement with experimental data, especially the Coulomb scattering while the magnetic form factors were less affected.

Radhi et al. (2014) [30] studied the effective charge and quadruple momentums for B (A=8, 10, 11, 12, 13, 14, 15) and Li (A=7, 8, 9, 11) on a p and large basis spsdpf-shell model spaces. The large-basis no-core excited the particles to higher orbits at 6 $\hbar$□ have been included and the effective charge for the p-shell and sd-shell nuclei are obtained for the neutron-rich B and Li isotopes which are smaller than the standard values. Their calculated results agree very well with the experimentally observed trends of the recent experimental data.

Ali A. Alzubadi et al. (2018) [31] calculated the transverse and longitudinal electroexcitation of positive and negative parity states in $^{17}$O using two different psdpn and zbme model spaces. The calculations have adopted one-body potential in Hartree-Fock theory and given a good agreement with experimental data form factors.

The transverse and longitudinal electron scattering form factors for $^{7}$Li and $^{10}$B nuclei were studied by Adie et al. (2019) [32]. Their calculation included 1p-1h excitation up to 12$\hbar$□. The transverse and longitudinal form factors and the behavior of the momentum transfer are described exactly for $^{7}$Li compared with 6$\hbar$□ energy.

## 1.5 Aim of the Present Work

The work aims to calculate the longitudinal, electrical and magnetic transverse form factors for elastic and inelastic electron scattering of several nuclei in the p- and sd-shell using different wave functions. The model space has also been expanded by introducing a mixture of the shell. Some interactions were also selected through which the best results were obtained, which were in better agreement with the experimental data from previous studies. The core-polarization calculation using the NuShell code[33].

# ***Chapter Two***
# ***Theoretical Bases***

## 2.1 General Theory

An electron scattering method is a potent tool for descriptions and studying nuclear charge density distributions. According to the first-Born approximation, the wave functions connected with electron scattering are interpreted as an exchange of a virtual photon carrying a momentum q between the electron and the nucleus. The Coulomb scattering of the electron with the charge distribution of the nucleus is considered as an exchange of a virtual photon with zero angular momentum along the direction of the momentum transfer q.  Second hand, in the nucleus the interaction of the electron with the spin and current distributions gives rise to the transverse scattering.

The differential cross-section from a nucleus of charge Ze, mass M and solid angle $d\Omega$ in the plane-wave Born approximation, is given [٣4]

$$\frac{\mathrm{d}\sigma}{\mathrm{d}\Omega} = \left(\frac{\mathrm{d}\sigma}{\mathrm{d}\Omega}\right)_{\mathrm{Mott}} \eta \sum_{\mathrm{J}} \left|\mathrm{F_J}(q,\theta)\right|^2 \qquad (2.1)$$

$$\left(\frac{\mathrm{d}\sigma}{\mathrm{d}\Omega}\right)_{\mathrm{Mott}} = \left[\frac{\mathrm{Z}\alpha\cos(\theta/2)}{2\mathrm{E_i}\sin^2(\theta/2)}\right]^2 \qquad (2.2)$$

Where $\left(\frac{\mathrm{d}\sigma}{\mathrm{d}\Omega}\right)_{\mathrm{Mott}}$ is the Mott scattering cross-section, Z is the atomic number, θ is the scattering angle, $\alpha = e^2/\hbar c = (1/137)$ is the scattering angle, and $E_i$ is the incident electron's energy [12, 35]. Where η is the nucleus recoil factor is given by:

$$\eta = \left[1 + \frac{2\mathrm{E_i}}{\mathrm{M}}\sin^2(\theta/2)\right]^{-1} \qquad (2.3)$$

where M is the mass of the target.

Electron scattering form factor (longitudinal and transverse) involving angular momentum J and momentum transfer q, between initial and final nuclear shell model state of spin $J_{i,f}$ and isospin $T_{i,f}$ is given by [36, 37]:

$$\left|F_J(q)\right|^2 = \left(\frac{q_\mu}{q}\right)^4 \left|F_J^L(q)\right|^2 + \left[\frac{q_\mu^2}{2q^2} + tan^2(\theta/2)\right]\left|F_J^T(q)\right|^2 \qquad (2.4)$$

$$q^2 \approx 4E^2\eta \sin^2\frac{\theta}{2}$$

The three and four-momentum transfers are the difference between the final and initial are given by:

$$\omega^2 = E_f - E_i$$

$$Q_\mu^2 = q^2 - (E_f - E_i)^2$$

The transverse (T) and longitudinal (L) form factors are given by [39]:

$$\left|F_J^L(q)\right|^2 = \sum_{J\geq 0}|(q)|^2\left|F_J^T\right|^2 \qquad (2.5)$$

$$\left|F_J^T(q)\right|^2 = \sum_{J>0}\left\{\left|F_J^M(q)\right|^2 + \left|F_J^E(q)\right|^2\right\} \qquad (2.6)$$

where $\left|F_J^M(q)\right|^2$ and $\left|F_J^E(q)\right|^2$ are the magnetic and electric transverse form factors, respectively. The angular momentum selection rule [3]:

$$|J_i - J_f| \leq J \leq J_i + J_f$$

$\pi_i\pi_f = (-1)^J$ for Coulomb (Electric) multiple

$\pi_i\pi_f = (-1)^{J+1}$ for magnetic multiple

The angular momentum J involving can be expressed in the electronic scattering form factors as [23]:

$$\left|F_J^\Lambda(q)\right|^2 = \frac{4\pi}{z^2}\frac{1}{2J_i+1}\left|\langle\Psi_{Jf}|\hat{T}_J^\Lambda(q)|\Psi_{Ji}\rangle\right|^2 \qquad (2.7)$$

Where $\Lambda$ selects the longitudinal or transverse form factors, $\hat{T}_J^\Lambda(q)$ is the electron scattering multiply operator [39]. Accordingly, the longitudinal and transverse form factor is defined as,

$$\left|F_J^L(q)\right|^2 = \frac{4\pi}{z^2}\frac{1}{2J_i+1}\sum_{J\geq 0}\left|\langle J_f\, M_{Jf}|\hat{T}_J^{Coul}(q)|J_I\, M_{Ji}\rangle\right|^2 \qquad (2.8)$$

$$\left|F_J^T(q)\right|^2 = \frac{4\pi}{z^2}\frac{1}{2J_i+1}\Sigma\left|\langle J_f\, M_{Jf}|\hat{T}_J^{el}(q)|J_I\, M_{Ji}\rangle\right|^2 + \left|\langle J_f\, M_{Jf}|\hat{T}_J^{mag}(q)|J_I\, M_{Ji}\rangle\right|^2 \qquad (2.9)$$

Where $J_i$ is the total angular momentum of the initial state and $J_f$ is the total angular momentum of the final state [39]. The multipole operator is defined by:

$$\hat{T}_J^{coul}(q) = \int \overrightarrow{dr}\, j_J(qr) Y_J^M(\Omega_r)\hat{\rho}(\vec{r}) \qquad (2.10)$$

$$\widehat{\mathrm{T}}_{\mathrm{J}}^{el}(\mathrm{q}) = \frac{1}{q}\int \overrightarrow{dr}\{\vec{\nabla}\times[j_J(qr)Y_{JJ_1}^{M}(\Omega_r)]\}.\hat{j}(\vec{r}) \tag{2.11}$$

$$\widehat{\mathrm{T}}_{\mathrm{J}}^{mag}(\mathrm{q}) = \int \overrightarrow{dr}\,[j_J(qr)Y_{JJ_1}^{M}(\Omega_r)].\hat{J}(\vec{r}) \tag{2.12}$$

Where $(\hat{J}(\vec{r})), (\hat{\rho}(\vec{r}))$ are current and charge density operators for the target, $j_J(qr)$ is the spherical Bessel function, and the $Y_{JJ_1}^{M}$ is spherical harmonics, given by [40].

$$\rho(\vec{r}) = \delta(r_i - r)e_i \tag{2.13}$$

$$\hat{J}(\vec{r}) = \delta(r_i - r)e_i\frac{1}{M_T}\,\vec{\nabla} \tag{2.14}$$

$$Y_{JJ_1}^{M}(\Omega_r) = \sum_{mm`}(Jm^1m`/JM)T_{J_1}^{M}(\Omega_r) \tag{2.15}$$

Where $e_i = \frac{(1+\tau_z(i))}{2}$ the nucleon charge, $Y_{J_1}^{M}(\Omega_r)$is the spherical harmonics and $\delta(r_i - r)$ is the Dirac delta function.

## 2.2 Corrections to the Form Factor

Electron scattering form factors for light nuclei can be calculated with confidence when corrections are scarred for the center of mass motion and finite size. The first is from the center of mass correction divides out the form factor due to the spurious motion which is ineradicable in the fixed center [10]. The center of mass correction factor $F_{cm}$ is given as [37]

$$\mathrm{F}_{\mathrm{c.m}} = \exp(\frac{\mathrm{q}^2\mathrm{b}^2}{4\mathrm{A}}) \tag{2. 16}$$

Where A is the mass number and b is the oscillator length parameter (or size parameter) chosen to reproduce the nucleus.

The other correction that adds to the form factor calculations is the inclusion of the finite nucleon size ($\mathrm{F}_{\mathrm{f.s}}$). This size correction is given by [41]

$$\mathrm{F}_{\mathrm{f.s}}(\mathrm{q}) = \left[1 + \left(\frac{\mathrm{q}}{4.33}\mathrm{fm}^{-1}\right)^2\right]^{-2} \tag{2.17}$$

The plane wave Born approximation (PWBA) is expected to characterize the electron scattering data very well for nuclei in which αZ«1, except in the region of the diffraction minima, where the PWBA goes to zero. The effect of the

Coulomb field is to raise the momentum transferred to the nucleus and an effective momentum transfer ($q_{eff}$) is related to q by [39]:

$$q_{eff} = q\left[1 + \frac{3\,ze^2}{2E_i R_c}\right] \tag{2.18}$$

Where $R_c = (\frac{5}{3})^{1/2}\, R_{rms}$ and $R_{rms}$ is the root main square charge radius, Z is the nuclear charge of the target nucleus and α is the fine structure constant. Ei and q are the incident electron energy and the three-momentum transfer respectively. And $e^2 = \alpha\hbar c = 1.44$ Mev $fm$.

Including these corrections, the form factor can be written as [42],

$$\left|F^{\Lambda}_{L.T}(q)\right|^2 = \frac{4\pi}{z^2(2J+1)}\left|\sum_{T=0,1}(-1)^{T_f-T_Z}\begin{pmatrix} T_f & T & T_i \\ -T_Z & 0 & T_Z\end{pmatrix}\langle J_f T_f \|\| T^{\Lambda}(q) \|\|\| J_i T_i\rangle\right|^2 \times |F_{f.s}F_{c.m}|^2 \tag{2.19}$$

## 2.3 Many-Particle Matrix Elements

In the microscopic theory, the core polarization effects can be explained as a mixed shell-model wave function and configuration with higher energy as particle-hole perturbation expansion. The reduced matrix element part of the electron scattering operator $\widehat{T}_J$ in the p- and sd-shell can be formed by the contribution of the core-polarization (CP) to the p- and sd-model spaces are added together [11].

The initial and final wave function of the electron scattering operator is specified as the adding over the one-body density matrix element-time the reduce single-particle element and taken as

$$\langle \Gamma_f \|\widehat{T}_6(q)\| \Gamma_i\rangle = \langle \Gamma_f \|\widehat{T}_6(q)\| \Gamma_i\rangle_{ms} + \langle \Gamma_f \|\delta\widehat{T}_6(q)\| \Gamma_i\rangle_{cp} \tag{2.20}$$

Where $\Gamma_i = J_i T_i$ is the inial state of the nucleus, $\Gamma_f = J_f T_f$ is the final state of the nucleus and б=LT is the multipolarity of the transition. In the p-shell, the model space matrix elements are indicated as the sum of the product single particle-matrix elements times the one-body density matrix elements that define as [43]:

$\langle \Gamma_f \| \hat{T}_6(q) \| \Gamma_i \rangle = \sum_{F_\alpha F_\beta} OBDM(\Gamma_f \Gamma_i F_\alpha F_\beta) \langle F_\alpha \| \hat{T}_6(q) \| F_\beta \rangle$

(2.21)

Where $F_\alpha$ refer to the initial model space states, $F_\beta$ refer to the final model space states OBMD contains all the information about the transition of a given multipolarity, the relation between these OBDM and the p/n OBDM is [43]:

$$\text{OBDM}(p/n) = (-1)^{\tau_f - \tau_Z} \begin{pmatrix} T_f & 0 & T_i \\ -T_Z & 0 & T_Z \end{pmatrix} \sqrt{2}\, \frac{OBDM(\Delta T=0)}{2}$$

$$(+/-)\tau Z (-1)^{J_f - J_Z} \begin{pmatrix} T_f & 1 & T_i \\ -T_Z & 0 & T_Z \end{pmatrix} \sqrt{6}\, \frac{OBDM(\Delta T=1)}{2} \qquad (2.22)$$

The multiparticle transition amplitudes are defined as:

$\text{OBDM}(\text{I}, \text{j}, \text{L}, \Delta\text{T}, j_1, j_2)$

$$= \frac{\langle J_f T_f \left\| \left[ \alpha^{\dagger}_{j_1 j_3} \otimes \tilde{\alpha}_{j_2 j_3} \right]^{\Gamma} \right\| J_i T_i \rangle \sqrt{2J_j + 1}}{\sqrt{2L+1}\sqrt{2\Delta T + 1}} \qquad (2.23)$$

where $j_3 = 1/2$ for neutron and $j_3 = -1/2$ for a proton.

In the single nucleon state ($j_2\, j_3$) the annihilation ($\tilde{\alpha}$) remove a neutron or proton, from the single nucleon state ($j_1\, j_3$) the corrosion ($\alpha^{\dagger}$) generate a neutron or proton.

## 2.4 The Harmonic-Oscillator Potential

The choice of the potential will impact the efficiency of the solution of a many-body problem. The Hamiltonian divides into a mean-field (single-particle) potential U plus a residual interaction W [44]:

$$H = \frac{1}{2m} \sum_i^A p_i^2 + \sum_i^A U(r_i) + \sum_{i<j}^A W(|\vec{r_i} - \vec{r_j}|) \qquad (2\text{-}36)$$

The harmonic-oscillator potential can be done separately and analytically in the private case:

$$\sum_i^A U^{HO}(r_i) = \frac{1}{2} m\omega^2 \sum_i^A r_i^2 = \frac{1}{2} m\omega^2 \sum_i^A \rho_i^2 + \frac{1}{2} A\omega^2 m R^2 \qquad (2\text{-}37)$$

Thus, Hamiltonian separates into

$$H = H_{int} + H_{cm'}^{ho} \tag{2-38}$$

$$H_{int} = \frac{1}{2}\sum_{1}^{A} q_i^2 + \frac{1}{7} m\omega^2 \sum_{1}^{A} \rho_i^2 + \sum_{i<j}^{A} W\left(\left|\vec{\rho}_i - \overrightarrow{\rho_j}\right|\right) \tag{2-39}$$

The center of mass must be in its lowest energy state of 0s ground state is referred to as the nonspurious state for the nucleus with mass $A_m$ in the potential $\frac{1}{2}Am\omega^2R^2$, with a center of mass-energy [44]:

$$\left\langle \psi \middle| H_{cm}^{hO} \middle| \psi \right\rangle = \frac{3}{2}\hbar\omega \tag{2-40}$$

## 2.5 Woods-Saxon Potential

The Woods-Saxon potential is an appropriated phenomenological choice for the one body in the Hartree-Fock theory. The woods-Saxon potential is a model of the single-particle wave functions, properties in the continuum and bound states so it is not dependent on a particular two-body interaction. The total binding energy cannot be calculated by Saxon potential (or any other one-body potential). The energies and radii of nuclear single particles are chosen to get match better Woods=Saxon parameters [45].

$$\mathrm{V(r)} = \mathrm{V}_o f_o(r) + \mathrm{V}_{so}(r)\vec{\ell}.\vec{s} + V_c(r) \tag{2.24}$$

Where $\mathrm{V}_o(r)$ is the central potential:

$$\mathrm{V_o\ (r) = V_o} f_\mathrm{o}\ \mathrm{(r)}$$

With a fermi shape

$$f_o(r) = \frac{1}{1+\left[e^{(r-R_{so})/\alpha_0}\right]} \tag{2.25}$$

$\mathrm{V}_{so}(r)$ is the spin-orbit potential:

$$\mathrm{V}_{so}(r) = \mathrm{V}_{so}\frac{1}{r}\frac{df_{so}(r)}{dr} \tag{2.26}$$

with $f_{so}(r) = \frac{1}{1+\left[e^{(r-R_{so})/\alpha_0}\right]}$ (2.27)

and the Coulomb potential for proton $V_c(r)$ specified by Coulomb potential for a sphere with $R_c$:

$$V_c(r) = \frac{Ze^2}{r} \quad for\, r > R_c \tag{2.28}$$

and

$$V_c(r) = \left[\frac{3Ze^2 - v}{2R^2{}_c} - \frac{r^2 Ze^2}{2R_c R_c^2}\right] for\, r < R_c \tag{2.29}$$

R is the sphere of radius, the radii $R_o$,$R_{so}$ and $R_c$ are usually expressed as: $R_i$=$r_i A^{1/3}$

The Woods-Saxon potential is written in terms of potential for our nucleus determined by Z and A. The potential of the protons will feel greater than the neutrons when the nuclei with a neutron increase. Thus, the average neutron-neutron (or proton-proton) potential is less strong than the average proton-neutron potential. Therefore, we take:

$$V_{op} = \mathrm{V}_o + \frac{(N-Z)}{A} V_1 \qquad for\, protons \tag{3.30}$$

$$V_{on} = \mathrm{V}_o - \frac{(N-Z)}{A} V_1 \qquad for\, neutrons \tag{3.31}$$

Theoretically, $R_O$ and $\alpha_o$ differences for protons and neutrons in a nucleus by a few N ≠ f. As a consequence, the six parameters in the spin-independent potential are possible. The strength $V_{so}$ for protons and neutrons could be different for N ≠ Z, but it exercises they are nearly the same. To provide a detailed account of the observed data the values of these parameters have been chosen [46].

## 2.6 The Skyrme Potential

The Skyrme force includes central, tensor and spin-orbit interaction, given by [47]

$$\mathrm{V}_{\mathrm{Skyrme}} = \widehat{\mathrm{V}}^{\mathrm{central}} + \widehat{\mathrm{V}}^{\mathrm{tensor}} + \widehat{\mathrm{V}}^{\mathrm{LS}} \tag{3.32}$$

The Skyrme interacts with the central two bodies [44]

$$\hat{V}^{\text{central}}(r_1, r_2) = \frac{1}{2}t_o\left(1 + \mathcal{X}_o\hat{P}_\sigma\right)\delta(r_1 - r_2) + \frac{1}{2}t_1\left(1 + \mathcal{X}_1\hat{P}_\sigma\right)\left[\hat{k}'^2\delta(r_1 - r_2) + \delta(r_1 r_2)\hat{k}^2\right] + t_2\left(1 + \mathcal{X}_2\hat{P}_\sigma\right)\hat{k}' \cdot \delta(r_1 - r_2)\hat{k} + \frac{1}{6}t_{31}\left(1 + \mathcal{X}_{31}\hat{P}_\sigma\right)\rho_o^{\alpha 1}(R) + \frac{1}{6}t_{32}\left(1 + \mathcal{X}_{32}\hat{P}_\sigma\right)\rho_o^{\alpha 2}(R) \quad (3.33)$$

where $\hat{P}_\sigma = \frac{1}{2}(1 + \hat{\sigma}_1.\hat{\sigma}_2)$ is the spin-exchange operator, $\rho_o(R)$ is the isoscalar density at $R \equiv \frac{1}{2}(r_1 - r_2)$, $\hat{k} \equiv \frac{1}{2i}(\nabla_1 - \nabla_2)$ is the relative momentum operator acting to the right and $\hat{k}'$ is the complex conjugate acting to the left. The spin-orbit part is given by [47]

$$\hat{V}^{LS}(r_1, r_2) = i\omega_o(\hat{\sigma}_1 + \hat{\sigma}_2) \cdot \hat{k}' \times \delta(r_1 - r_2)\hat{k} \quad (2\text{-}34)$$

And the last term is the tensor part [48]:

$$\hat{V}^{\text{tensor}}(r_1, r_2) = \frac{1}{2}t_e\left\{\left[3(\sigma_1.k')(\sigma_2.k') - (\sigma_1 \cdot \sigma_2)k'^2\right]\delta(r_1 - r_2) + \delta(r_1 r_2)[3(\sigma_1.k)(\sigma_2.k) - (\sigma_1 \cdot \sigma_2)k^2]\right\} + \frac{1}{2}t_o\{[3(\sigma_1.k)\delta(r_1 - r_2)(\sigma_2.k) - (\sigma_1 \cdot \sigma_2)k' \cdot \delta(r_1 - r_2)k] + [3(\sigma_2.k')\delta(r_1 - r_2)(\sigma_1.k) - (\sigma_1 \cdot \sigma_2)k \cdot \delta(r_1 - r_2)k']\}$$

(2.35)

# ***Chapter Three Results, Discussion, and Conclusion***

## 3.1 Introduction

In the p-shell model, the nucleons are distributed over the $1p_{3/2}$ $1p_{1/2}$ orbits. The large-basis of the psd shell model has included two shells (1p, 1d-2s) while the large-basis no core spsdpf shell model has included four shells (1s, 1p, 1d-2s, 1f-2p) [6]. The psd model space was calculated using the psdmwk interaction. The large-basis no core spsdpf was calculated using the wbm, while the p-shell used the ckpot interaction. Large scale calculations were done using the single-particle of the radial wave function of Harmonic-Oscillator (HO), Woods-Saxon (WS), and Skyrme (Ska) [49] potentials. The core-polarization calculation using the NuShell code was included through the Tessie model. The oscillator length parameter was chosen b = 1.76 $fm^{-1}$.

## 3.2 The Nucleus $^{10}$B

The Boron-10 nucleus is especially interesting because it is the second oddest-odd nuclei in the p-shell region [21]. In this study, the longitudinal form factors were calculated for the nucleus states which is excited from the ground state ($J^{\pi}$ T=$3^+$ 0) to the positive parity states ($J^{\pi}$ T=$1^+$ 0, $1^+$ 0, $2^+$ 0, $4^+$ 0) by the incident electron in this transition with excitation energy ($E_x$=0.718, 2.154, 3.587, 6.025) MeV. Also, the transverse form factors were calculated for the nucleus states ($J^{\pi}$ T=$3^+$ 0, $0^+$ 1) with energy ($E_x$=0.00, 1.74) MeV.

### 3.2.1 The Longitudinal Form Factors for (1,0) State at (0.718 MeV)

The longitudinal inelastic (C2) form factors are calculated at $E_x$=0.718 MeV state using Harmonic-Oscillator (HO) potential as shown in figure (3-1). The p-shell (dashed line) calculation results are compared with the large-basis psd (solid line) model space and spsdpf (dashed-dot line) model space truncation up to $2\hbar$□. The results of psd model space form factors with default effective charge (0.35, 0.35) were in good agreement with experimental data except the region $1 \geq q \leq 2\ fm^{-1}$. While the results of p-shell and spsdpf-shell were underestimating the experimental data at $q \leq 2.5\ fm^{-1}$.

The longitudinal inelastic (C2) form factors are calculated for the $J^{\pi}\ T = 1^{+}\ 0$ using Woods-Saxon (WS) potential is displayed in figure (3-2), while the calculation with Skyrme (Ska) potential is shown in figure (3-3). The calculating results with WS potential were closer to the experimental data than the Harmonic-Oscillator calculations. The calculating form factors with Skyrme (Ska) potential give remarkable agreement with experimental results at all momentum transfers.

The calculating longitudinal inelastic (C2) form factors for the $J^{\pi}\ T = 1^{+}\ 0$ truncated up to $2\hbar$ □ using all potentials for the psd model are displayed in figures (3-4). The results of Ska potential form factors were in agreement with experimental data for lower momentum transfer values $q \leq\ 1.2\ fm^{-1}$. But the results of higher momentum transfer values are incompatible with experimental -data and fall rapidly. The One-Body Density Matrix (OBDM) element values for transition (C2) calculated using psd model space are displayed in a table (3.1).

Table (3.1): The calculated C2 inelastic transition OBDM element values for $J^{\pi}\ T = 1^{+}\ 0\ \ (E_x = 0.718\ MeV)$in $^{10}$B nucleus.

| **$^{10}$B** | | **C2** |
|---|---|---|
| $j_i$ | $j_f$ | OBDM (ΔT=0) |
| $1p_{3/2}$ | $1p_{3/2}$ | 0.01045 |
| $1p_{3/2}$ | $1p_{1/2}$ | -0.02702 |
| $1p_{1/2}$ | $1p_{3/2}$ | 0.08352 |
| $1d_{5/2}$ | $1d_{5/2}$ | -0.00552 |
| $1d_{5/2}$ | $1d_{3/2}$ | -0.01677 |
| $1d_{5/2}$ | $2s_{1/2}$ | -0.01683 |
| $1d_{3/2}$ | $1d_{5/2}$ | 0.05685 |
| $1d_{3/2}$ | $1d_{3/2}$ | 0.01844 |

| | | |
|---|---|---|
| $1d_{3/2}$ | $2s_{1/2}$ | 0.16883 |
| $2s_{1/2}$ | $1d_{5/2}$ | -0.01773 |
| $2s_{1/2}$ | $1d_{3/2}$ | -0.18997 |

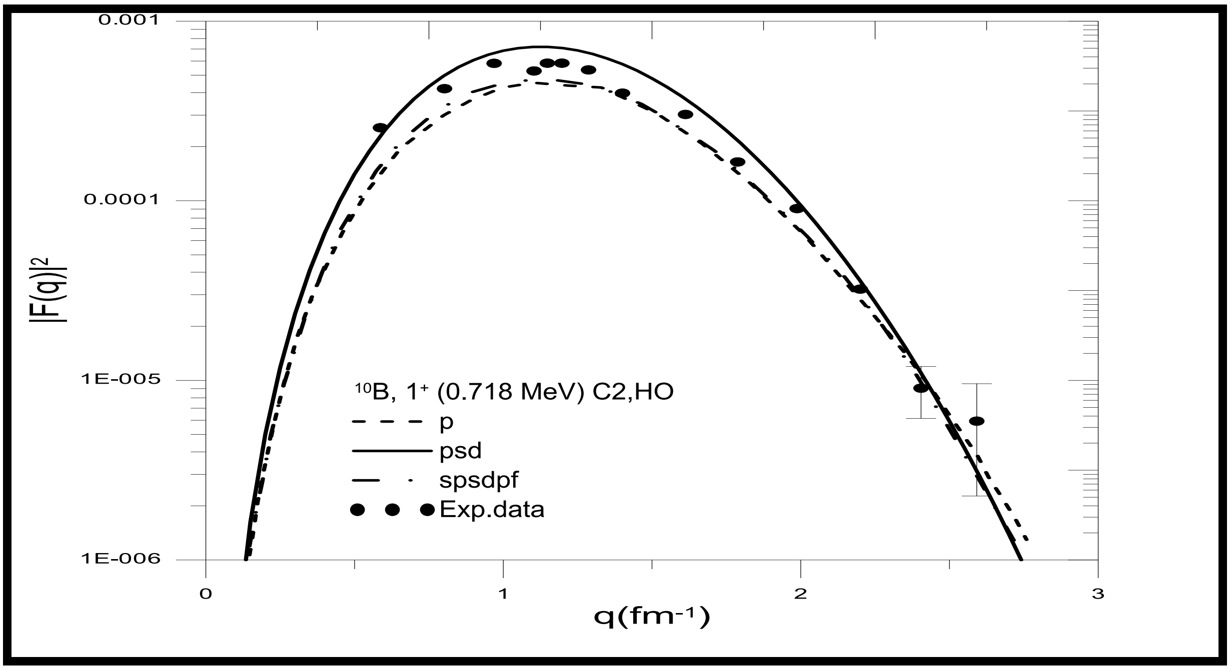


Fig. (3-1): The longitudinal inelastic (C2) form factors for the transition to the $1^+$ (0.718 MeV) state in $^{10}$B calculated using HO potential for different models space. The experimental data are taken from reference [24]

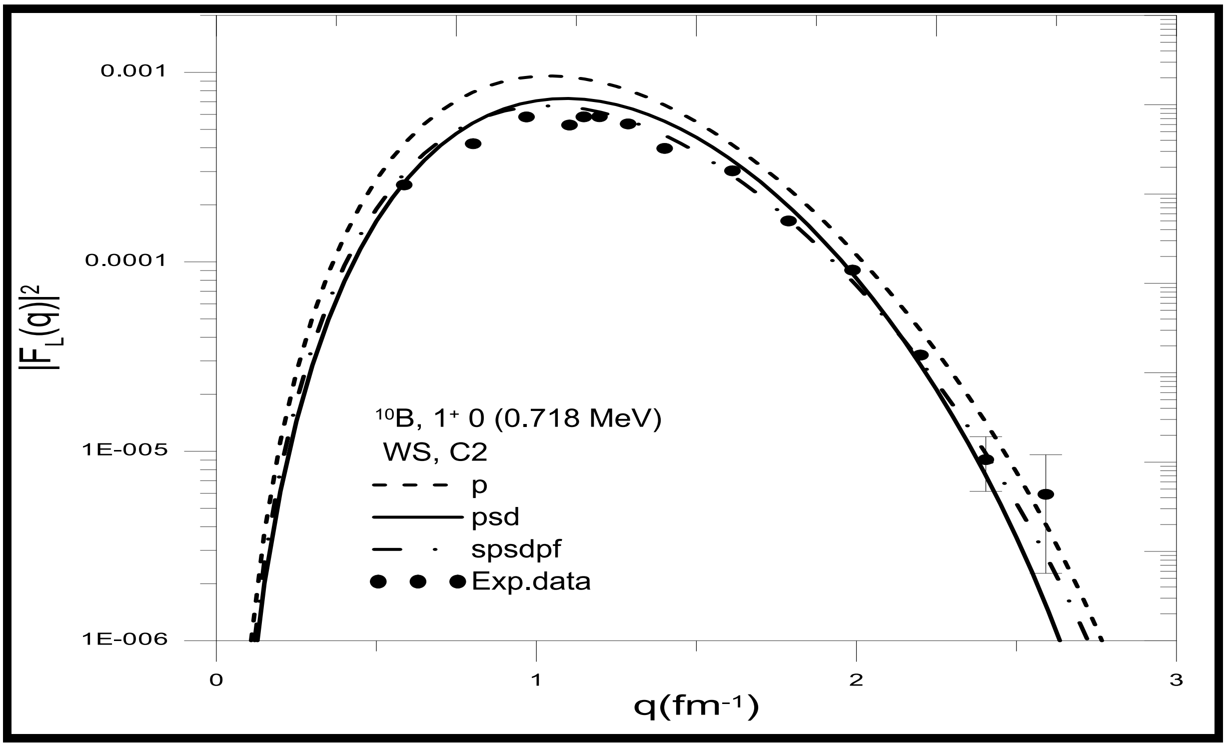

Fig. (3-2): The longitudinal inelastic (C2) form factors for the transition to the $1^+$ (0.718 MeV) state in $^{10}$B calculated using WS potential for different models space. The experimental data are taken from reference [24]

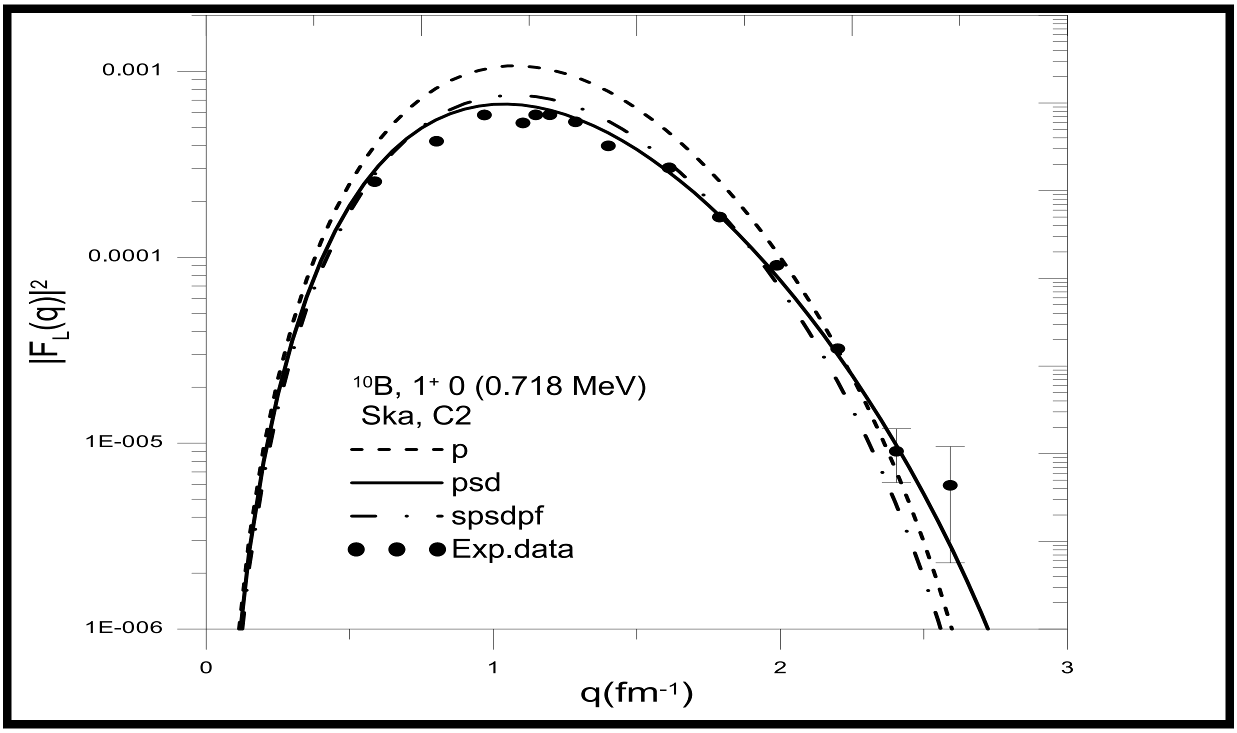


Fig. (3-3): The longitudinal inelastic (C2) form factors for the transition to the $1^+$ (0.718 MeV) state in $^{10}$B calculated using Ska potentials for different models space. The experimental data are taken from reference [24]

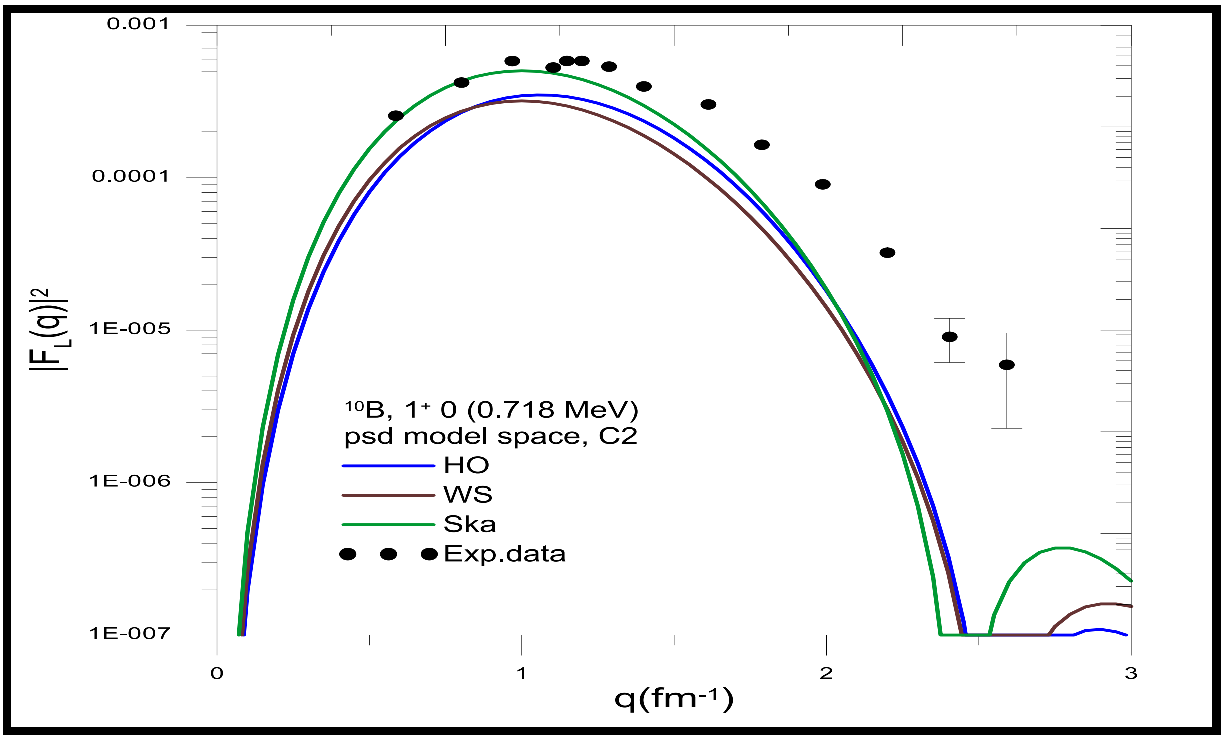

Fig. (3-4): The longitudinal inelastic (C2) form factors for the transition to the $1^+$ (0.718 MeV) state in $^{10}$B calculated using psd models space truncation at $2\hbar$ for different potentials. The experimental data are taken from reference [24]

### 3.2.2 The Longitudinal Form Factors for (1,0) State at (2.154 MeV)

The psd model calculation for the longitudinal inelastic (C2) form factors at $E_x$=2.154 MeV state using HO potential is plotted in figure (3-5). The calculating results with effective charge (0.1, 0.1) for proton and neutron respectively overestimate the experimental data shape at $q \geq 2.4\, fm^{-1}$. While the other calculation with p-shell and spsdpf-shell truncation up to $2\hbar$ underestimates the experimental data in all momentum transfers.

The longitudinal inelastic (C2) form factors were calculated for the $J^\pi\, T = 1^+\, 0$ at $E_x = 2.154\, MeV$ state using WS potential is displayed in figure (3-6), while the calculation with Skyrme (Ska) potential is shown in figure (3-7). The calculating results for the psd model space with the contribution of the effective charge agree well and reproduce the shape of the experimental data. The calculation results of the psd and spsdpf models space using WS and Ska potentials give a good agreement and are closer than the results of the p model in $q \leq 1.5\, fm^{-1}$.. The One-Body Density Matrix (OBDM) element values for (C2) calculated using psd model space are displayed in tables (3.2).

Table (3.2): the calculated C2 inelastic transition OBDM element values for $J^\pi\, T = 1^+\, 0$ ($E_x$ =2.154 MeV) in $^{10}$B nucleus.

| $^{10}$B | | C2 |
|---|---|---|
| $j_i$ | $j_f$ | OBDM (ΔT=0) |
| $1p_{3/2}$ | $1p_{3/2}$ | -0.34014 |
| $1p_{3/2}$ | $1p_{1/2}$ | -0.13950 |
| $1p_{1/2}$ | $1p_{3/2}$ | 0.06995 |
| $1d_{5/2}$ | $1d_{5/2}$ | 0.00395 |
| $1d_{5/2}$ | $1d_{3/2}$ | 0.00297 |
| $1d_{5/2}$ | $2s_{1/2}$ | -0.00420 |

| | | |
|---|---|---|
| $1d_{3/2}$ | $1d_{5/2}$ | -0.00326 |
| $1d_{3/2}$ | $1d_{3/2}$ | 0.00921 |
| $2s_{1/2}$ | $1d_{5/2}$ | -0.00466 |
| $2s_{1/2}$ | $1d_{3/2}$ | -0.02120 |

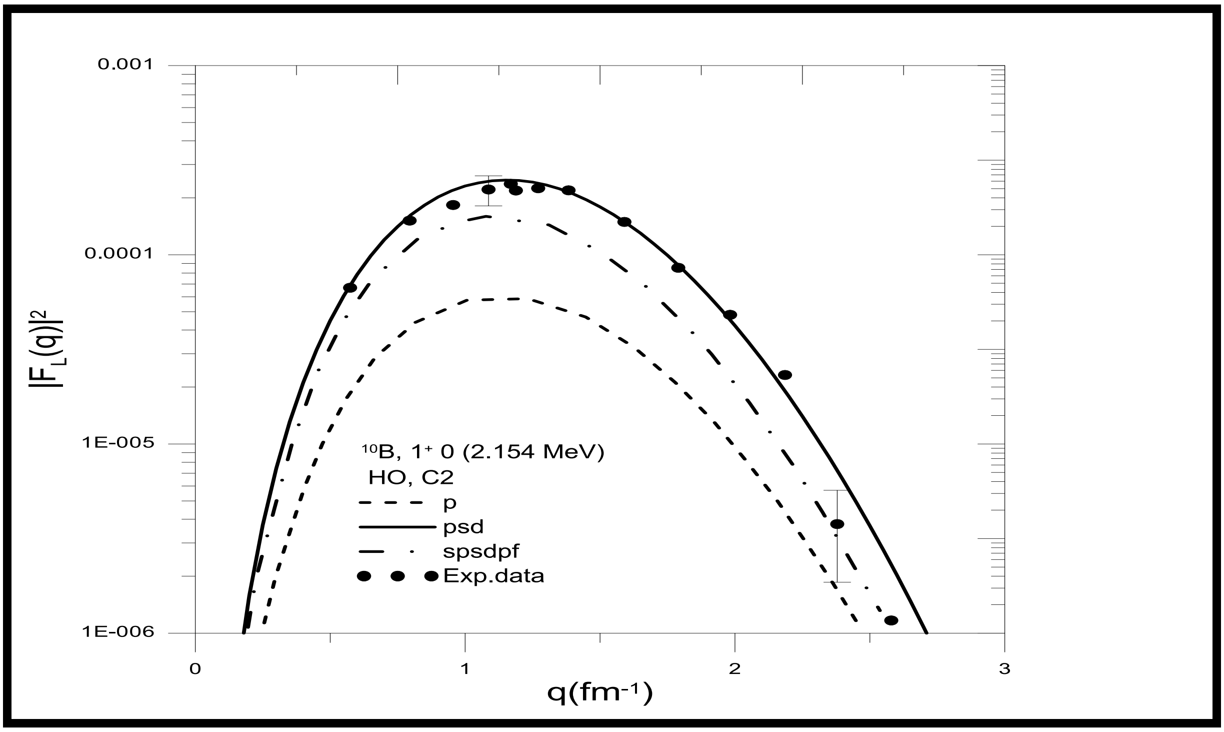


Fig. (3-5): The longitudinal inelastic (C2) form factor for the transition to the $1^+$ (2.154 MeV) state calculated using HO for different models space truncation at $2\hbar$ □. The experimental data are taken from reference [24]

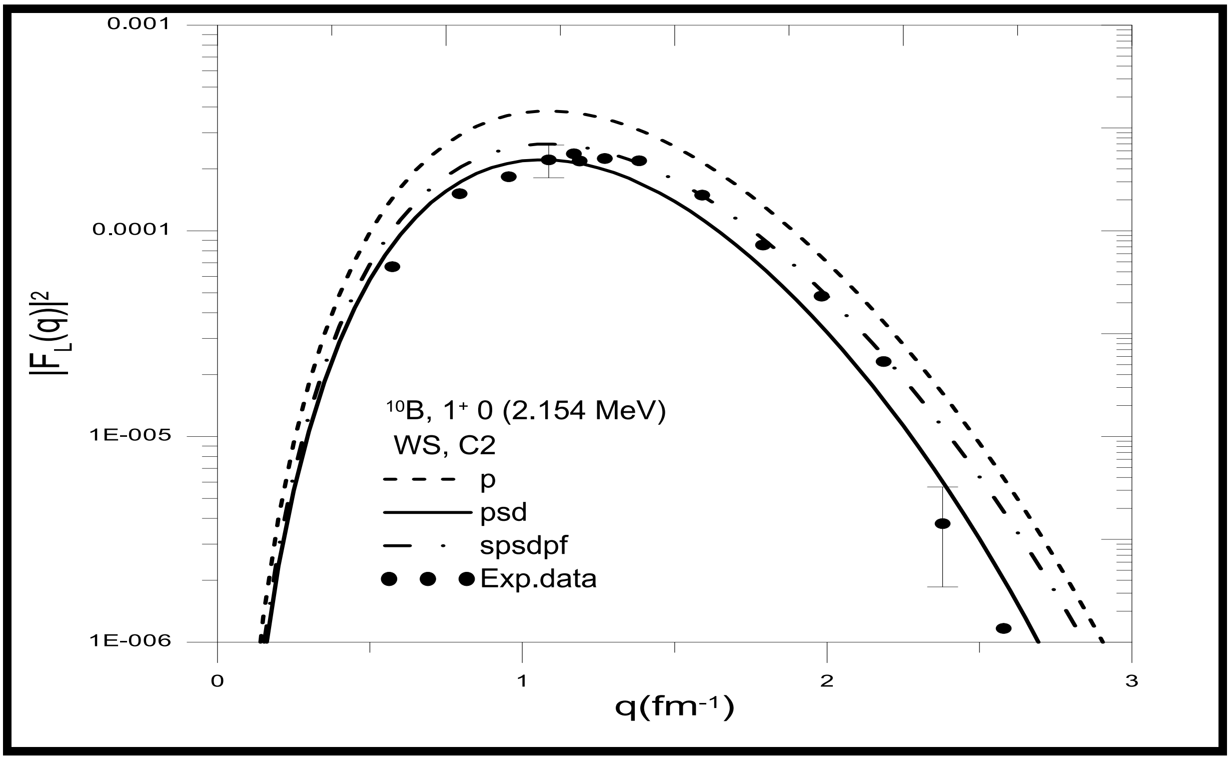


Fig. (3-6): The longitudinal inelastic (C2) form factors for the transition to the $1^+$ (2.154 MeV) state calculated using p, psd, and spsdpf models space. The experimental data are taken from reference [24]

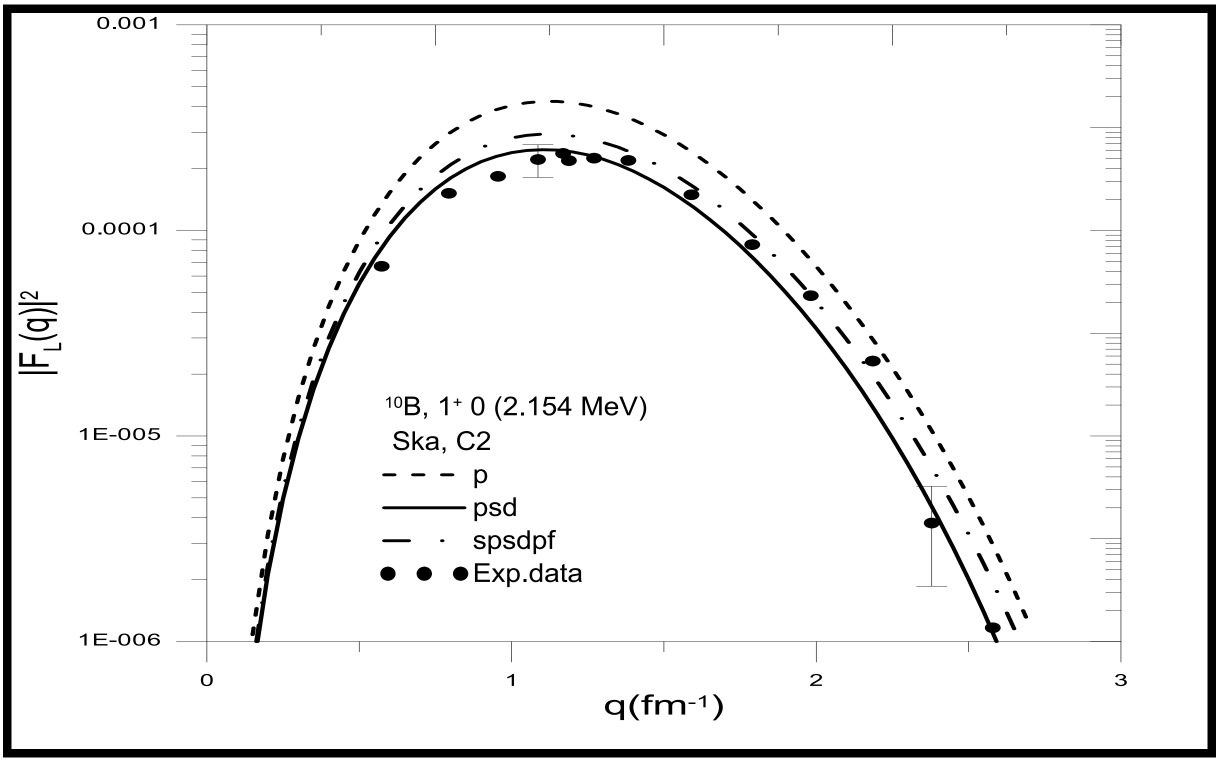


Fig. (3-7): The longitudinal inelastic (C2) form factors for the transition to the $1^+$ (2.154 MeV) state calculated using Ska for different models space. The experimental data are taken from reference [24]

### 3.2.3 The Longitudinal Form Factors for (2, 0) State at (3.587 MeV)

The calculation of longitudinal inelastic (C2) form factors of the $J^{\pi}T = 2^{+}\,0$ states at $E_x = 3.587\,MeV$ state using HO potential is displayed in figure (3-8). The calculation results using the psd model space without effective charge (1, 0) give good agreement with experimental data, especially at higher momentum transfer values.

The longitudinal inelastic (C2) form factors are calculated using WS potential displayed in figure (3-9) and using Skyrme (Ska) potentials in figure (3-10). The p calculation results are compared with the large-basis psd and spsdpf models. The calculations results with the large-basis psd model with WS potential agree well with experimental data at all momentum transfer values and give better results than another potential. While the results of p-shell were incompatible with experimental data at $q \geq 2.2\,fm^{-1}$. The calculation results with the large-basis spsdpf model slightly underestimated the experimental data at all momentum transfer values. The One-Body Density Matrix element values for this transition (C2) calculated using psd model space are shown in tables (3.3).

Table (3.3): The calculated C2 transition OBDM element values for $J^{\pi}T = 2^{+}\,0$ ($E_x = 3.587\,MeV$) in $^{10}$B nucleus

| $^{10}$B | | C2 |
|---|---|---|
| $j_i$ | $j_f$ | OBDM (ΔT=0) |
| $1p_{3/2}$ | $1p_{3/2}$ | -0.00932 |
| $1p_{3/2}$ | $1p_{1/2}$ | -0.01358 |
| $1p_{1/2}$ | $1p_{3/2}$ | -0.00009 |
| $1d_{5/2}$ | $1d_{5/2}$ | 0.45211 |
| $1d_{5/2}$ | $1d_{3/2}$ | 0.00571 |
| $1d_{5/2}$ | $2s_{1/2}$ | -0.00531 |
| $1d_{3/2}$ | $1d_{5/2}$ | -0.03385 |
| $1d_{3/2}$ | $1d_{3/2}$ | 0.03018 |
| $1d_{3/2}$ | $2s_{1/2}$ | -0.07931 |

| | | |
|---|---|---|
| $2s_{1/2}$ | $1d_{5/2}$ | **-0.00940** |
| $2s_{1/2}$ | $1d_{3/2}$ | **-0.01209** |

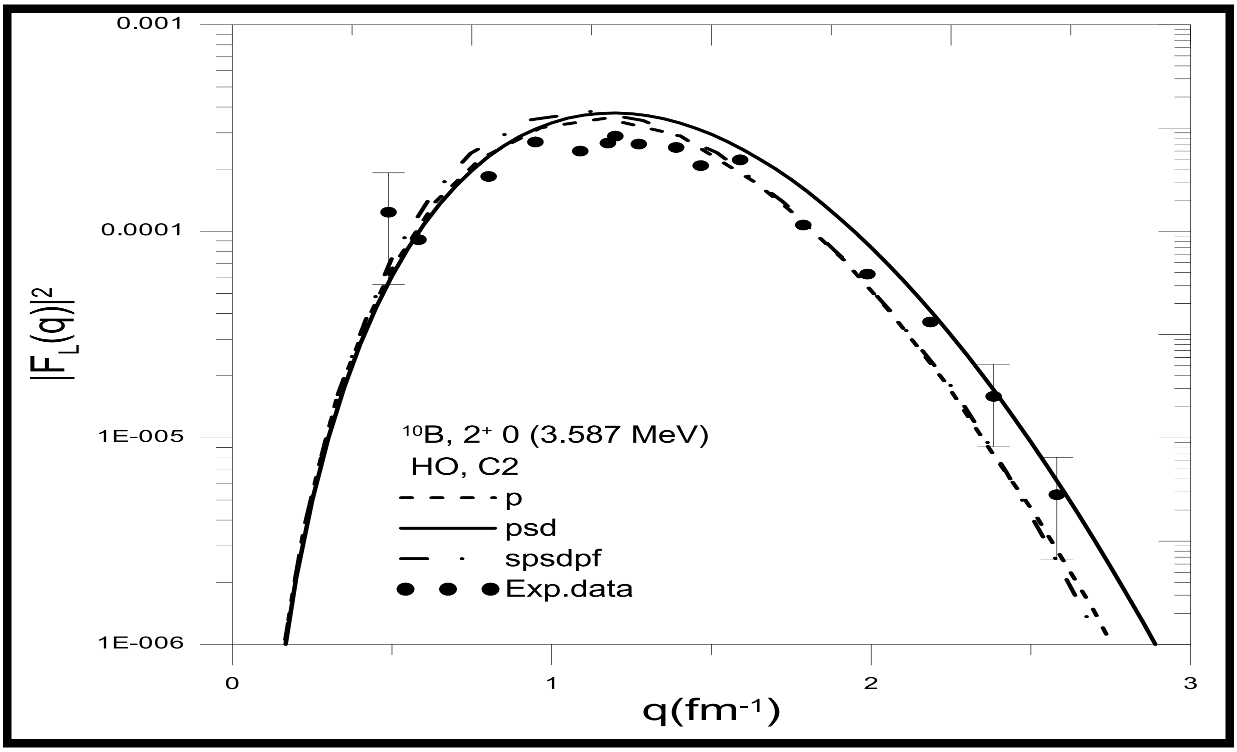


Fig. (3-8): The longitudinal inelastic (C2) form factors for the transition to the $2^+$ (3.587 MeV) state in $^{10}B$ calculated using HO potential for different models space. experimental data are taken from reference [24]

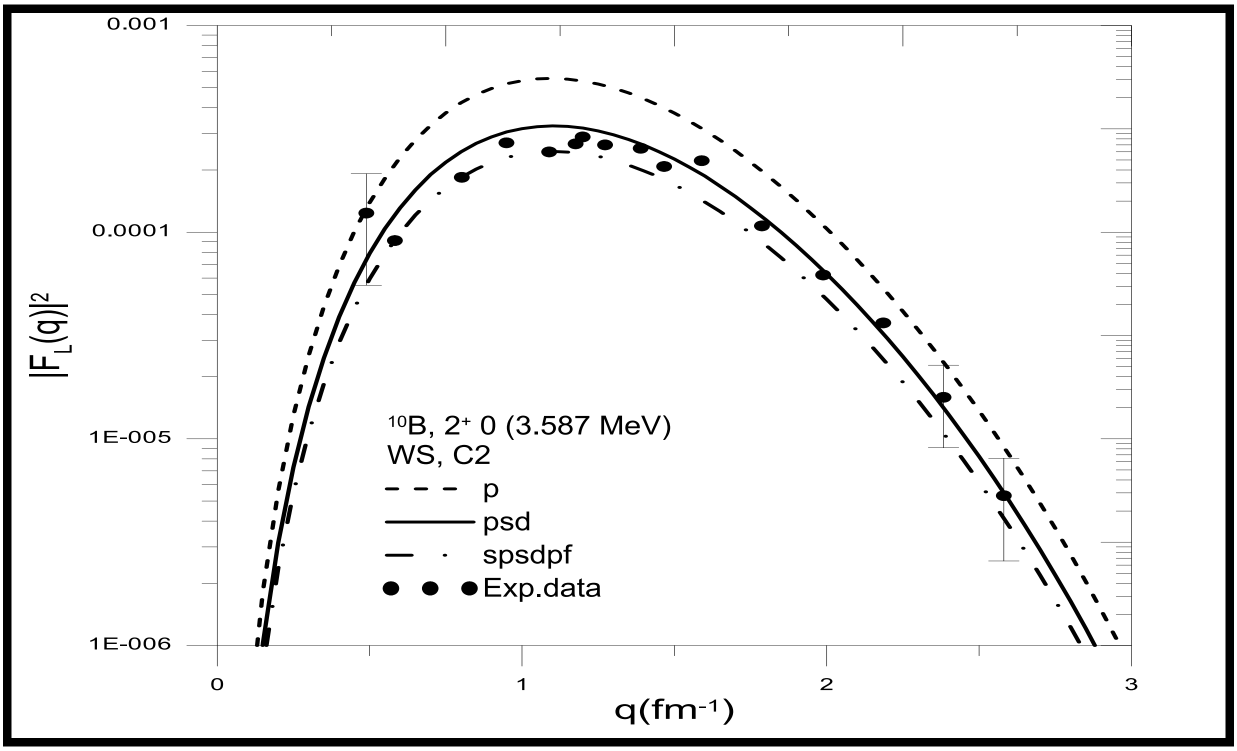


Fig. (3-9): The longitudinal inelastic (C2) form factors for the transition to the $2^+$ (3.587 MeV) state calculated using WS potential for different models space. The experimental data are taken from reference [24]

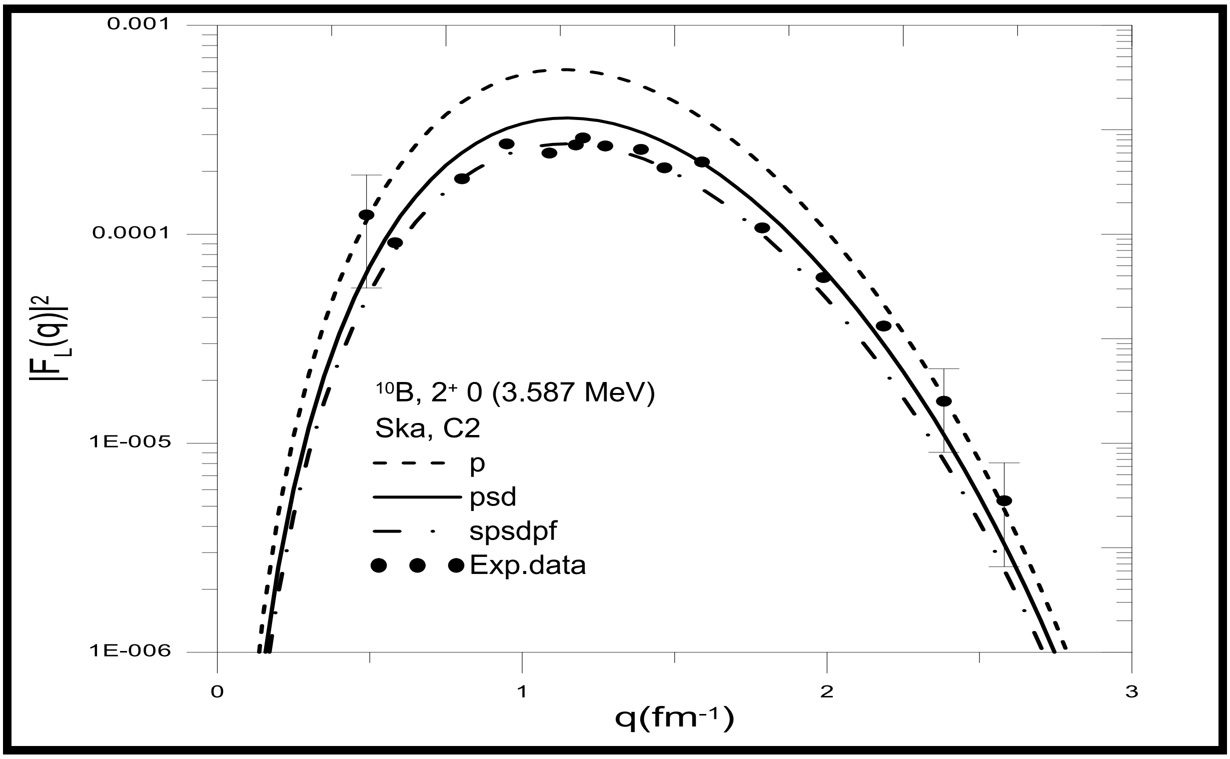


Fig. (3-10): The longitudinal inelastic (C2) form factors for the transition to the $2^+$ (3.587 MeV) state calculated using Ska potential for different models space. The experimental data are taken from reference [24]

### 3.2.4 The Longitudinal Form Factors for (4, 0) State at (6.025 MeV)

The longitudinal inelastic (C2) form factors for the $J^{\pi}T = 4^{+}\ 0$ state at $E_x = 6.025$ MeV calculated by using Harmonic-Oscillator (HO) potential displayed in figure (3-11). The p-shell calculation results are compared with the large-basis psd and spsdpf models with effective charge values equal to (0.9, 0.5) for proton and neutron respectively. The calculating results for psd model space with the contribution of the effective charge are given a good agreement with experimental data at $q\ \leq 1.5\ fm^{-1}$. .

The longitudinal inelastic (C2) form factors calculated using WS and Skyrme (Ska) potential are displayed in Figures (3-12), and (3-13), respectively. The calculation results using WS potential for psd model space in agreement for lower momentum transfer q ≤ 0.9 $fm^{-1}$. While the results of form factors fall rapidly at higher momentum transfer. The calculating results with the contribution of the effective charge using Ska potential are given a good agreement with experimental data at $q\ \leq 1.5\ fm^{-1}$. The One-Body Density Matrix element values for this transition (C2) calculated using psd model space are given in tables (3.4).

Table (3.4): The calculated C2 transition OBDM element values for $J^{\pi}T = 4^{+}\ 0$ ($E_x = 6.025$ MeV) in $^{10}$B nucleus

| $^{10}$B | | C2 |
|---|---|---|
| $j_i$ | $j_f$ | OBDM (ΔT=0) |
| $1p_{3/2}$ | $1p_{3/2}$ | -0.00174 |
| $1p_{3/2}$ | $1p_{1/2}$ | 0.00101 |
| $1p_{1/2}$ | $1p_{3/2}$ | 0.0.3204 |
| $1d_{5/2}$ | $1d_{5/2}$ | 0.08327 |
| $1d_{5/2}$ | $1d_{3/2}$ | 0.00207 |
| $1d_{5/2}$ | $2s_{1/2}$ | -0.10938 |
| $1d_{3/2}$ | $1d_{5/2}$ | 0.01766 |
| $1d_{3/2}$ | $1d_{3/2}$ | 0.09765 |
| $1d_{3/2}$ | $2s_{1/2}$ | 0.00158 |
| $2s_{1/2}$ | $1d_{5/2}$ | 0.06036 |
| $2s_{1/2}$ | $1d_{3/2}$ | -0.05188 |

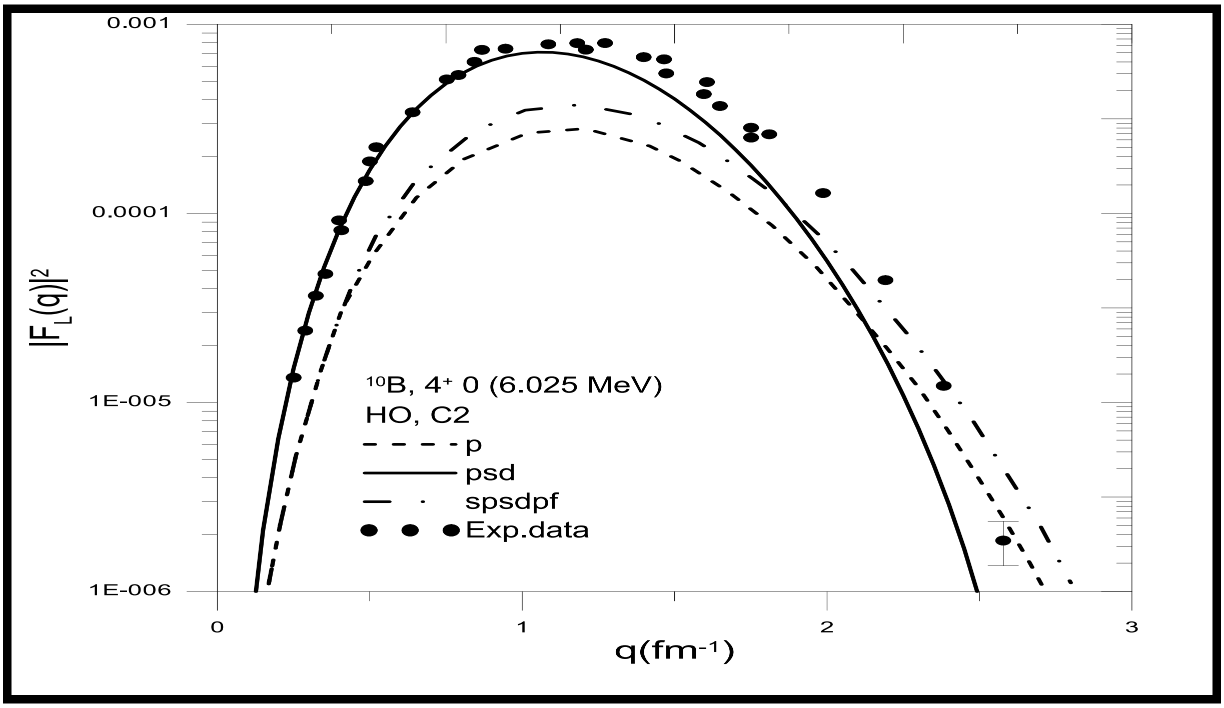


Fig. (3-11): The longitudinal inelastic (C2) form factors for the transition to the $4^+$ (6.025 MeV) state in $^{10}$B calculated using HO potential for different models space. The experimental data are taken from reference [24]

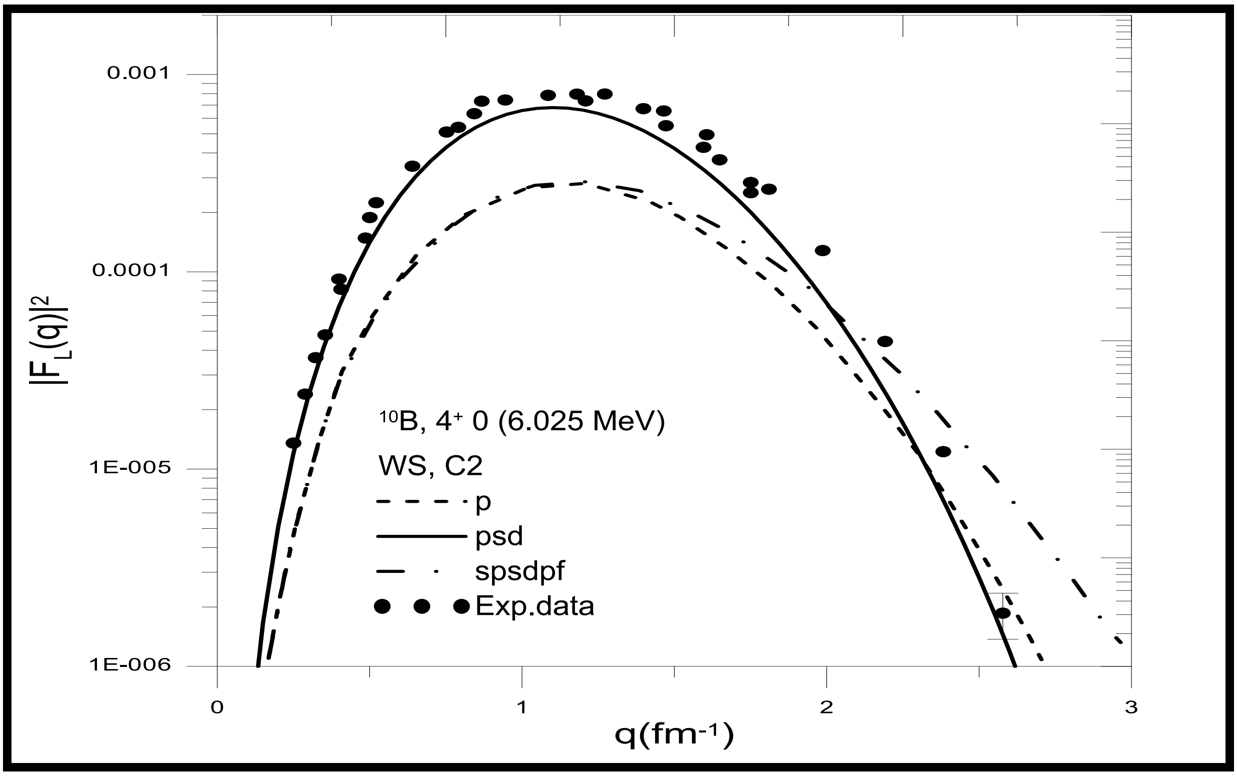


Fig. (3-12): The longitudinal inelastic (C2) form factors for the transition to the $4^+$ (6.025 MeV) state in $^{10}$B calculated using WS potential for different models space. The experimental data are taken from reference [24]

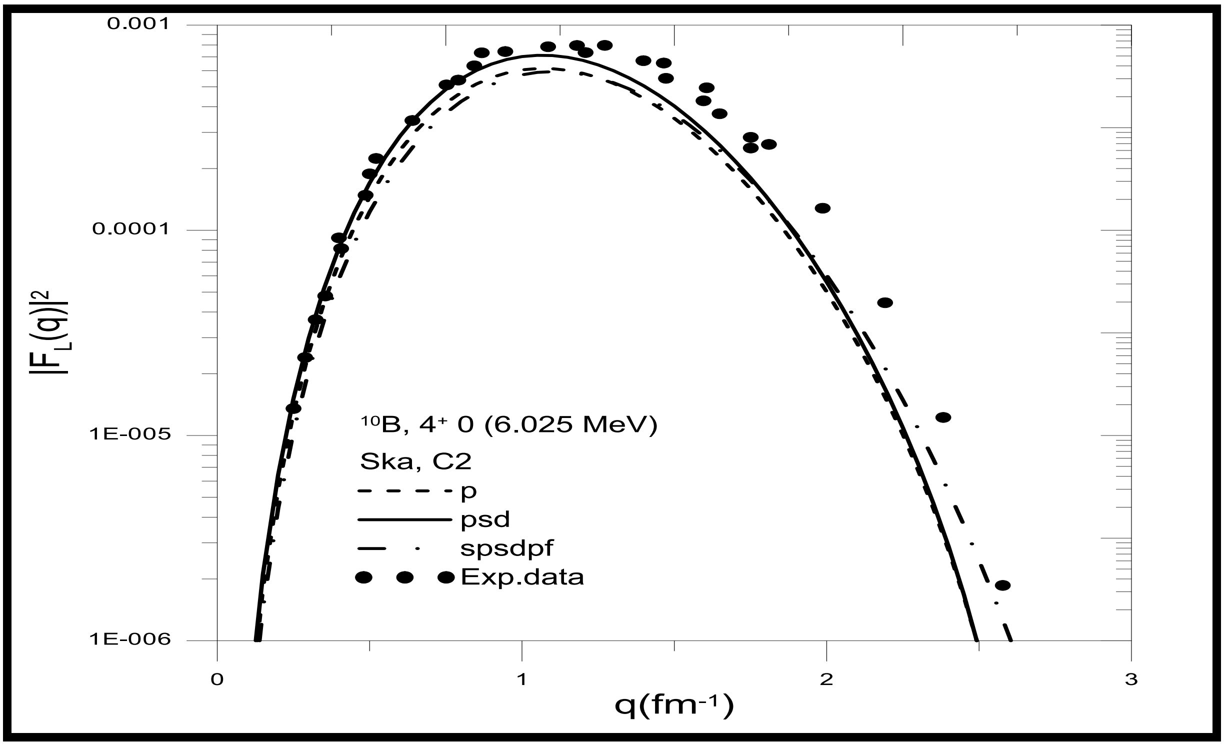


Fig. (3-13): The longitudinal inelastic (C2) form factors for the transition to the $4^+$ (6.025 MeV) state in $^{10}$B calculated using Ska potential for different models space. The experimental data are taken from reference [24]

### 3.2.5 The Transverse Form Factors for (3, 0) State at (0.00 MeV)

The transverse elastic form factors for M1, M3, and total (M1+M3) for the $3^+$ calculated using HO potential are shown in Figures (3-14). The M1 (dash line) component dominates the transition to $2^+$ at $q \leq 2\ fm^{-1}$ after then, the M3 (dash-double-dotted line) contribution becomes dominant in the transition. The exchange of influence between M1 and M3 indicates that the one-body values were well computed in this model space.

Figure (3-15) shows the total elastic transverse (M1+M3) calculated form factors of the $J^\pi\, T = 3^+\, 0$ states in $^{10}$B using HO potential. The p-shell calculation results are compared with the large-basis psd and spsdpf models at (0+2) $\hbar$ □. The results of the calculations using Skyrme (ska) potential for the psd model space with default effective charge agree well with experimental data at $0.7 \geq q \leq 1.5\ fm^{-1}$. .

The transverse elastic form factors contribute M1, M3, and the total (M1+M3) for the $3^+$ transition using WS and Ska potentials shown in Figure (3-16), (3-

18). The calculated results for all potential (HO, WS, and Skyrme) have the same results.

The form factors of elastic magnetic mixed multipolarity (M1+M3) were calculated using WS and Ska potentials for all models displayed in figure (3-17), (3-19). The p-shell calculation results are compared with the large-basis psd and spsdpf models at (0+2) $\hbar\omega$. The calculation results using the psd model space with default effective charge give a good description of the experimental data best from the p and spsdpf models.

The total transverse form factor for (M1+M3) was calculated using HO, WS, and Ska potential displayed in figure (3-20). The calculation results using psd truncation at $2\hbar\omega$ acceptable with experimental data at lower momentum transfer than being after that fall rapidly for higher values of momentum transfer at $q = 2\ fm^{-1}$. The form factors of elastic magnetic mixed multipolarity (M1+M3) calculated using all potentials are shown in figure (3-21). The calculation results using psd model space truncation at $4\hbar\omega$ compatible with the experimental data in the momentum transfers region at $0.7 \geq q \leq 1.5\ fm^{-1}$. Whereas, the psd model space using Skyrme (ska) potential truncated to (0+2) $\hbar\omega$ gave better results. The One-Body Density Matrix element values for this transition (M1 and M3) calculated using psd model space are shown in tables (3.5), and (3.6) respectively.

Table (3.5): The calculated M1 transition OBDM element values for $J^{\pi}T = 3^{+}\ 0\ (E_x = 0.00\ MeV)$ in $^{10}$B nucleus.

| $^{10}$B | | M1 |
|---|---|---|
| $j_i$ | $j_f$ | OBDM (ΔT=0) |
| $1p_{3/2}$ | $1p_{3/2}$ | 0.66179 |
| $1p_{3/2}$ | $1p_{1/2}$ | 0.23454 |
| $1p_{1/2}$ | $1p_{3/2}$ | -0.23454 |
| $1p_{1/2}$ | $1p_{1/2}$ | 0.09020 |
| $1d_{5/2}$ | $1d_{5/2}$ | 0.03837 |
| $1d_{5/2}$ | $1d_{3/2}$ | 0.06883 |
| $1d_{3/2}$ | $1d_{5/2}$ | -0.6883 |

| | | |
|---|---|---|
| $1d_{3/2}$ | $1d_{3/2}$ | **1.14126** |
| $1d_{3/2}$ | $2s_{1/2}$ | **0.22886** |
| $2s_{1/2}$ | $2s_{1/2}$ | **-0.54704** |

Table (3.6): The calculated M3 transition OBDM element values for $J^{\pi}T = 3^{+}\,0\;(E_x = 0.00\ MeV)$ in $^{10}$B nucleus.

| $^{10}$**B** | | **M3** |
|---|---|---|
| $j_i$ | $j_f$ | **OBDM (ΔT=0)** |
| $1p_{3/2}$ | $1p_{3/2}$ | **-0.09113** |
| $1d_{5/2}$ | $1d_{5/2}$ | **0.00557** |
| $1d_{5/2}$ | $1d_{3/2}$ | **0.04175** |
| $1d_{5/2}$ | $2s_{1/2}$ | **-0.01307** |
| $1d_{3/2}$ | $1d_{5/2}$ | **-0.01475** |
| $1d_{3/2}$ | $1d_{3/2}$ | **-0.30892** |
| $2s_{1/2}$ | $1d_{5/2}$ | **-0.01307** |

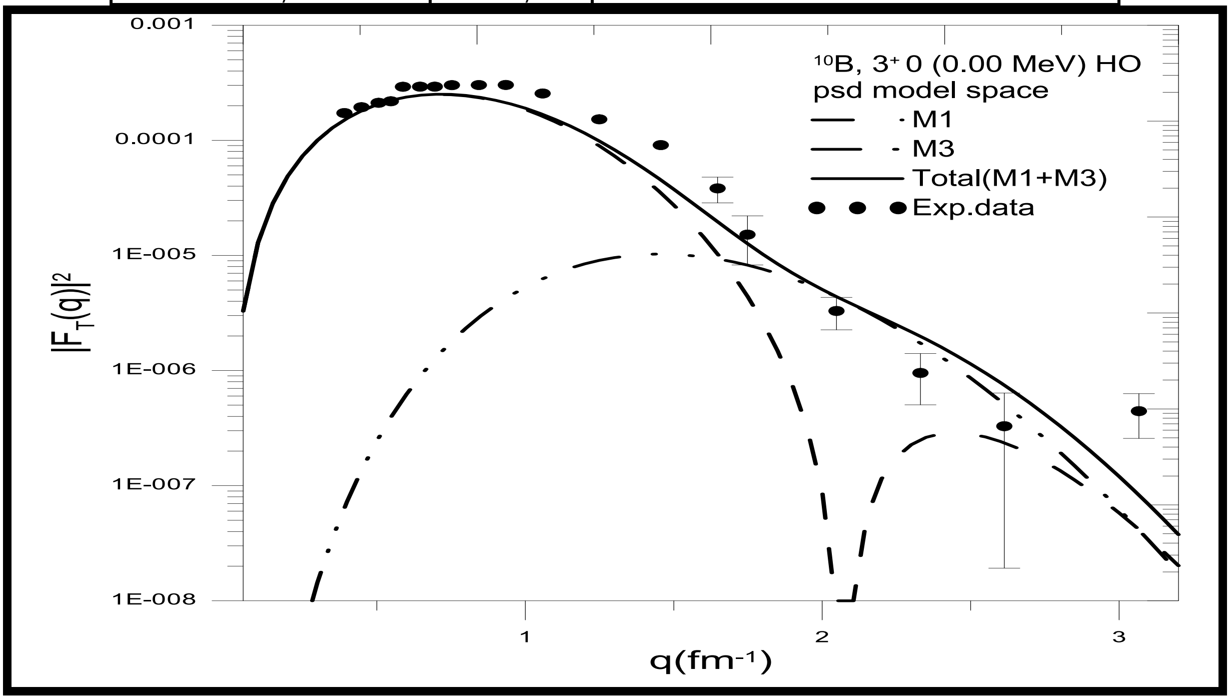


Fig. (3-14): The total transverse elastic (M1+M3) form factors for the transition to the $2^{+}$ (0.00 MeV) state in $^{10}$B calculated using HO potential for psd model space truncation at (0+2) $\hbar$ □. The experimental data are taken from reference [22]

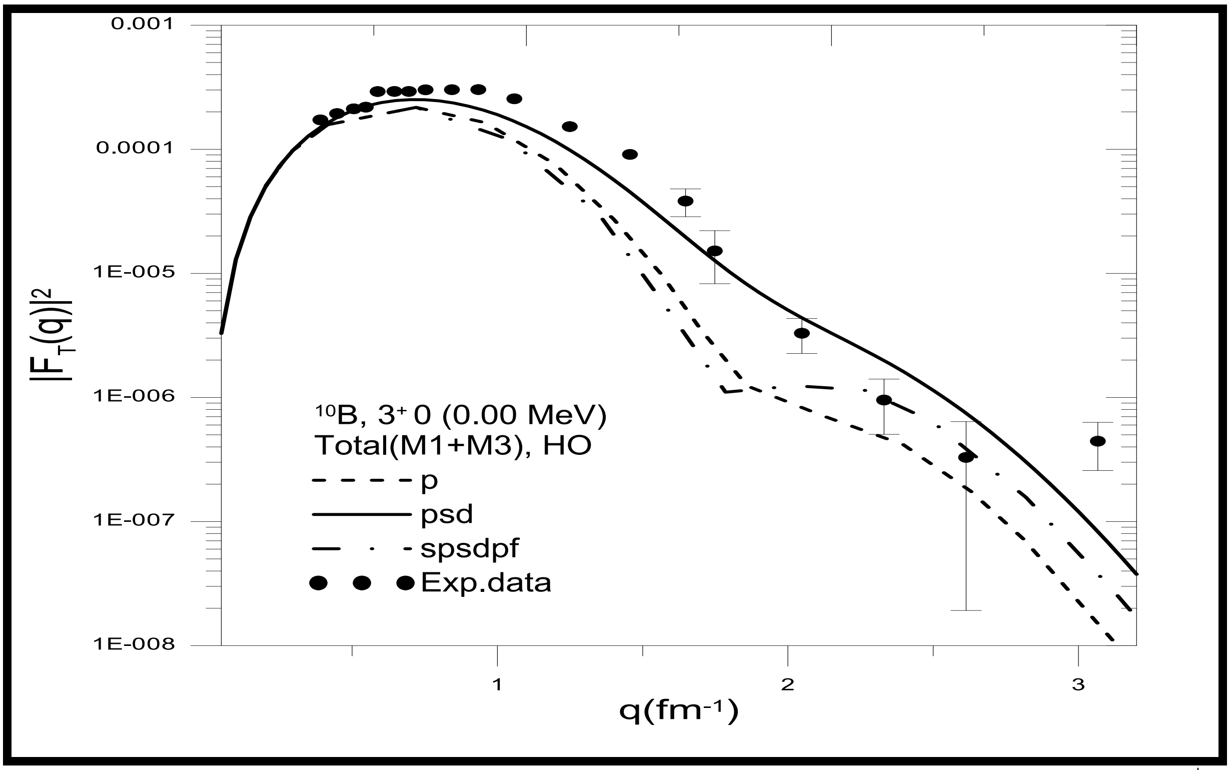


Fig. (3-15): The total transverse (M1+M3) form factors for the transition $3^+$ (0.00 MeV) state calculated using HO potential for different models space truncation at (0+2) $\hbar$ □. The experimental data are taken from reference [22]

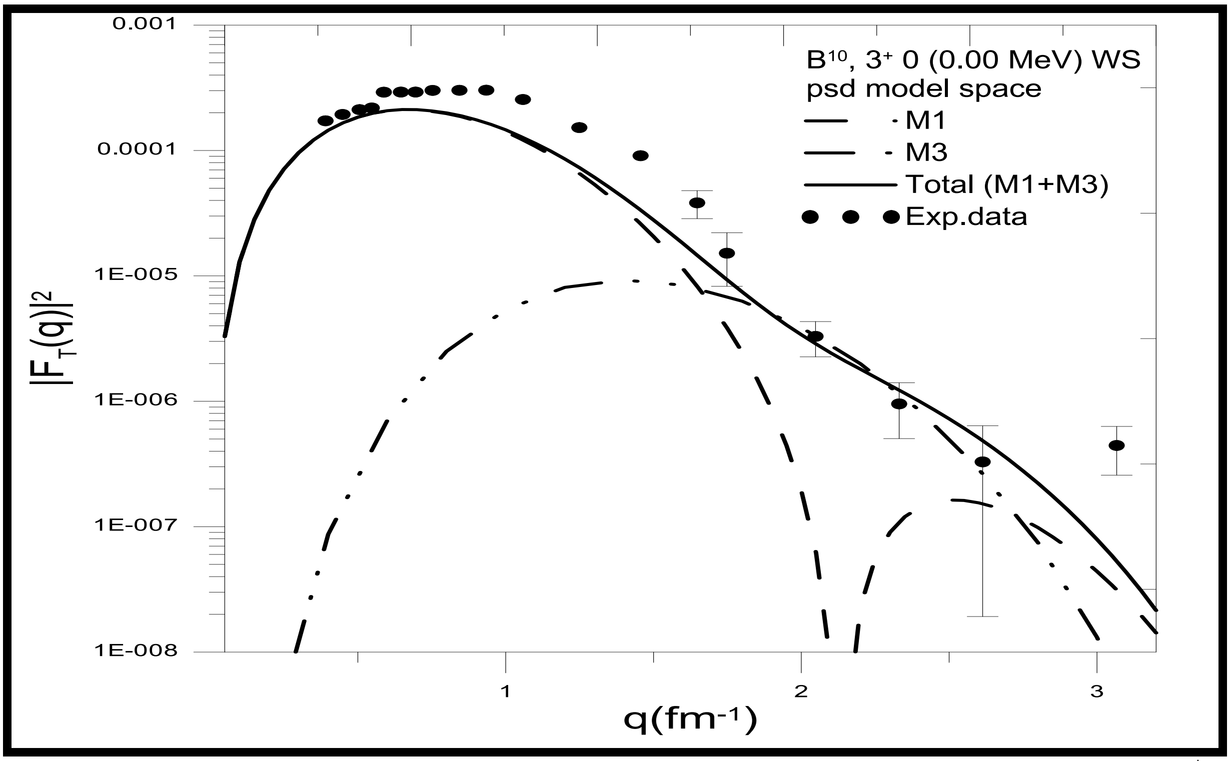


Fig. (3-16): The total transverse (M1+M3) form factors for the transition $3^+$ (0.00 MeV) state calculated using WS potential for psd model space truncation at (0+2) $\hbar$ □. The experimental data are taken from reference [22]

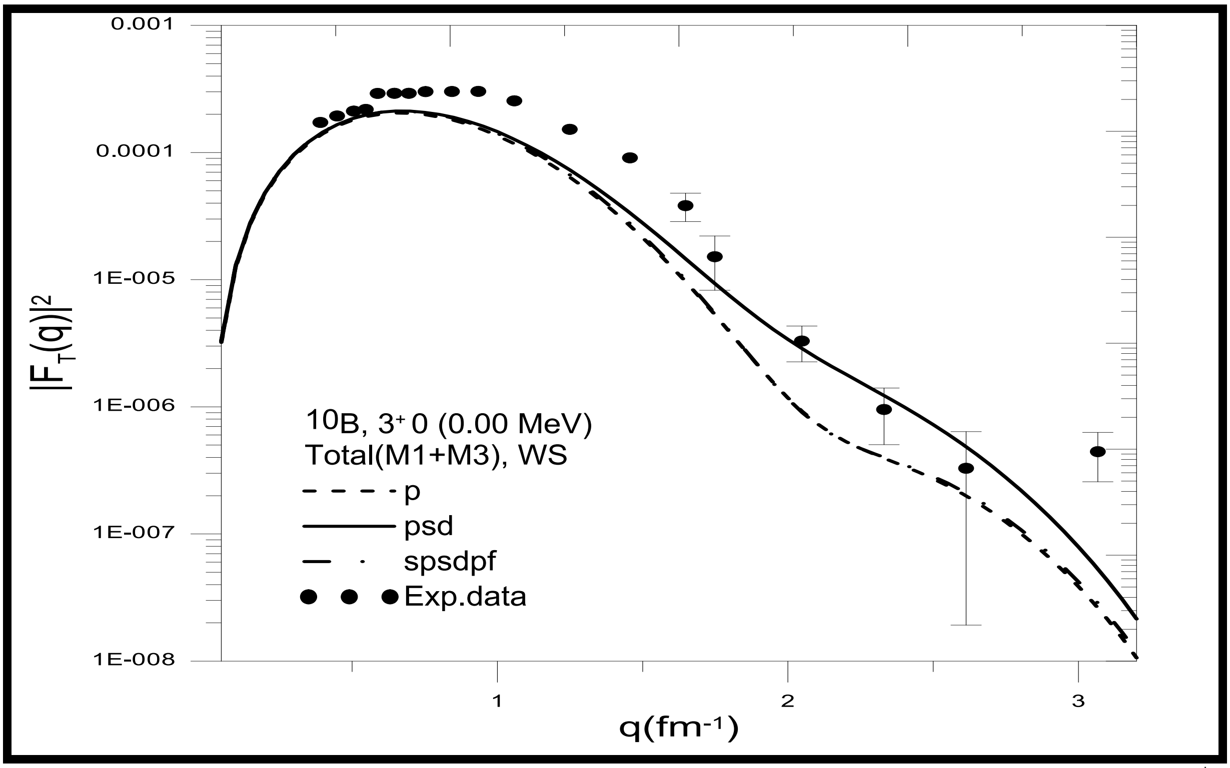


Fig. (3-17): The total transverse (M1+M3) form factors for the transition 3$^+$ (0.00 MeV) state calculated using Ska potential for different model's space truncation at (0+2) ℏ □. The experimental data are taken from reference [22]

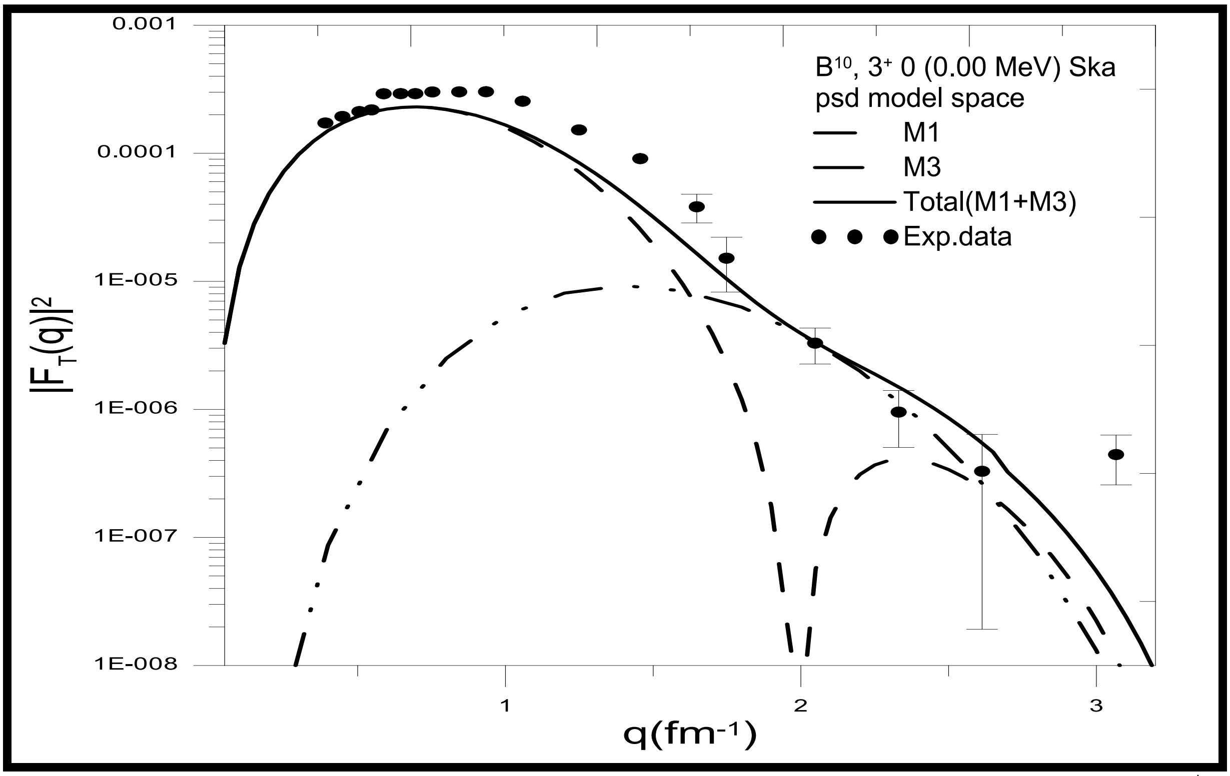


Fig. (3-18): The total transverse (M1+M3) form factors for the transition 3$^+$ (0.00 MeV) state calculated using Ska potential for psd model space truncation at (0+2) ℏ □. The experimental data are taken from reference [22]

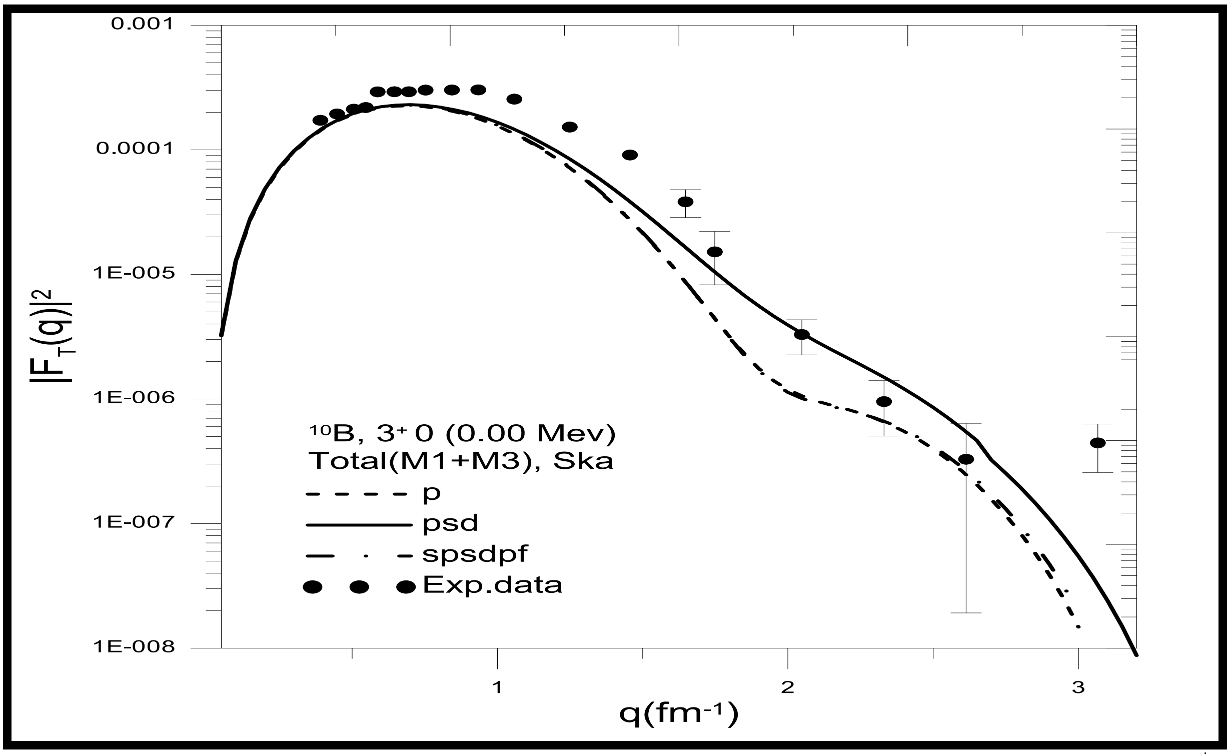


Fig. (3-19): The total transverse (M1+M3) form factor for the transition $3^+$ (0.00 MeV) state calculated using Ska potential for different model's space truncation at (0+2) $\hbar$ □. The experimental data are taken from reference [22]

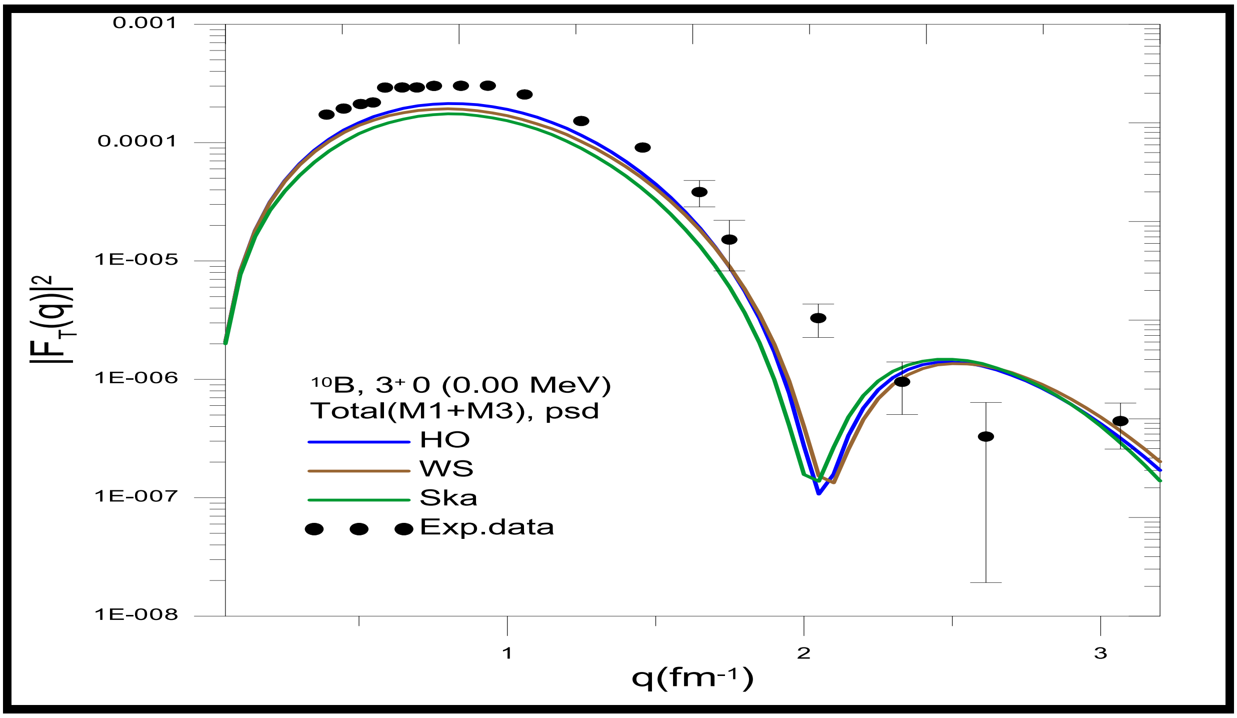


Fig. (3-20): The total transverse (M1+M3) form factors for the transition $3^+$ (0.00 MeV) state calculated using psd model space truncation at $2\hbar$ □ for different potentials. The experimental data are taken from reference [22]

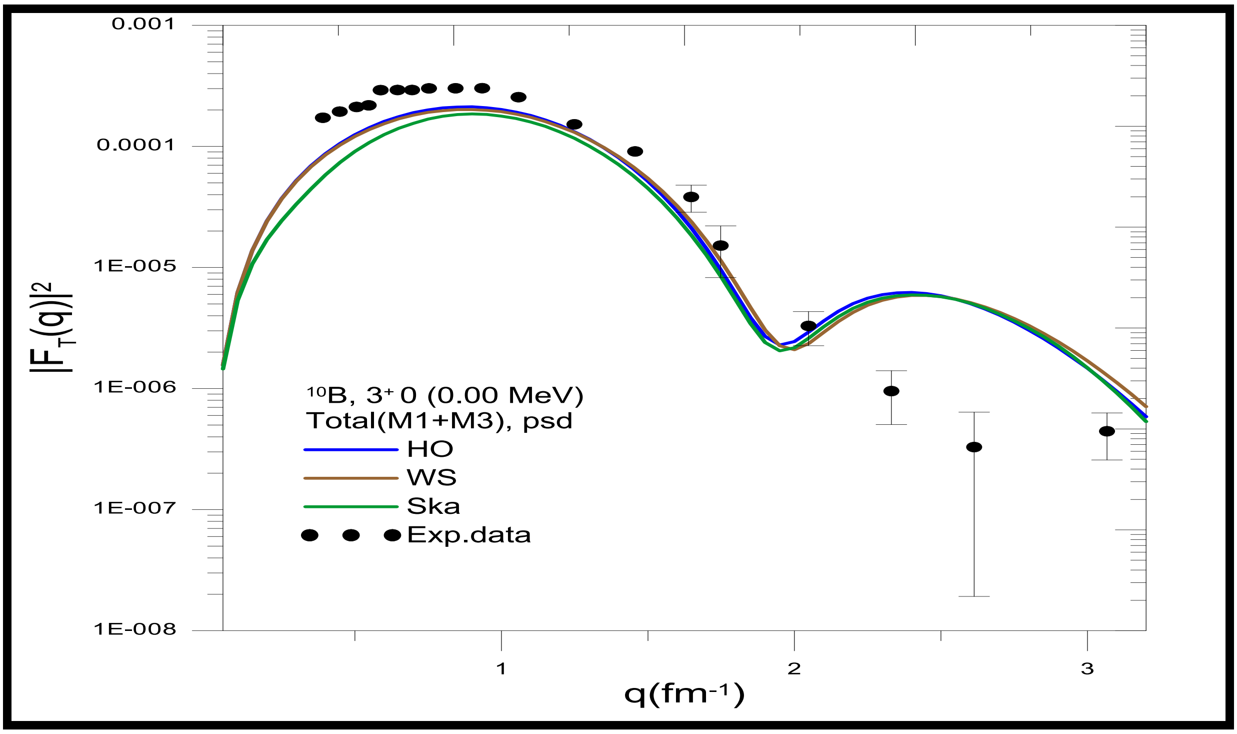


Fig. (3-21): The total transverse (M1+M3) form factors for the transition $3^+$ (0.00 MeV) state calculated using psd model space truncation at $4\hbar\omega$ for different potentials. The experimental data are taken from reference [22]

### 3.2.6 The Transverse Form Factors for (0, 1) State at (Ex=1.74 MeV)

The pure M3 of inelastic magnetic form factors of the $J^{\pi}T = 0^{+}\,1$ transition at $E_x = 1.74\ MeV$ states calculated using HO potential. The p-shell calculation results are compared with the large-basis psd and spsdpf models at (0+2) $\hbar\omega$ displayed in Figures (3-22). The calculation results give good agreement at first maximum then after that begins to deviate and show a decline in values in the second part.

The inelastic magnetic form factors for the M3 transition of the $J^{\pi}T = 0^{+}\,1$ at $E_x = 1.74\ MeV$ state were calculated using WS and Ska potentials shown in figures (3-23), and (3-24), respectively. The calculation results using psd model space truncation up to (0+2) $\hbar\omega$ give good agreement with the experimental data at lower values of momentum transfer q ≥ 2 $fm^{-1}$. Whereas, the calculation results are in falling below the experimental data at high momentum transfer. The consistency of the psd model space is seen to be good and shape agreement with experimental data, but the p and spsdpf models space are underestimated.The calculation form factors for all potential in this transition produced the same output shape. The One-Body Density Matrix element value values for this transition (M3) calculated using psd model space are shown in table (3.7).

Table (3.7): The calculated M3 transition OBDM element value for $J^{\pi}T = 0^{+}\,1$ $(E_x = 1.74\ MeV)$ in $^{10}$B nucleus.

| $^{10}$B | | M3 |
|---|---|---|
| $j_i$ | $j_f$ | OBDM ($\Delta$T=1) |
| $1p_{3/2}$ | $1p_{3/2}$ | -0.08321 |
| $1d_{5/2}$ | $1d_{5/2}$ | -0.0074 |
| $1d_{5/2}$ | $1d_{3/2}$ | -0.01568 |
| $1d_{5/2}$ | $2s_{1/2}$ | 0.00539 |
| $1d_{3/2}$ | $1d_{5/2}$ | 0.04903 |
| $1d_{3/2}$ | $1d_{3/2}$ | 0.24606 |
| $2s_{1/2}$ | $1d_{5/2}$ | -0.00831 |

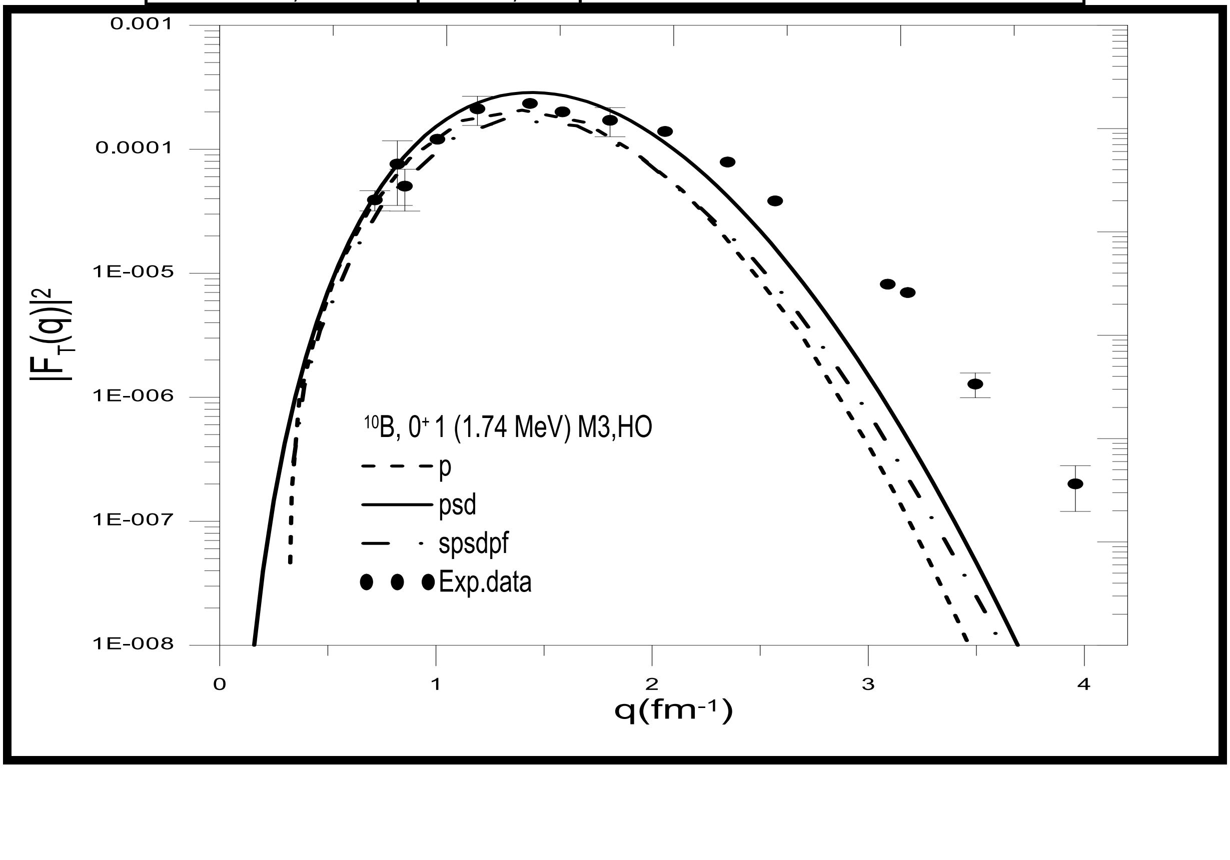

Fig. (3-22): The transverse inelastic (M3) form factors for the $0^+$ (1.74 MeV) state calculated using HO potential for different models space. The experimental data are taken from ref. [22]

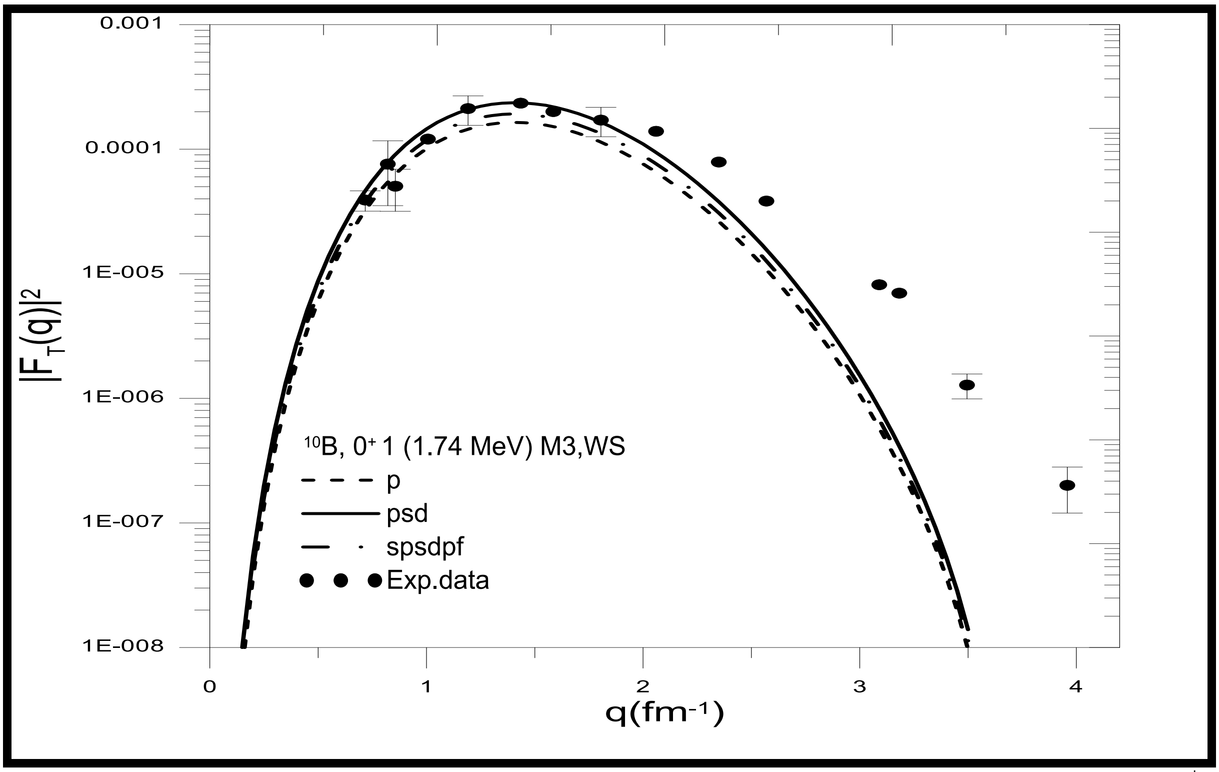


Fig. (3-23): The transverse inelastic (M3) form factors for the transition $0^+$ (1.74 MeV) state calculated using WS potential for different models space. The experimental data are taken from reference [23]

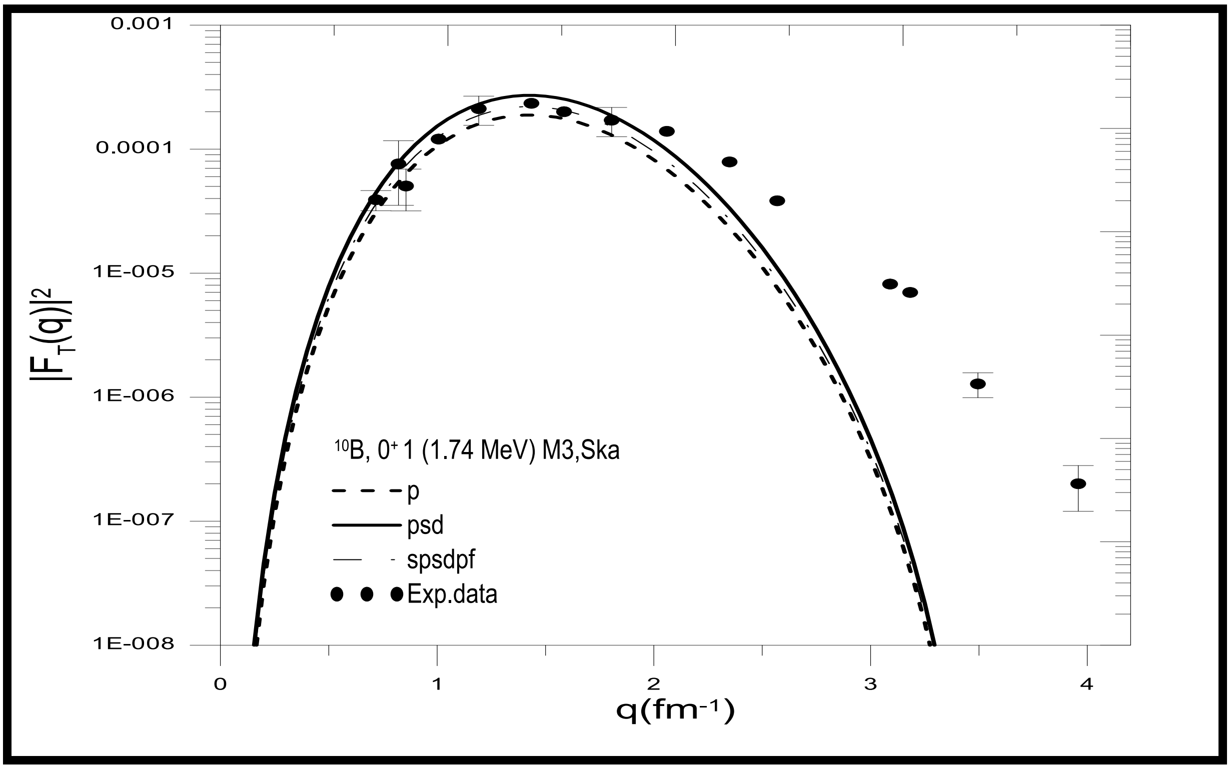

Fig. (3-24): The transverse inelastic (M3) form factors for the transition $0^+$ (1.74 MeV) state calculated using Ska potential for different models space. The experimental data are taken from reference [22]

### 3.2.7 The Transverse Form Factors for (3, 0) State at (Ex=0.00 MeV)

The transverse elastic form factor for the M1 transition of the $J^{\pi}T = 3^{+}\ 0$ in $^{10}B$ was calculated using the HO potential displayed in figure (3-25). The p-shell calculation results are compared with the large-basis psd and spsdpf truncation at $2\hbar\omega$ models. The calculating results very well at $q \geq 1\ fm^{-1}$ and the diffraction minimum is shifting to higher momentum transfer.

The transverse elastic form factor for M1 transition was calculated using WS and Ska potentials shown in Figures (3-26), and (3-27), respectively. The calculation results with default effective charge are done to produce an appropriate characterization of the experimental data for the momentum transfer region using models (p, psd, and spsdpf), especially at momentum transfer $q\ \leq\ 1.2\ fm^{-1}$. It is noticed HO potential results gave better results.

The psd model space truncation up to $2\hbar\omega$ calculation form factors using all potentials (HO, WS, and Ska) as shown in the figure (3-28). The calculation results using psd model space with default effective charge were close to the experimental data at overall momentum transfer regions.

The form factor was calculated for psd model space at $4\hbar\omega$ by using all potentials displayed in figure (3-29). The calculation results in some momentum transfer regions $q \leq 2\ fm^{-1}$ in qualitative agreement with the experimental data.

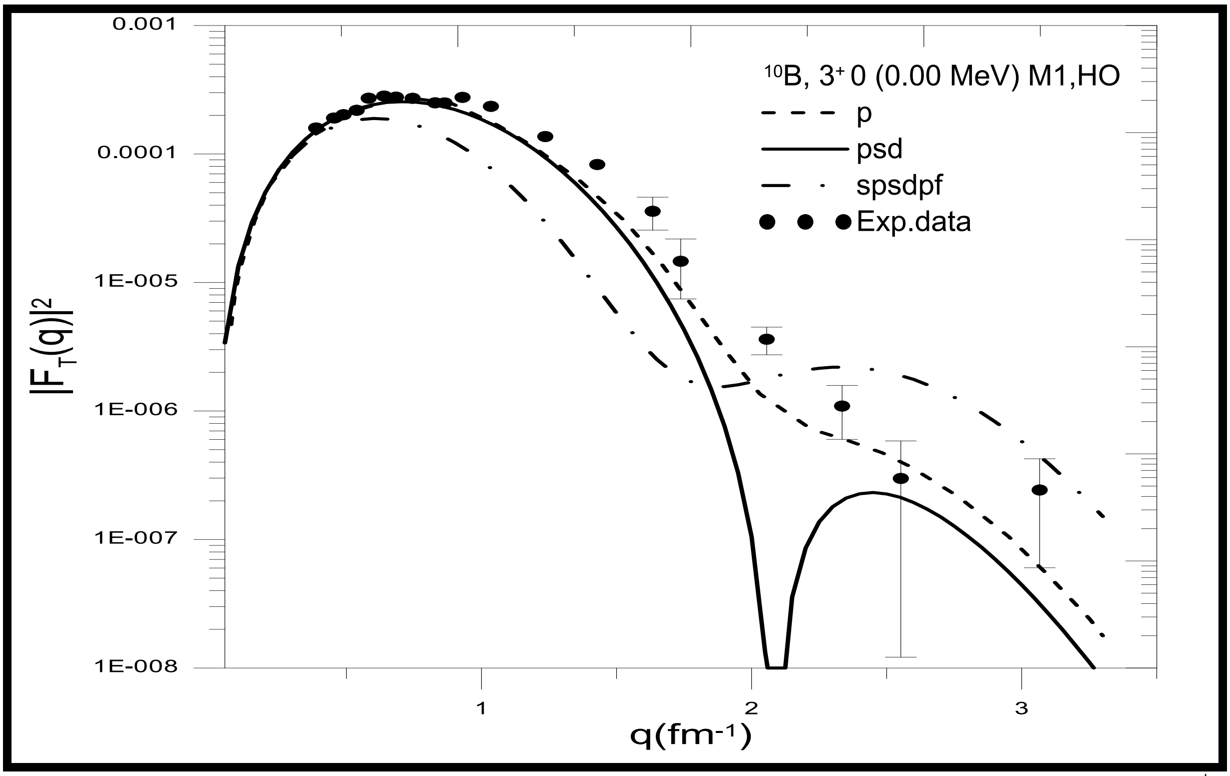


Fig. (3-25): The transverse elastic (M1) form factors for the transition to the $3^+$ (0.00 MeV) state calculated using HO potential for different models space. The experimental data are taken from reference [24]

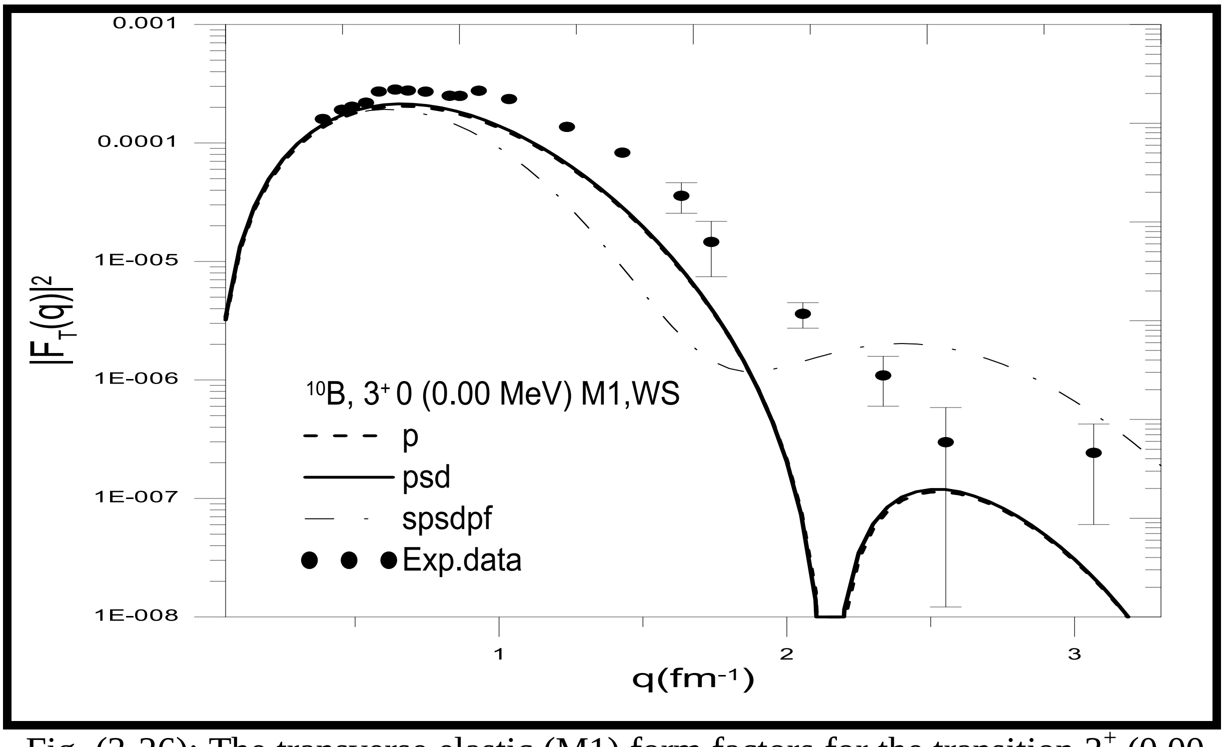


Fig. (3-26): The transverse elastic (M1) form factors for the transition $3^+$ (0.00 MeV) state calculated using WS potential for different models space. The experimental data are taken from reference [24]

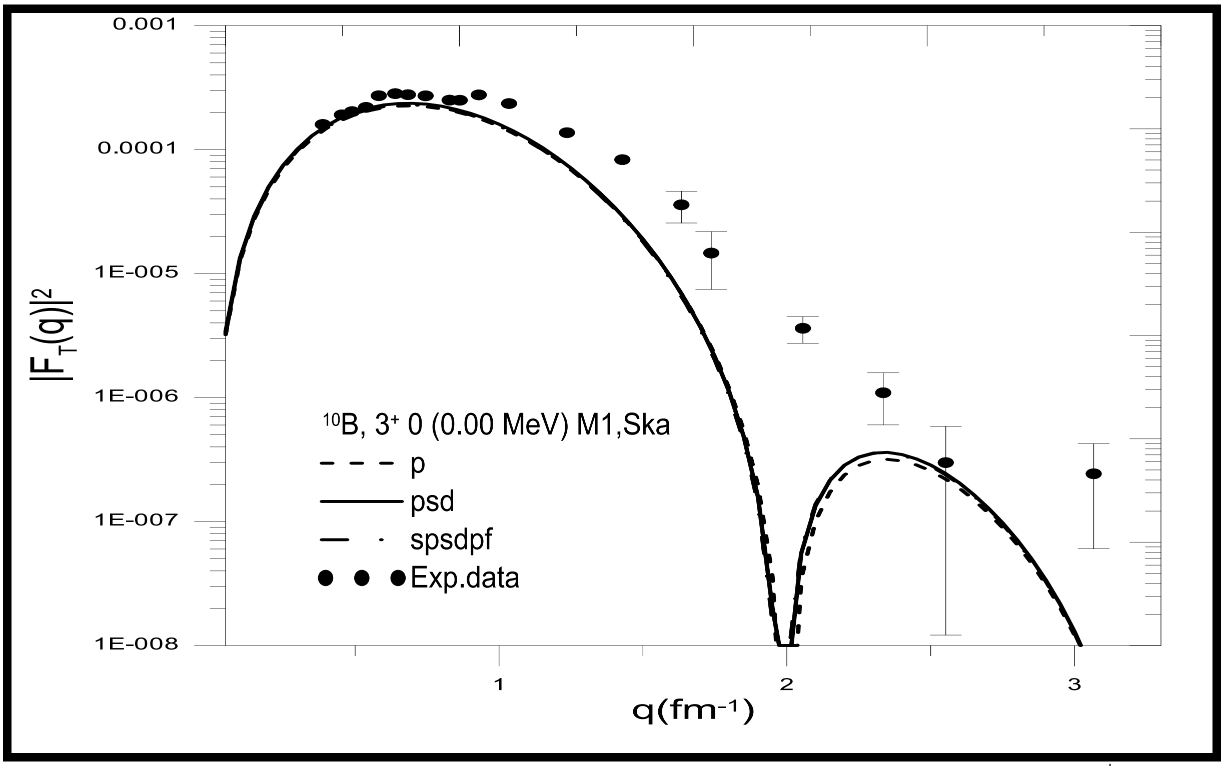


Fig. (3-27): The transverse elastic (M1) form factors for the transition $3^+$ (0.00 MeV) state calculated using Ska potential for different models space. The experimental data are taken from reference [24]

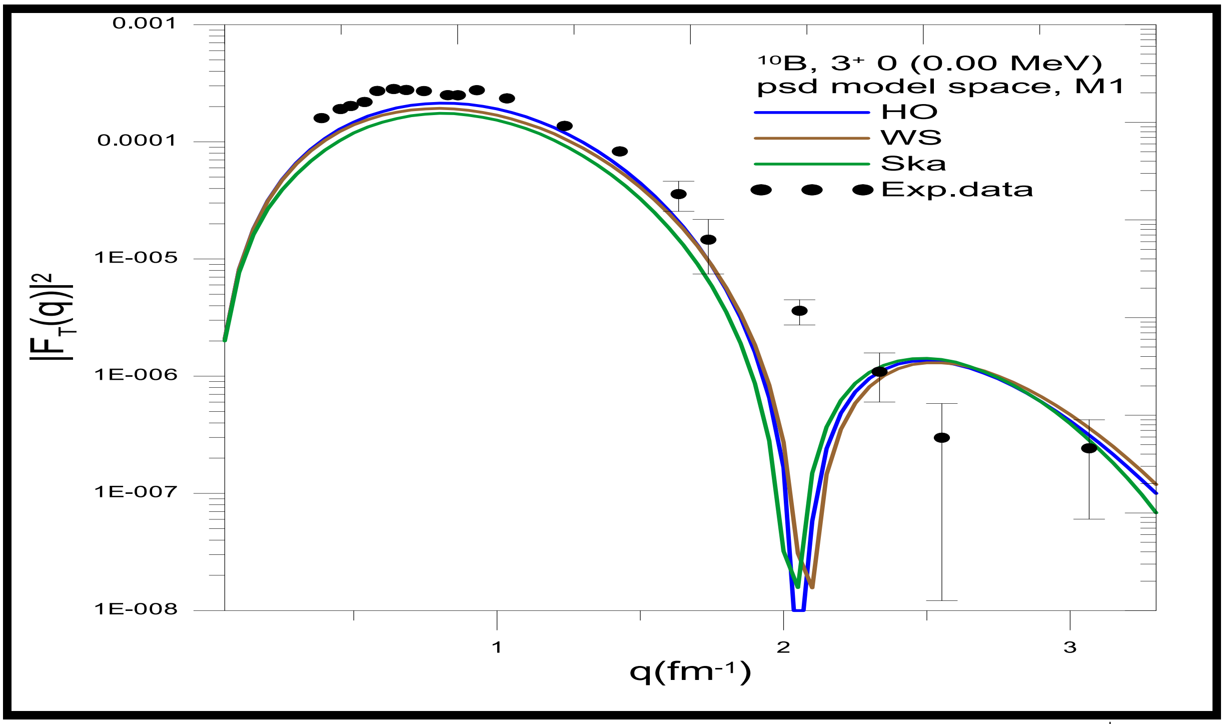


Fig. (3-28): The transverse elastic (M1) form factors for the transition $3^+$ (0.00 MeV) state calculated using psd model space truncation at $2\hbar\omega$ for different potentials. The experimental data are taken from reference [24]

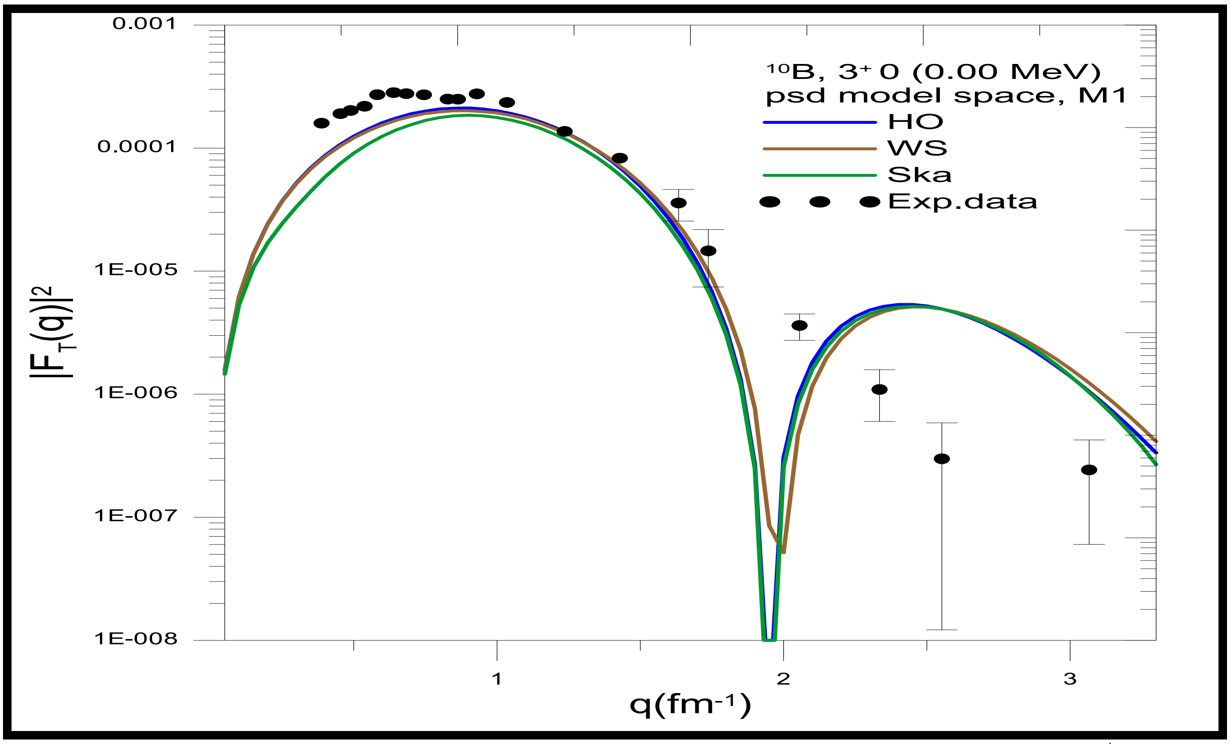


Fig. (3-29): The transverse elastic (M1) form factors for the transition $3^+$ (0.00 MeV) state calculated using psd model space truncation at $4\hbar$ for different potentials. The experimental data are taken from reference [24]

## 3.3 The Nucleus $^{12}C$

The longitudinal electron scattering form factors for the C2 transition from the ground state ($J^{\pi}\ T = 0^+\ 0$) to the ($J^{\pi}\ T = 2^+\ 0$) states at $E_x = 4.439\ MeV$ calculated by using (HO) potential is displayed in figure (3-30). The p-shell calculation results are compared with the large-basis psd and spsdpf models. The calculation form factors with p-shell model space give the best results for different potentials. Also, the same results were obtained when using WS and Ska potentials which are shown in figures (3-31), and (3-32) respectively. The One-Body Density Matrix element values for this transition C2 calculated using psd model space are shown in table (3.8).

Table (3.8): The calculated C2 transition OBDM element values for $J^{\pi}\ T = 2^{+}\ 0\ (E_x = 4.439\ MeV)$ in $^{12}$C nucleus.

| $^{10}$C | | C2 |
|---|---|---|
| $j_i$ | $j_f$ | OBDM (ΔT=0) |
| $1p_{3/2}$ | $1p_{3/2}$ | -0.80976 |
| $1p_{3/2}$ | $1p_{1/2}$ | -0.10946 |
| $1p_{1/2}$ | $1p_{3/2}$ | 0.00987 |
| $1d_{5/2}$ | $1d_{5/2}$ | 0.42198 |
| $1d_{5/2}$ | $1d_{3/2}$ | 0.00096 |
| $1d_{5/2}$ | $2s_{1/2}$ | -0.0655 |
| $1d_{3/2}$ | $1d_{5/2}$ | 0.04430 |
| $1d_{3/2}$ | $1d_{3/2}$ | 0.93215 |
| $1d_{3/2}$ | $2s_{1/2}$ | 0.00097 |
| $2s_{1/2}$ | $1d_{5/2}$ | 0.77510 |
| $2s_{1/2}$ | $1d_{3/2}$ | -0.00512 |

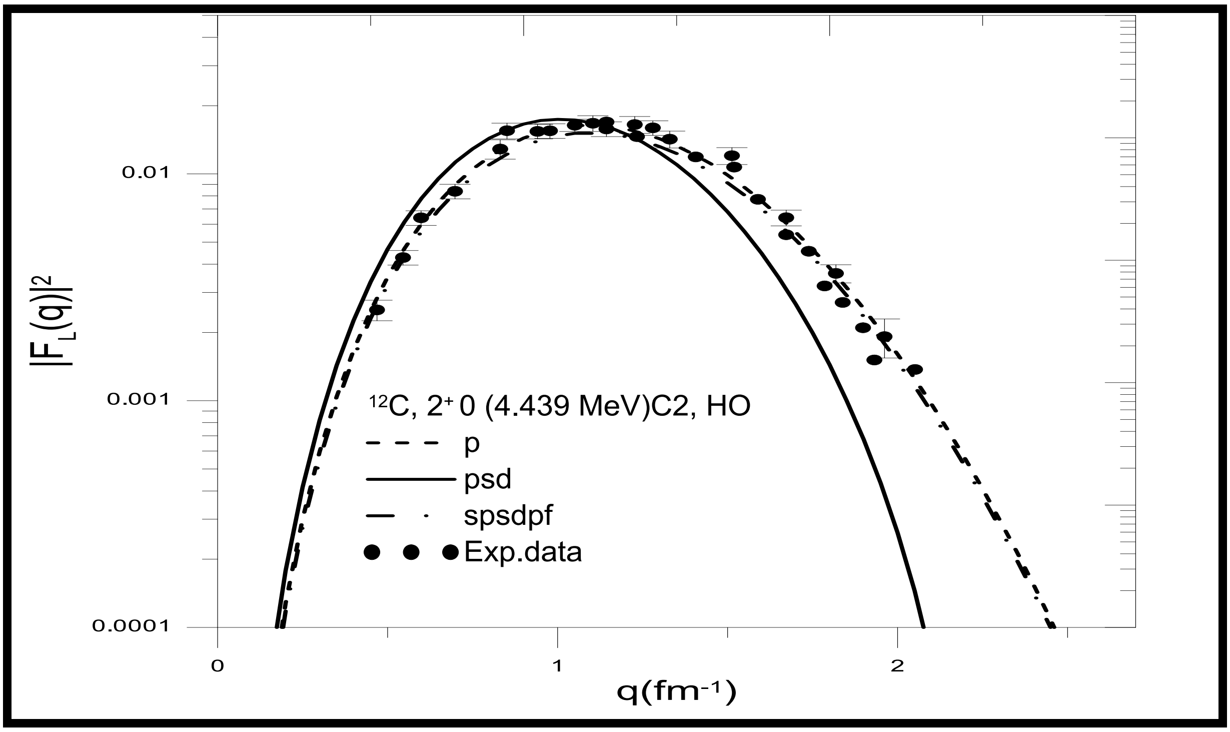


Fig. (3-30): The longitudinal inelastic (C2) form factors for the transition 2$^{+}$ (4.439 MeV) state calculated using HO potential for different models space. experimental data are taken from reference [15]

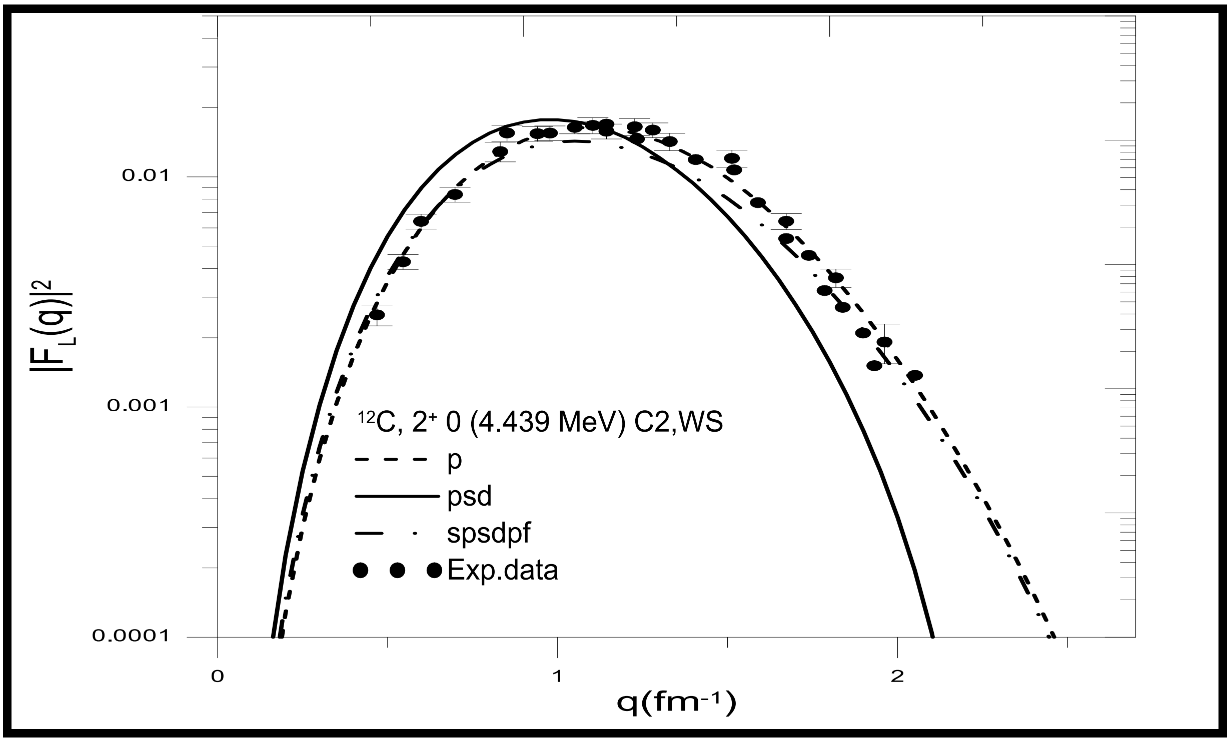


Fig. (3-31): The longitudinal inelastic (C2) form factors for the transition $2^+$ (4.439 MeV) calculated using WS potential for different models space. The experimental data are taken from reference [15]

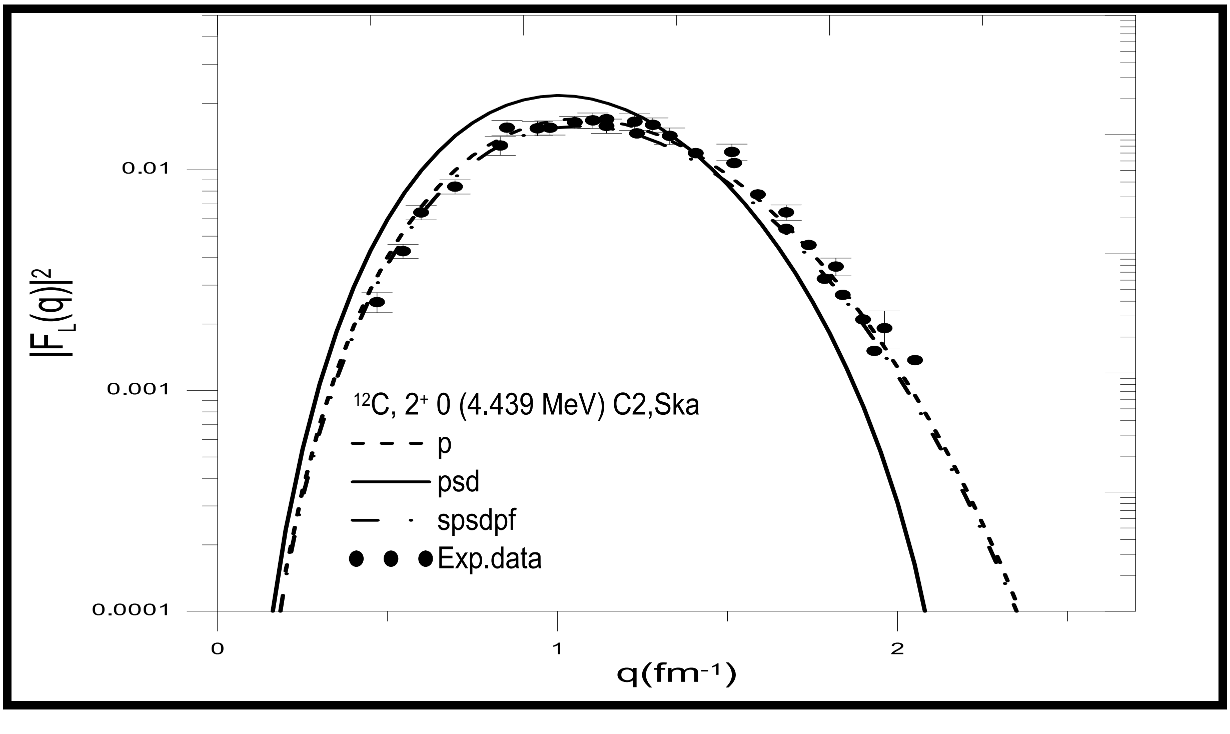


Fig. (3-32): The longitudinal inelastic (C2) form factors for the transition $2^+$ (4.439 MeV) state calculated using Ska potential for different models space. The experimental data are taken from reference [15]

## 3.4 The Nucleus $^{17}$O

The incident electron in this transition excited the $^{17}$O nucleus from the ground state $J^{\pi}\,T = 5/2^{+}\,1/2$ to the $1/2^{+}$ (0.870 $MeV$), $1/2^{+}$ (7.956 $MeV$), $7/2^{+}$ (7.576 $MeV$), $5/2^{+}$ (8.402 $MeV$), $5/2^{+}$ ( 6.862 $MeV$), $3/2^{+}$ (5.084$MeV$), $5/2^{+}$ (0.870 $MeV$) . Also, inelastic scattering is allowed for the transverse multiples M1, M3, and M5, and the longitudinal multipoles C0, C2, and C4. The calculations of these multipoles included using the zbme model space with the rewile interaction. In the zbme model space, the nucleons are distributed over the $1p_{1/2}$ $1d_{5/2}$. The oscillator length parameter was chosen $b = 1.76\ fm^{-1}$.

### 3.4.1 The Longitudinal Form Factors for ($1/2^{+}$,1/2) State at (0.870 MeV)

The inelastic longitudinal Coulomb C2 form factors for the $1/2^{+}$ state of the $^{17}$O at $E_x = 0.870\ MeV$ are calculated using zbme model space are plotted in figure (3-33). The calculation results using all potentials (HO, WS, Ska, and Bsk9 [52]) with default effective charge are in good agreement with the experimental data in all regions of momentum transfer. Also, it illustrates that the results are best by using potentials (ska and WS). The One-Body Density Matrix element values for this transition (C2) calculated using zbme model space are shown in table (3.9).

Table (3.9): The calculated C2 transition OBDM element values for $1/2^{+}$ ($E_x = 0.870\ MeV$) in $^{17}$O nucleus

| $^{17}$O | | C2 | |
|---|---|---|---|
| $j_i$ | $j_f$ | OBDM(T=0) | OBDM(T=1) |
| $1d_{5/2}$ | $1d_{5/2}$ | 0.06497 | -0.02773 |
| $1d_{5/2}$ | $2s_{1/2}$ | 0.00650 | -0.02564 |
| $2s_{1/2}$ | $1d_{5/2}$ | 0.96292 | 0.92851 |

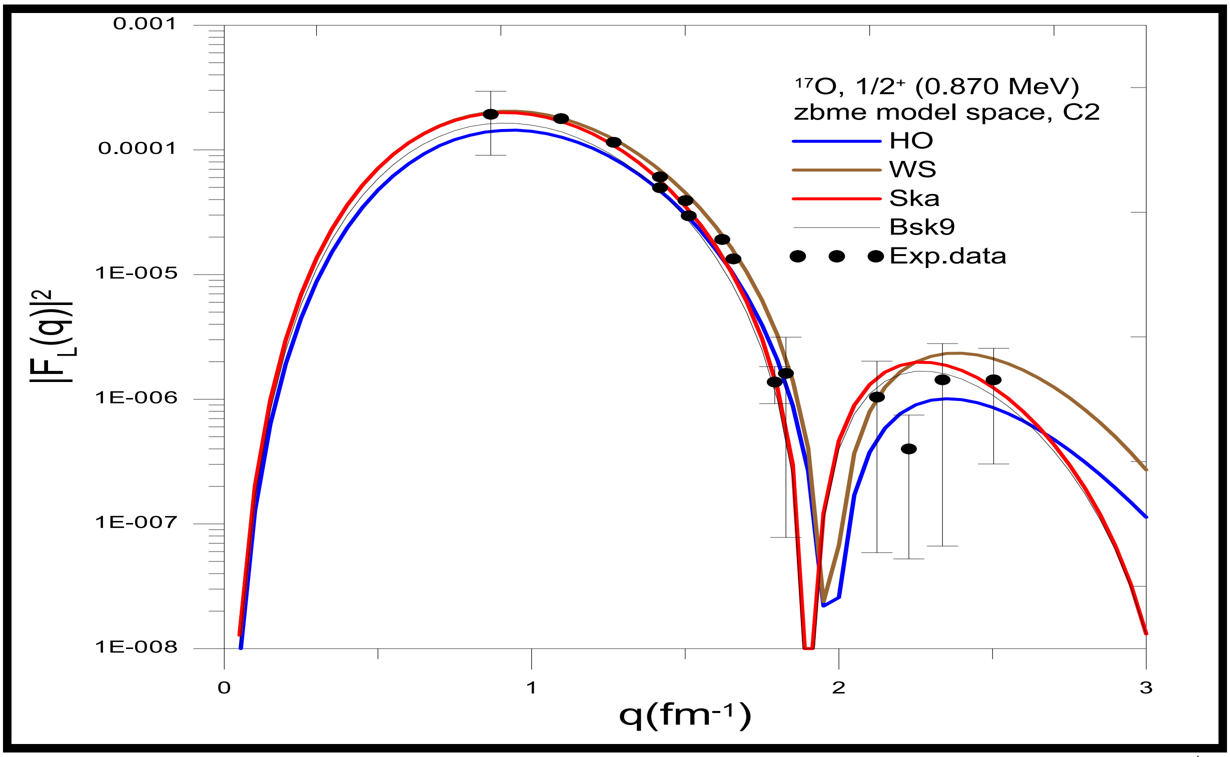


Fig. (3-33): The longitudinal inelastic (C2) form factors for the transition 1/2$^+$ (0.870 MeV) state calculated using zbme model space for different potentials. The experimental data are taken from reference [31]

### 3.4.2 The Longitudinal Form Factors for (1/2$^+$, 1/2) state at (7.956 MeV)

The longitudinal C2 form factors for the 1/2$^+$ state for the $^{17}$O at $E_x = 7.956\ MeV$ calculated using zbme model space are shown in figure (3-34). The form factors calculation results using HO, WS, Ska, and Bsk9 potentials with default effective charge a give good agreement at $q \le 1.8\ fm^{-1}$. And then show the minimum diffraction, and start deviating from the experimental data values. The calculation form factors for all potentials appear to be similar but the best of them is the Skyrme(ska) potentials. The One-Body Density Matrix element values for this transition (C2) calculated using zbme model space are shown in table (3.10).

Table (3.10) The calculated C2 transition OBDM element values for 1/2$^+$ ($E_x = 7.956\ MeV$ ) in $^{17}$O nucleus

| $^{17}$O | | C2 | |
|---|---|---|---|
| $j_i$ | $j_f$ | OBDM (ΔT=0) | OBDM (ΔT=1) |
| $1d_{5/2}$ | $1d_{5/2}$ | 0.07583 | -0.03093 |
| $1d_{5/2}$ | $2s_{1/2}$ | 0.00186 | -0.01712 |
| $2s_{1/2}$ | $1d_{5/2}$ | -0.05839 | -0.17391 |

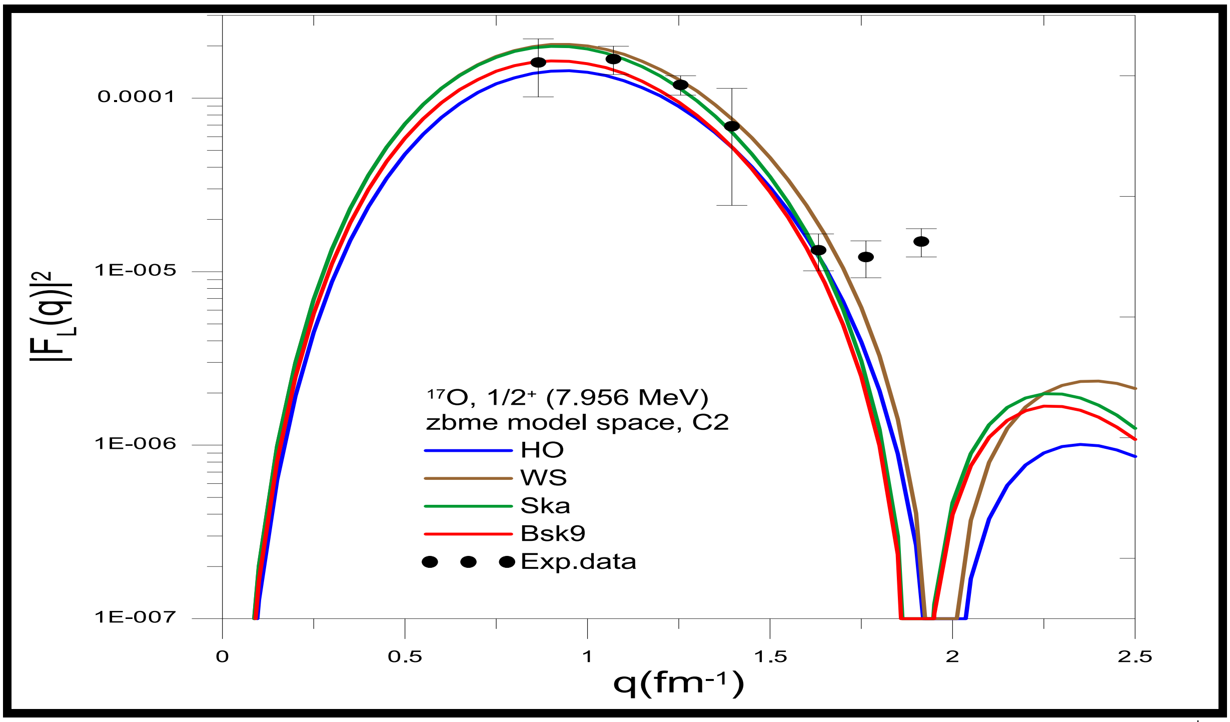


Fig. (3-34): The longitudinal inelastic (C2) form factors for the transition 1/2$^+$ (7.956 MeV) state calculated using zbme model space for different potentials. The experimental data are taken from reference [31]

### 3.4.3 The Longitudinal Form Factors for (7/2$^+$,1/2) State at (7.576 MeV)

Figure (3-35) shows the inelastic longitudinal C2 form factors for the 7/2$^+$ at $E_x = 7.576\ MeV$ calculated using the zbme model space for all potentials (HO, WS, Ska, Bsk9). The calculating results using the zbme model space with default effective charge using Skyrme (ska) potential exhibit qualitative similarity to the shape of the experimental data in$q \leq 1.6\ fm^{-1}$ and give the best result compared with another potential. The One-Body Density Matrix element values for this transition (C2) calculated using zbme model space are shown in table (3.11).

Table (3.11): The calculated C2 transition OBDM element values for $7/2^+$ $(E_x = 7.576\ MeV)$ in $^{17}O$ nucleus

| $^{17}$O | | C2 | |
|---|---|---|---|
| $j_i$ | $j_f$ | OBDM (ΔT=0) | OBDM (ΔT=1) |
| $1d_{5/2}$ | $1d_{5/2}$ | 0.09860 | -0.04386 |
| $1d_{5/2}$ | $2s_{1/2}$ | 0.15039 | 0.00790 |
| $2s_{1/2}$ | $1d_{5/2}$ | 0.38911 | 0.10313 |

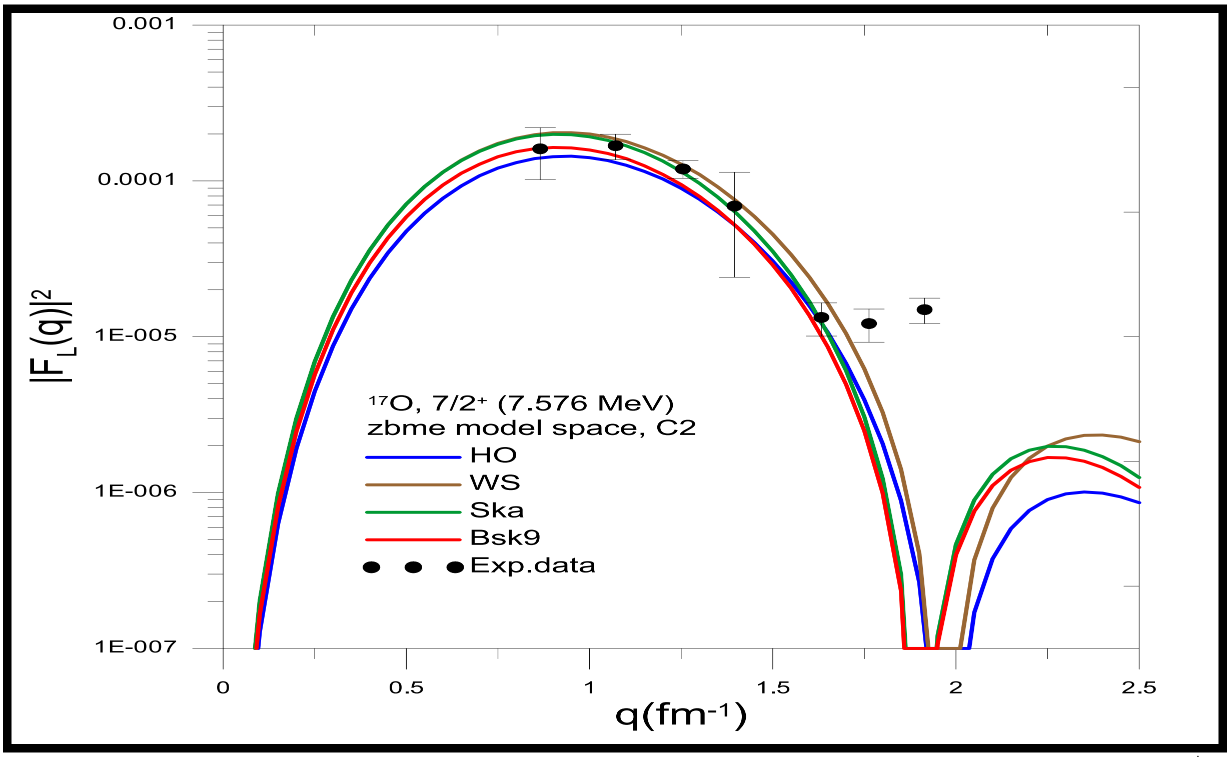


Fig. (3-35): The longitudinal inelastic (C2) form factors for the transition $7/2^+$ (7.576 MeV) state calculated using zbme model space for different potentials. The experimental data are taken from reference [31]

### 3.4.4. The Longitudinal Form Factors for ($5/2^+$, 1/2) State at (8.402 MeV)

The longitudinal C2 form factors were calculated using all potentials for the $5/2^+$ state (8.402 MeV) shown in figure (3-36). The calculation results using the zbme model space with an effective charge (0.8, 0.5) for proton and neutron respectively. In this transition, all potential give acceptable results compared with experimental data at $q \geq 1.5\ fm^{-1}$, then that falls off slightly less rapidly. The One-Body Density Matrix element values for this transition (C2) calculated using zbme model space are shown in table (3.12)

Table (3.12): The calculated C2 transition OBDM element values for $5/2^+$ $(E_x = 8.402\ MeV)$ in $^{17}O$ nucleus

| $^{17}O$ | | C2 | |
|---|---|---|---|
| $j_i$ | $j_f$ | OBDM (ΔT=0) | OBDM (ΔT=1) |
| $1d_{5/2}$ | $1d_{5/2}$ | -0.12890 | -0.06878 |
| $1d_{5/2}$ | $2s_{1/2}$ | -0.00304 | -0.00436 |
| $2s_{1/2}$ | $1d_{5/2}$ | -0.00890 | -0.02998 |

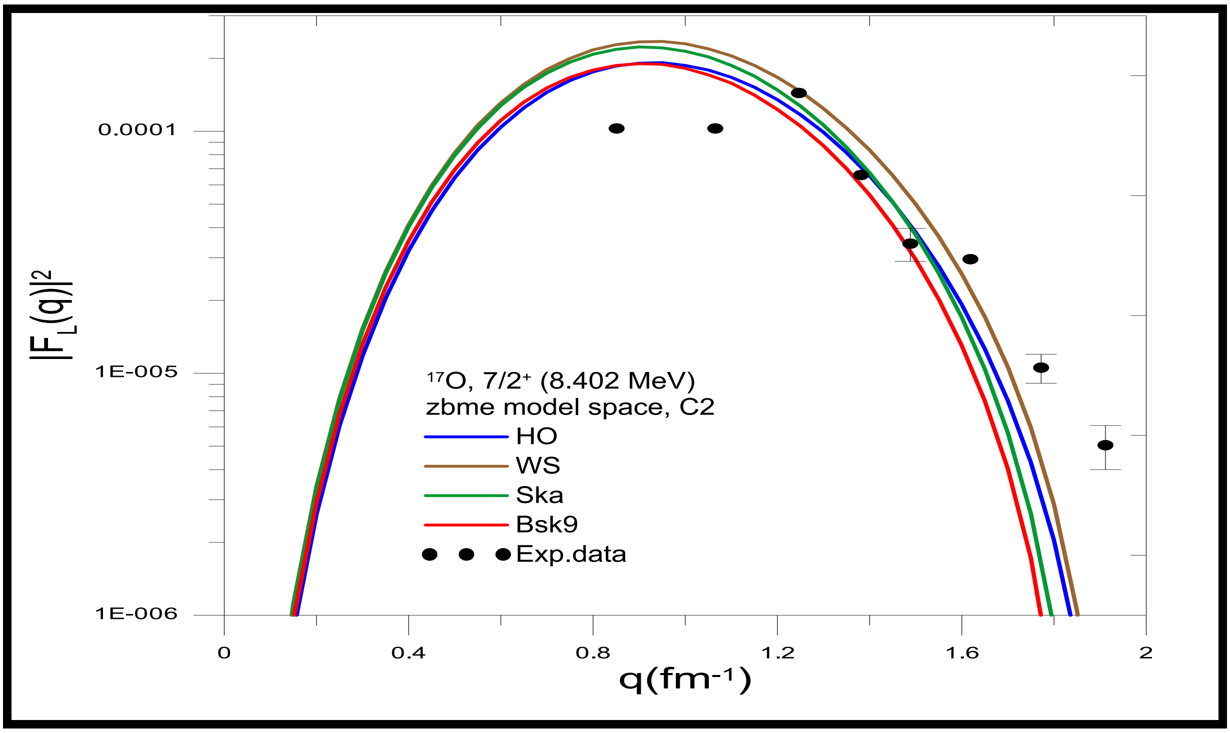


Fig. (3-36): The longitudinal inelastic (C2) form factor for the transition $5/2^+$ (8.402 MeV) state calculated using zbme model space for different potentials. The experimental data are taken from reference [31]

**3.4.5 The Longitudinal Form Factors for ($5/2^+$, 1/2) State at (6.862 MeV)**

The inelastic longitudinal C0 and C2 form factors calculated for the $5/2^+$ at 6.862 MeV state using HO potential is shown in figure (3-37). The total (C0+C2) form factors using zbme model space with an effective charge value equal to (2.1, 1.4) for proton and neutron respectively is produced in the shape and agree well of the experimental data form factors, especially at higher momentum transfer.

The total longitudinal (C0+C2) form factor and their individual contributions were calculated at 6.862 MeV for the $5/2^+$ state using WS potential with an effective charge value equal to (1.6, 0.8) for proton and neutron respectively, while with using Ska potential was effective charge value equal to (2.4, 1.4) for proton and neutron respectively are shown in figure (3-38), (3-39). Also, the effective charge value using Bsk9 potential is equal to (1.8, 0.8) for proton and neutron respectively as shown in figure (3-40). The calculated results using Skyrme (ska) potential with effective charge contribution are in good agreement with experimental data at $q \geq 1.4\ fm^{-1}$.

The zbme model calculation for the total longitudinal inelastic (C0+C2) form factors of the $5/2^+$ at $E_x = 6.862\ MeV$ state with effective charge shown in figure (3-41). The calculation results well agree and can produce the form factors that match the experimental data shape at high transfers momentum. The One-Body Density Matrix element values for this transition (C0 and C2) calculated using zbme model space are shown in tables (3.13), and (3.14).

Fig. (3.13): The calculated C0 transition OBDM element values for $5/2^+$ ($E_x = 6.862\ MeV$) in $^{17}O$ nucleus

| **$^{17}$O** | | **C0** | |
|---|---|---|---|
| $j_i$ | $j_f$ | **OBDM (ΔT=0)** | **OBDM (ΔT=1)** |
| $1p_{1/2}$ | $1p_{1/2}$ | **0.92040** | **0.06636** |
| $1d_{5/2}$ | $1d_{5/2}$ | **-0.33302** | **-0.03811** |
| $2s_{1/2}$ | $2s_{1/2}$ | **-0.34359** | **-0.0036** |

Table (3.14): The calculated C2 transition OBDM element values for $5/2^+$ $(E_x = 6.862\ MeV)$ in $^{17}$O nucleus

| $^{17}$O | | C2 | |
|---|---|---|---|
| $j_i$ | $j_f$ | **OBDM (ΔT=0)** | **OBDM (ΔT=1)** |
| $1d_{5/2}$ | $1d_{5/2}$ | **0.11178** | **0.09531** |
| $1d_{5/2}$ | $2s_{1/2}$ | **-0.01417** | **0.00192** |
| $2s_{1/2}$ | $1d_{5/2}$ | **-0.01951** | **0.00008** |

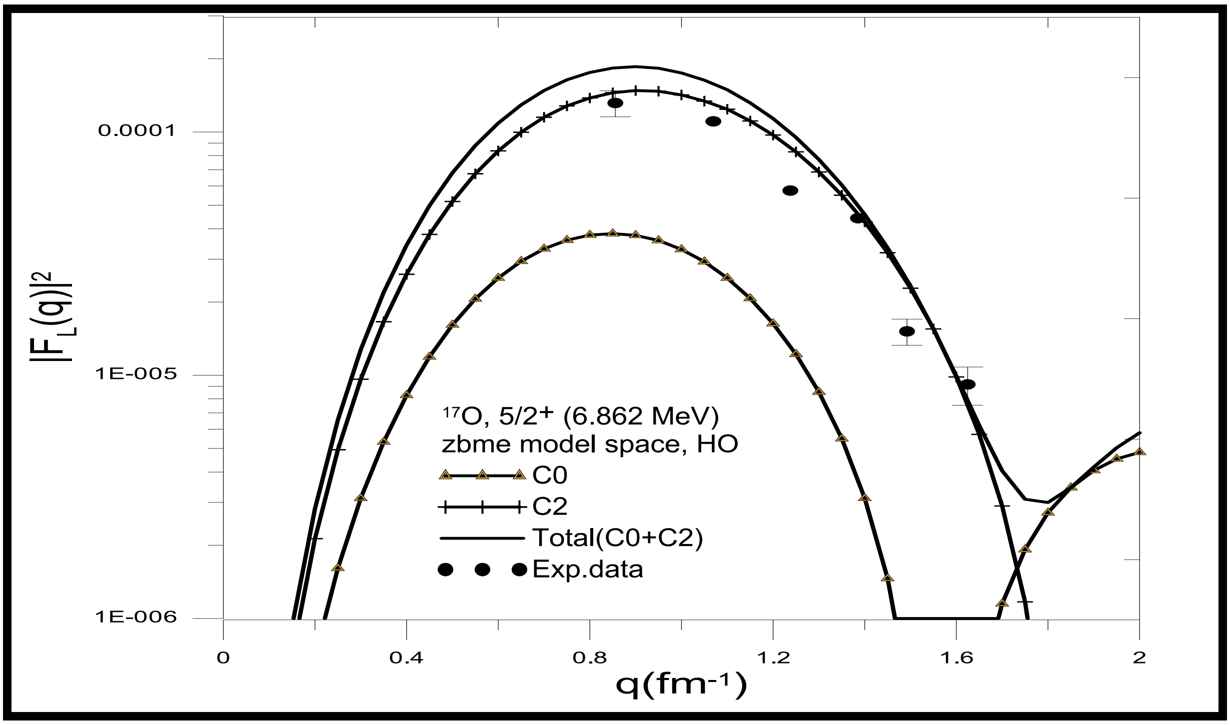


Fig. (3-37): The total longitudinal inelastic (C0+C2) form factors for the transition $5/2^+$ (6.862 MeV) state calculated using HO potential for zbme model space. The experimental data are taken from reference [31]

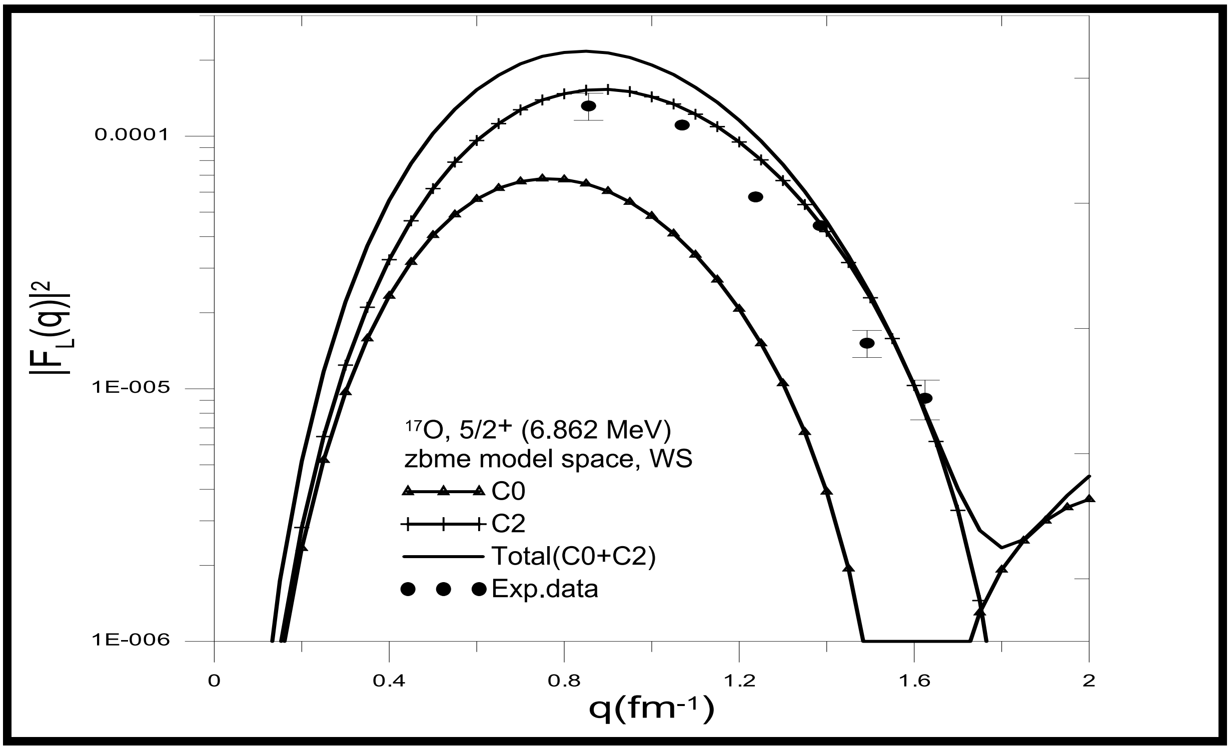


Fig. (3-38): The total longitudinal inelastic (C0+C2) form factors for the transition $5/2^+$ (6.862 MeV) state calculated using WS potential for zbme model space. The experimental data are taken from reference [31]

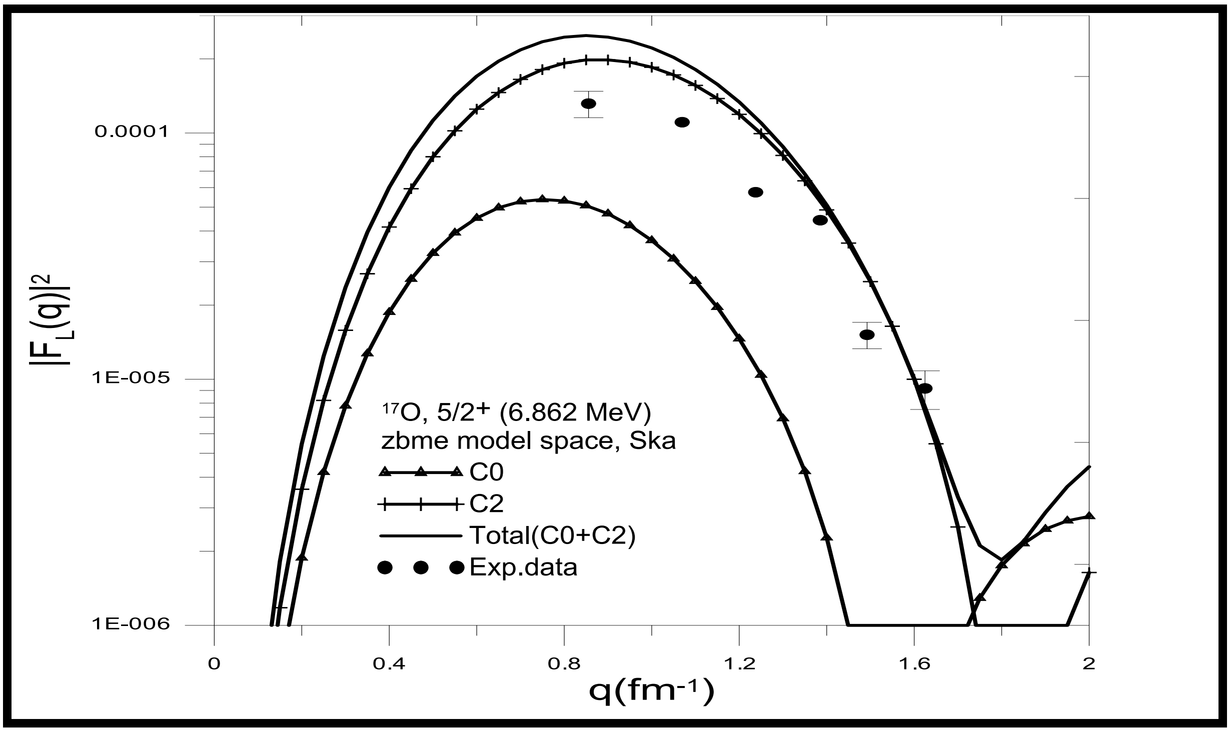


Fig. (3-39): The total longitudinal inelastic (C0+C2) form factors for the transition $5/2^+$ (6.862 MeV) state calculated using Ska potential for zbme model space. The experimental data are taken from reference [31]

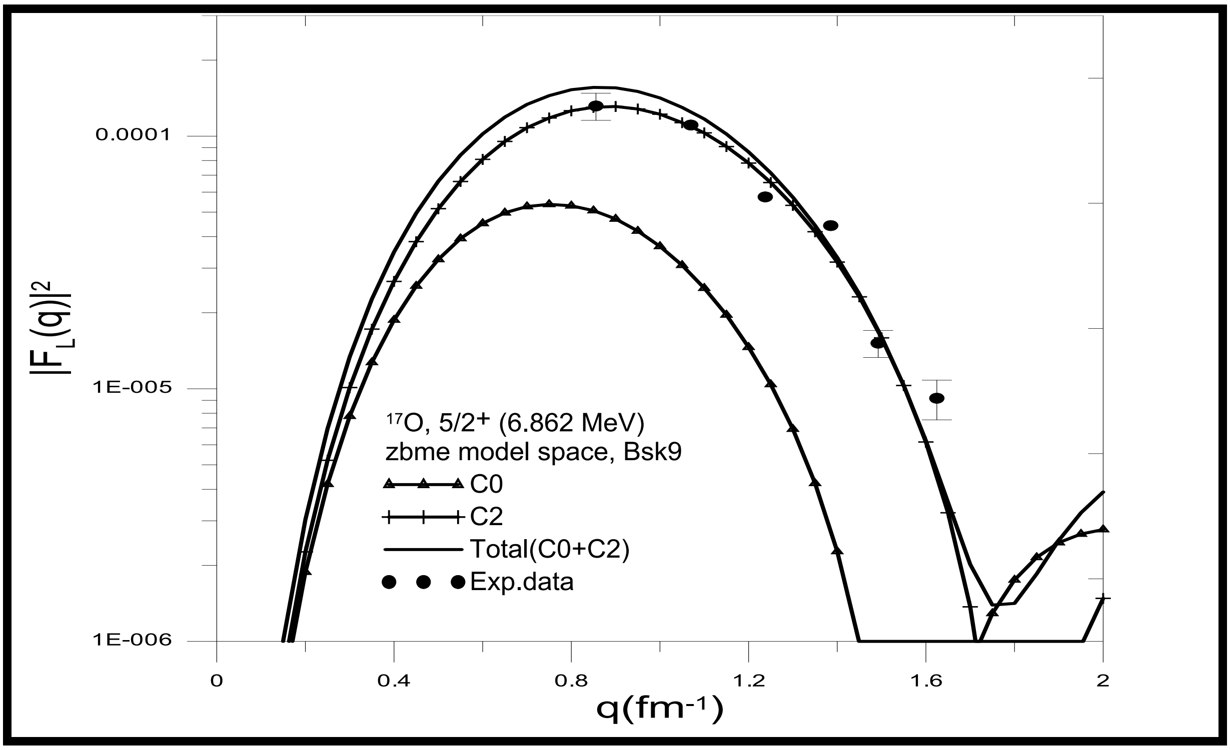


Fig. (3-40): The total longitudinal inelastic (C0+C2) form factors for the transition $5/2^+$ (6.862 MeV) state calculated using Bsk9 potential for zbme model space. The experimental data are taken from reference [31]

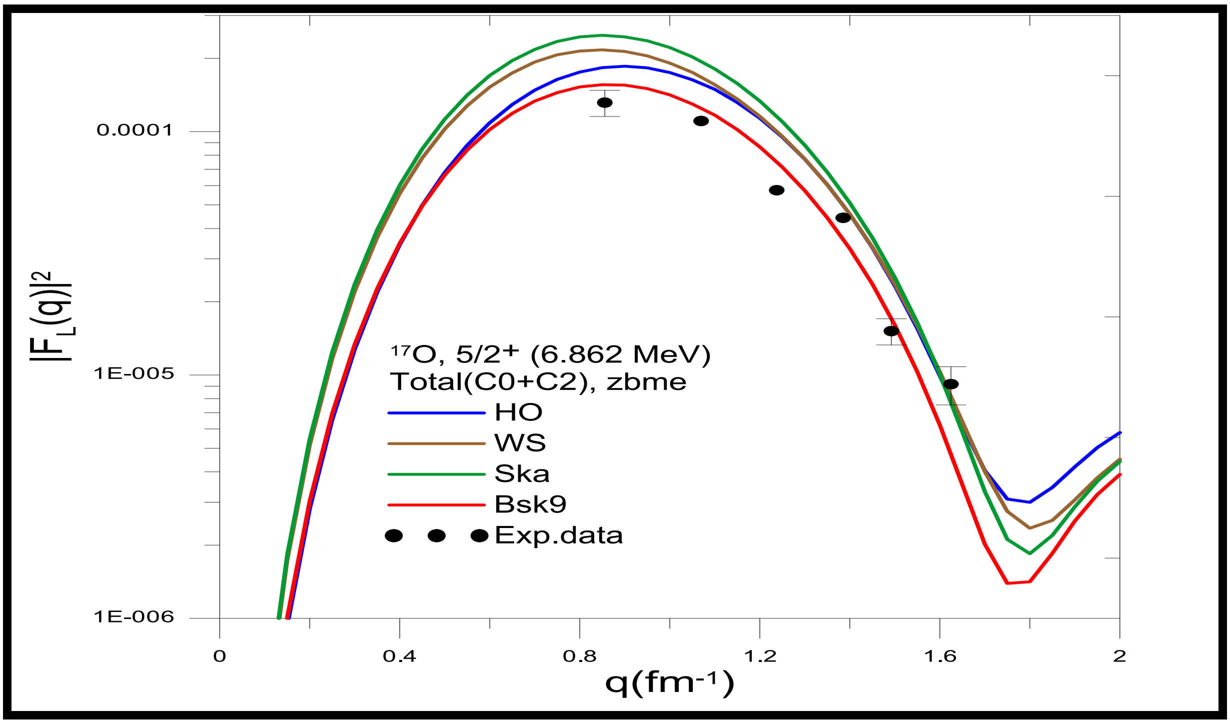


Fig. (3-41): The total longitudinal inelastic (C0+C2) form factors for the transition $5/2^+$ (6.862 MeV) state calculated using zbme model space for different potentials. The experimental data are taken from reference [31]

### 3.4.6 The Longitudinal Form Factors for ($3/2^+$, 1/2) State at (5.084 MeV)

The total longitudinal (C2+C4) and their individual contributions form factors calculated for the $3/2^+$ at $E_x = 5.084\ MeV$ state using HO, WS, and Ska potentials with default effective charge are shown in figures (3-42), (3-43), and (3-44) respectively. All results in figures for this state using zbme model space are in good agreement with the experimental data in $q \leq 1.7\ fm^{-1}$, but the best one is the Skyrme (Bsk9) potential. The One-Body Density Matrix element values for this transfer (C2 and C4) calculated using zbme model space are shown in tables (3.15), and (3.16).

Table (3.15): The calculated C2 transition OBDM element value for $3/2^+$ ($E_x = 5.084\ MeV$) in $^{17}O$ nucleus

| $^{17}$O | | C2 | |
|---|---|---|---|
| $j_i$ | $j_f$ | OBDM (ΔT=0) | OBDM (ΔT=1) |
| $1d_{5/2}$ | $1d_{5/2}$ | 0.96321 | 0.96321 |
| $1d_{5/2}$ | $2s_{1/2}$ | 0.01710 | 0.01710 |
| $2s_{1/2}$ | $1d_{5/2}$ | 0.10432 | 0.10432 |

Table (3.16): The calculated C4 transition OBDM element value for $3/2^+$ ($E_x = 5.084\ MeV$) in $^{17}O$ nucleus

| $^{17}$O | | C4 | |
|---|---|---|---|
| $j_i$ | $j_f$ | OBDM (ΔT=0) | OBDM (ΔT=1) |
| $1d_{5/2}$ | $1d_{5/2}$ | -0.08321 | 0.01704 |

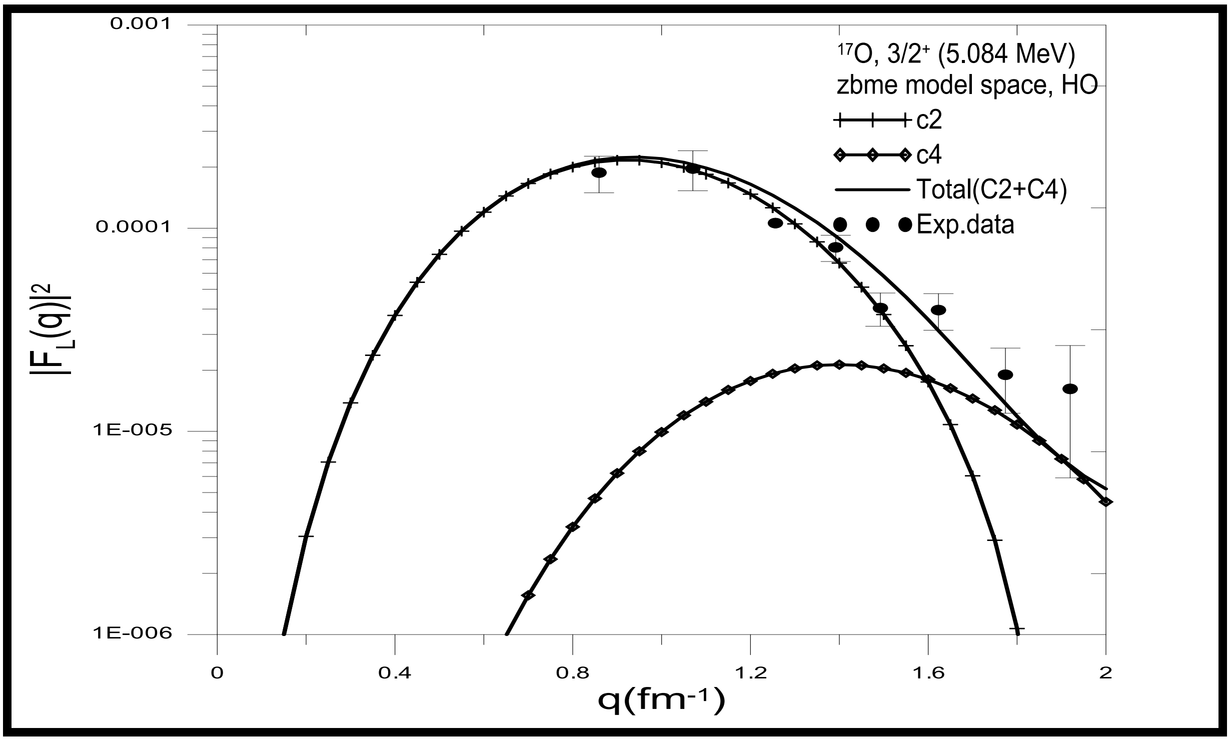


Fig. (3-42): The total longitudinal inelastic (C2+C4) form factors for the transition $3/2^+$ (5.084 MeV) state calculated using HO potential for zbme model space. The experimental data are taken from reference [31]

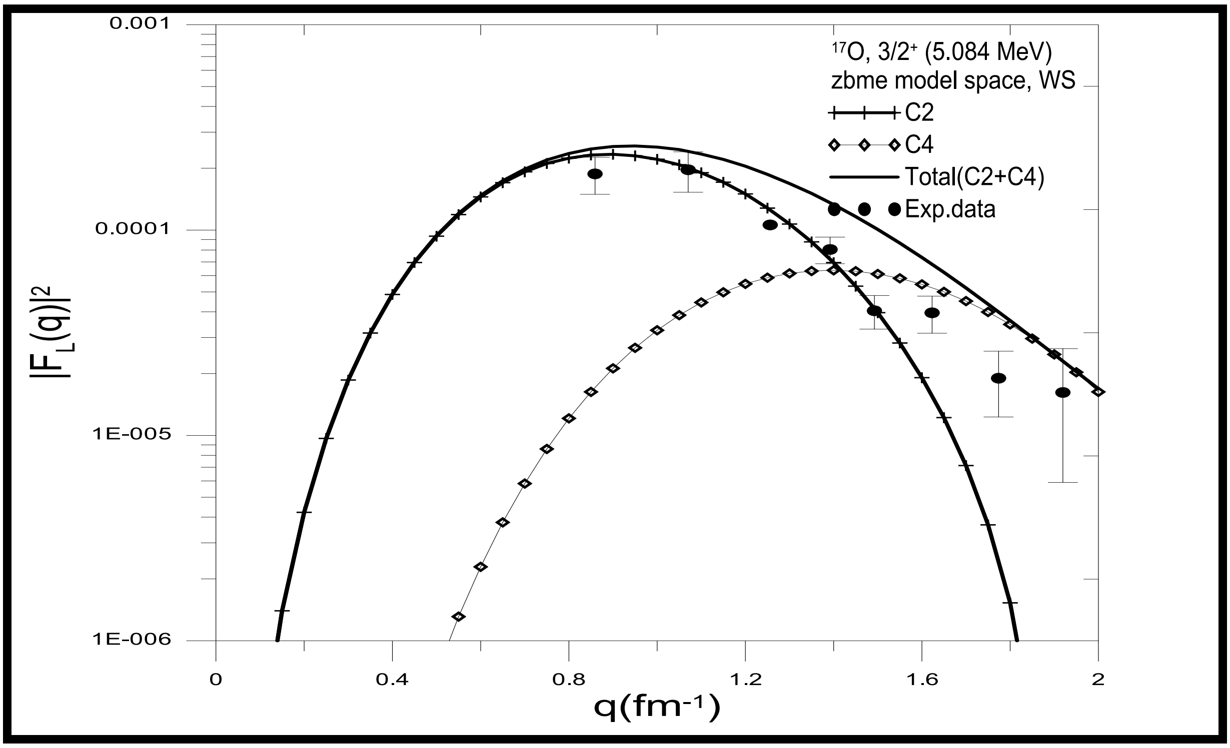


Fig. (3-43): The total longitudinal inelastic (C2+C4) form factors for the transition $3/2^+$ (5.084 MeV) state calculated using WS potential for zbme model space. The experimental data are taken from reference [31]

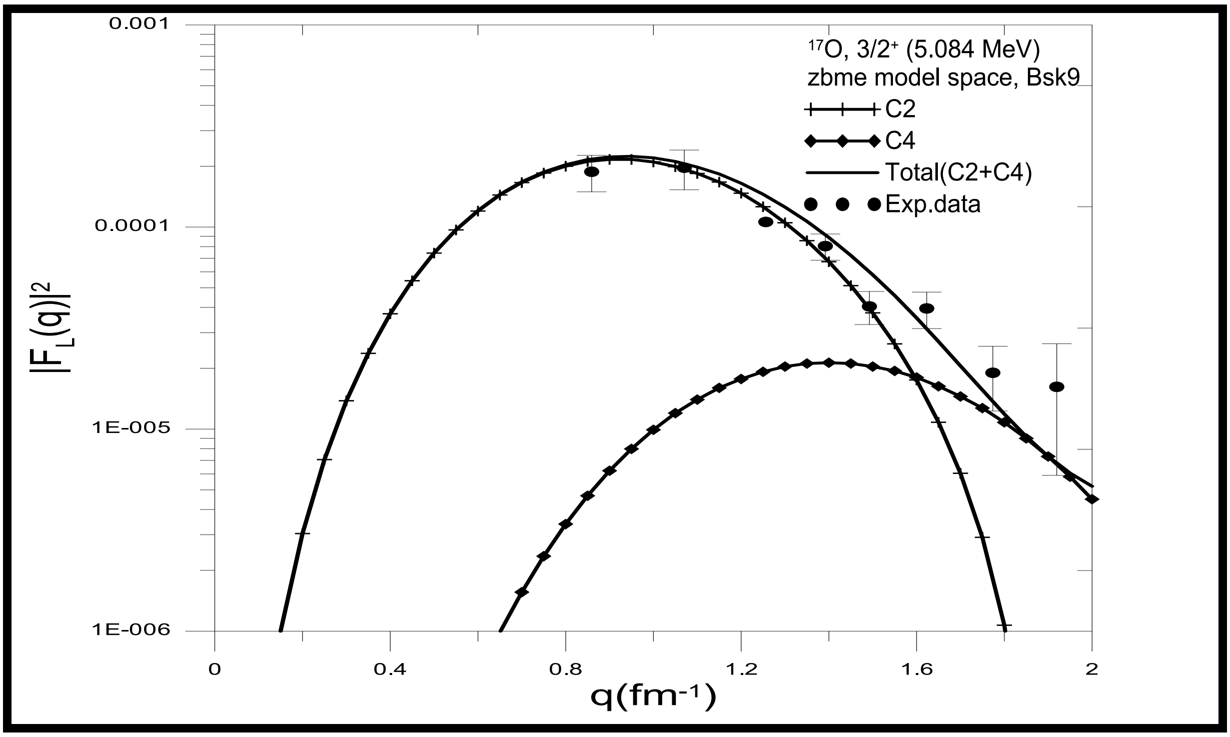


Fig. (3-44): The total longitudinal inelastic (C2+C4) form factors for the transition $3/2^+$ (5.084 MeV) state calculated using Bsk9 potentials for zbme model space. The experimental data are taken from reference [31]

### 3.4.7 The Transverse Form Factors for ($1/2^+$, 1/2) State at (0.870 MeV)

The inelastic transverse (M3) form factors for the transition $1/2^+$ ($E_x = 0.870\ MeV$) the state was calculated using HO, WS, Ska, and Bsk9 potentials with default effective charge as shown in figure (3-45). The results using zbme model space calculation using Skyrme (ska) potential give good agreement with experimental data at lower values of momentum transfer $q \leq 1.5\ fm^{-1}$, after which the calculation results are less than the value of the experimental data at higher values of momentum transfer. The One-Body Density Matrix element values for this transition (M3) calculated using zbme model space are shown in table (3.17)

Table (3.17): The calculated M3 transition OBDM element values for $1/2^+$ ($E_x = 0.870\ MeV$) in $^{17}O$ nucleus

| $^{17}$O | | M3 | |
|---|---|---|---|
| $j_i$ | $j_f$ | OBDM (ΔT=0) | OBDM (ΔT=1) |
| $1d_{5/2}$ | $1d_{5/2}$ | 0.00291 | -0.02189 |
| $1d_{5/2}$ | $2s_{1/2}$ | 0.04098 | -0.00313 |
| $2s_{1/2}$ | $1d_{5/2}$ | 0.92791 | 0.93939 |

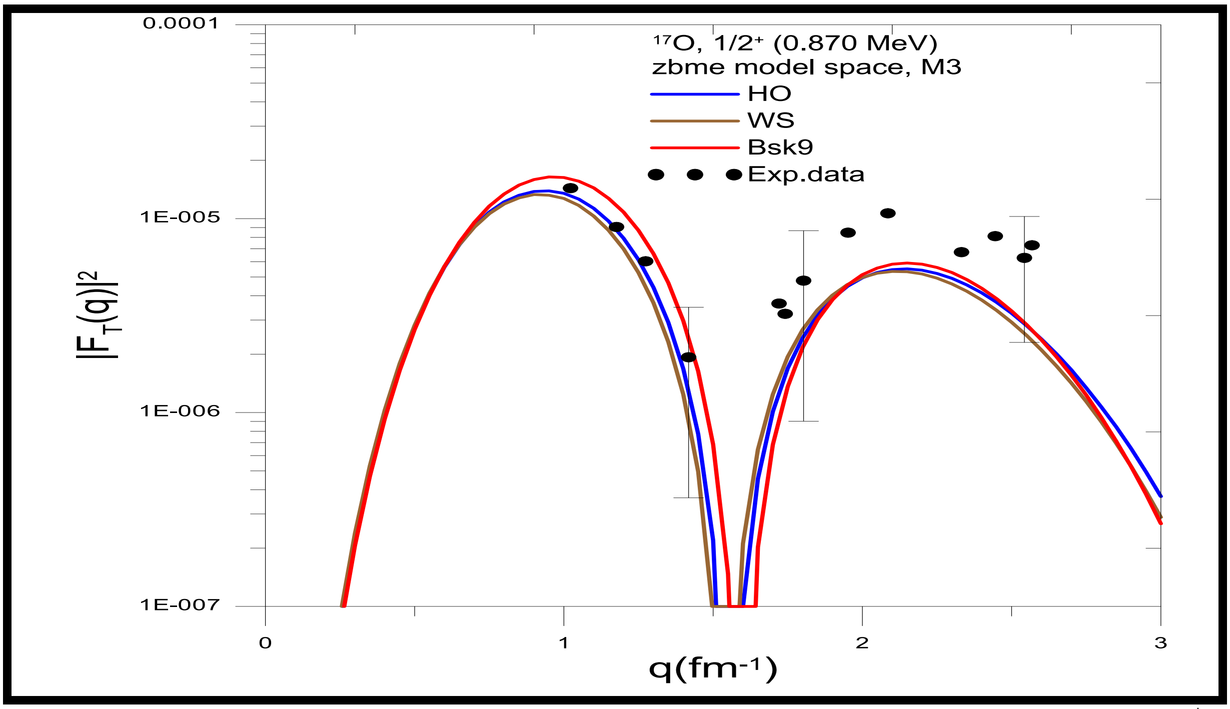


Fig. (3-45): The transverse inelastic (M3) form factors for the transition 1/2$^+$ (0.870 MeV) state calculated using zbme model space for different potentials. The experimental data are taken from reference [31]

### 3.4.8 The Transverse Form Factors for (1/2$^+$, 1/2) State at (0.870 MeV)

The M3 and E2 (dash-dash-dotted line) multipoles contribution form factors for the transition 1/2$^+$ at $E_x = 0.870\ MeV$ state calculated using HO potential are shown in figure (3-46). The results calculation using zbme model space gives good agreement with experimental data overall momentum transfer regions.

The total transverse inelastic (M3+ E2) and their individual contributions form factors for the transition 1/2$^+$ at $E_x = 0.870\ MeV$ was calculated using WS and Bsk9 potentials displayed in figures (3-47), and (3-48) respectively. The results of the calculations using of zbme model space with default effective charge agree well with experimental data at $q \geq 1.3\ fm^{-1}$.

The total transverse inelastic (M3+ E2) form factors $1/2^{+}$ were calculated at $E_x = 0.870\ MeV$ state using HO, WS, and Bsk9 potentials displayed in figure (3-49). The calculating results using zbme model space using WS potential give remarkable agreement with experimental data. The One-Body Density Matrix element values for this transition (E2) calculated using zbme model space are shown in table (3.18).

Table (3.18): The calculated E2 transition OBDM element values for $1/2^{+}$ ($E_x = 0.870\ MeV$) in $^{17}O$ nucleus

| $^{17}$O | | E2 | |
|---|---|---|---|
| $j_i$ | $j_f$ | OBDM (ΔT=0) | OBDM (ΔT=1) |
| $1d_{5/2}$ | $1d_{5/2}$ | 0.06497 | -0.02773 |
| $1d_{5/2}$ | $2s_{1/2}$ | 0.00650 | -0.02564 |
| $2s_{1/2}$ | $1d_{5/2}$ | 0.96292 | 0.92851 |

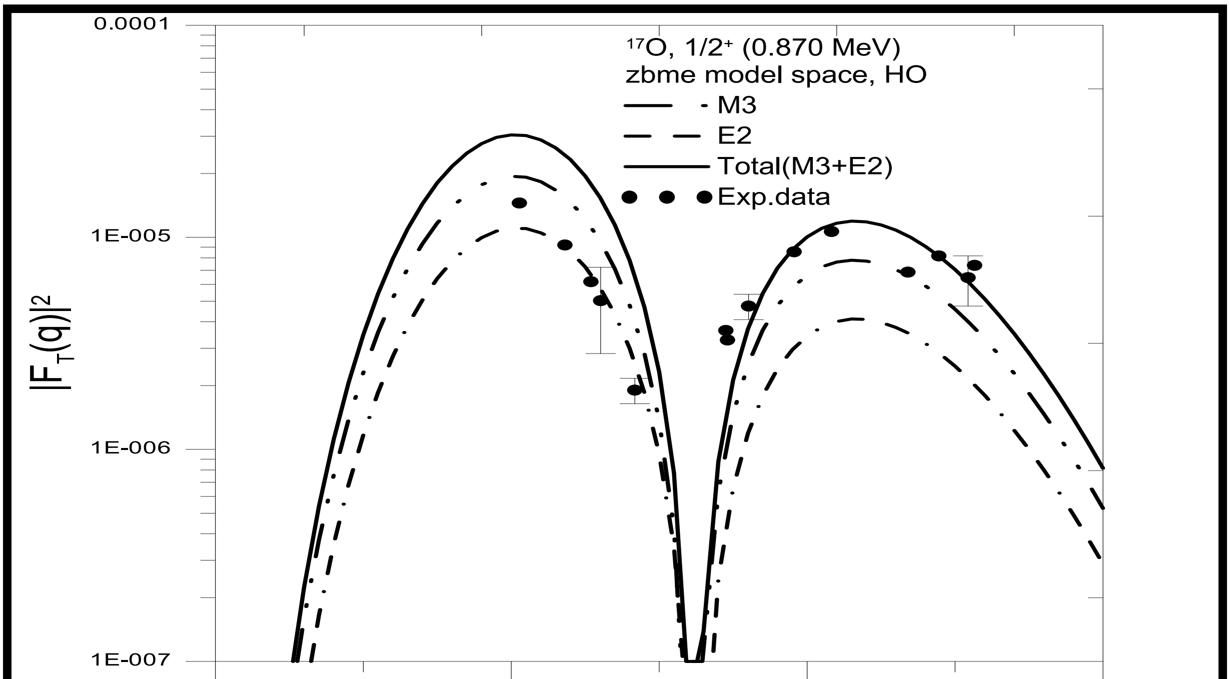

Fig. (3-46): The total transverse inelastic (M3+E2) form factors for the transition 1/2+ (0.870 MeV) state calculated using HO potential for zbme model space. The experimental data are taken from reference [31]

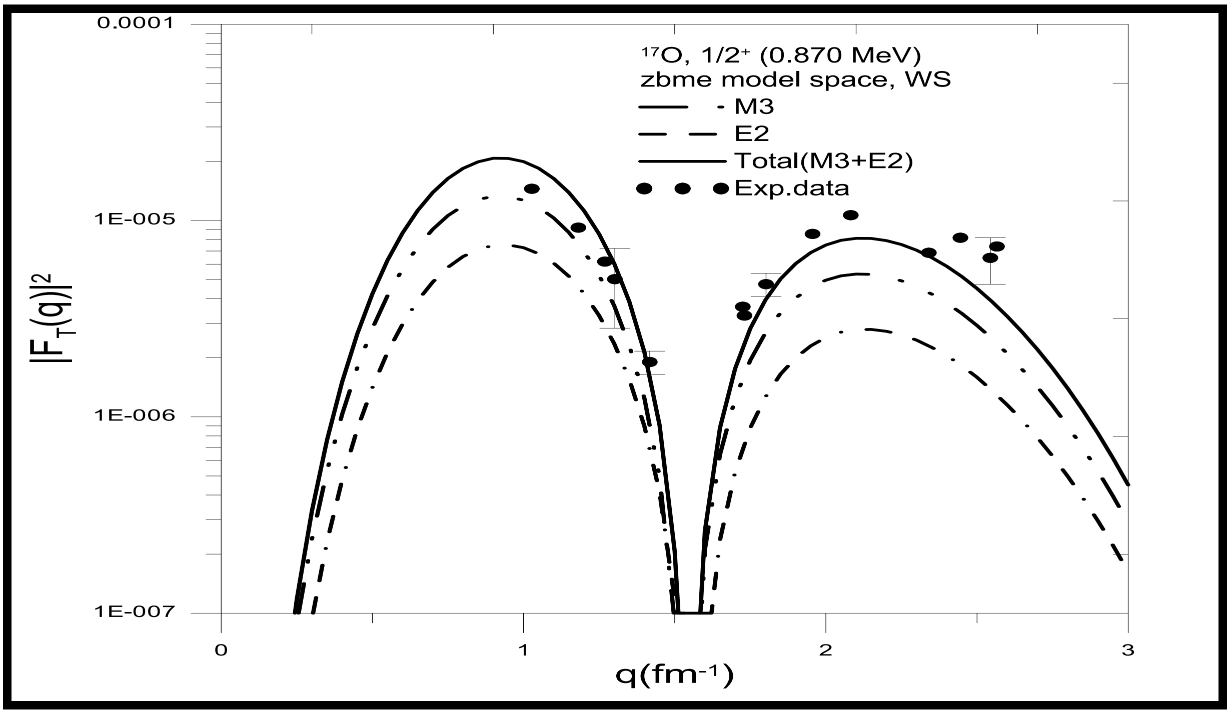


Fig. (3-47): The total transverse inelastic (M3+E2) form factors for the transition 1/2+ (0.870 MeV) state calculated using WS potential for zbme model space. The experimental data are taken from reference [31]

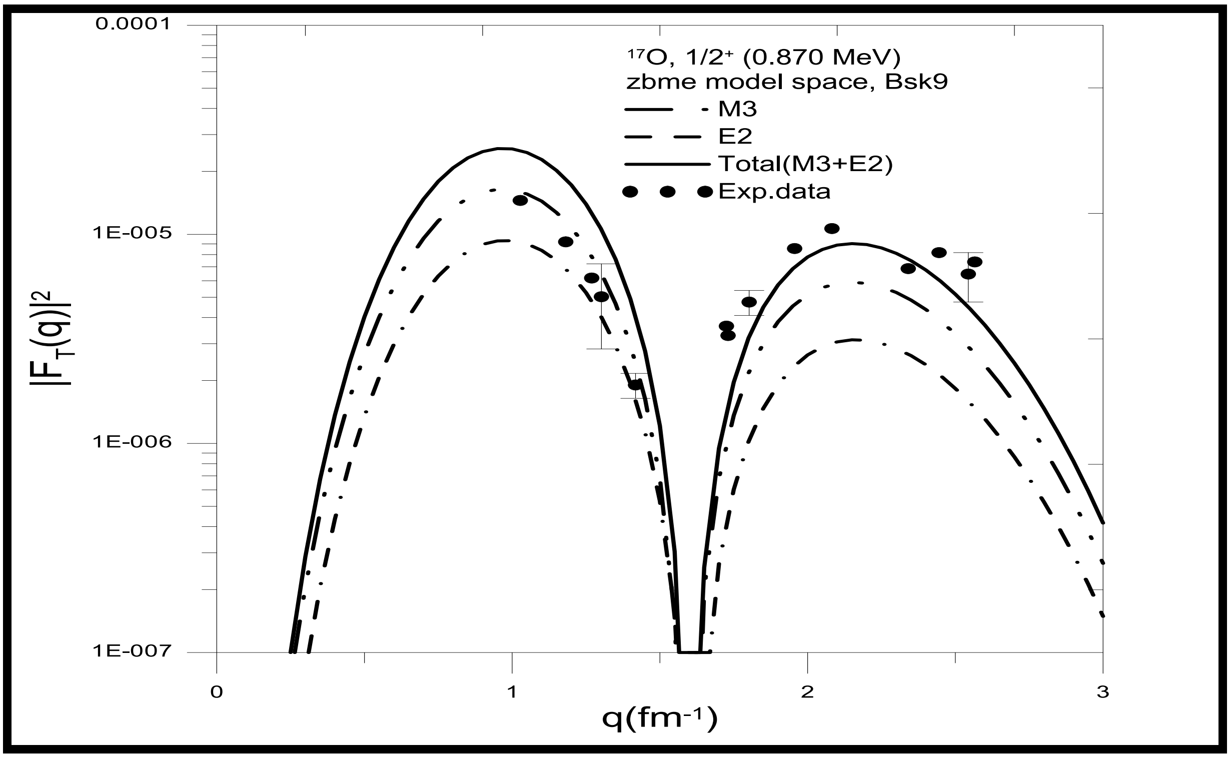


Fig. (3-48): The total transverse inelastic (M3+E2) form factors for the transition 1/2+ (0.870 MeV) state calculated using Bsk9 potential for zbme model space. The experimental data are taken from reference [31]

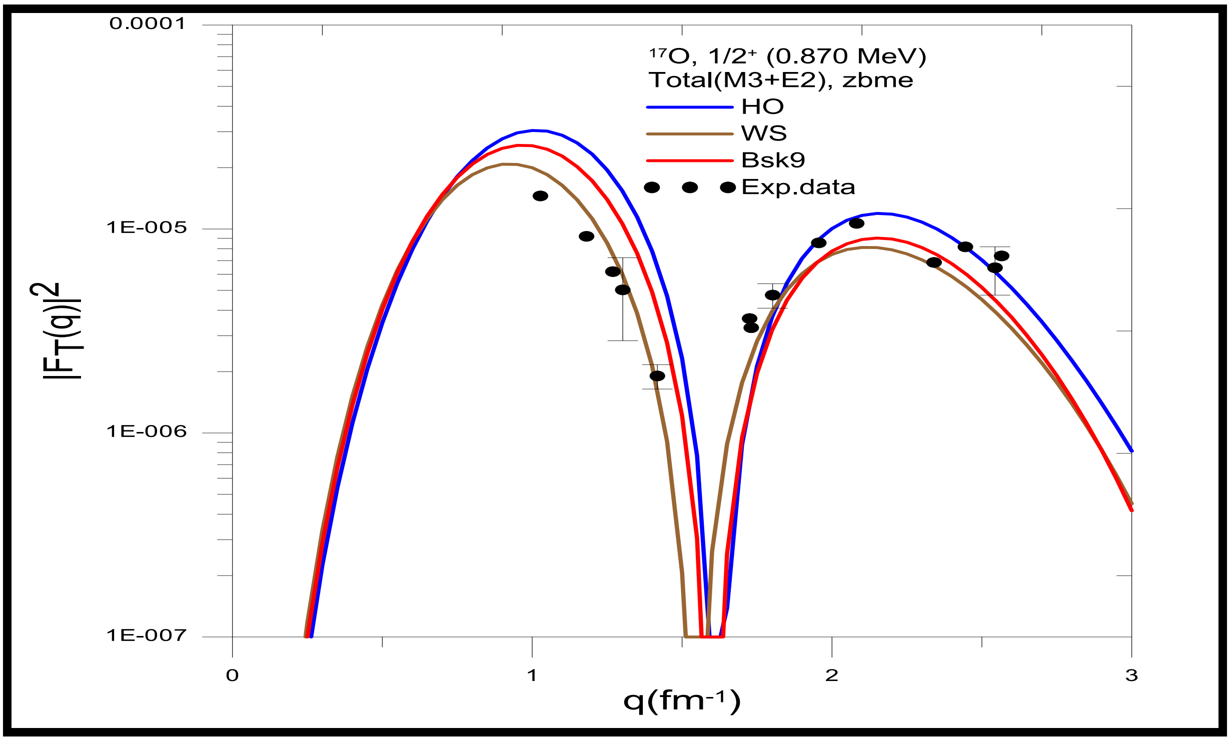


Fig. (3-49): The total transverse inelastic (M3+E2) form factors for the transition $1/2^+$ (0.870 MeV) state calculated using zbme model space for different potentials. The experimental data are taken from reference [31]

### 3.4.9 The Transverse Form Factors for ($5/2^+$, 1/2) State at (0.870 MeV)

The total transverse inelastic M1, M3, and M5 (dash-dot-dot-dotted line) form factors and their individual contributions for the transition $5/2^+$ at $E_x = 0.870\, MeV$ state calculated using HO, WS, and Bsk9 potentials displayed in figures (3-50), (3-51), and (3-52), respectively. The results calculated using the zbme model space with default effective charge showed good agreement with the experimental data in some transfer momentum regions.

Figure (3-53) shows the comparison between HO, WS, and Bsk9 potentials using zbme model space to calculate the total transverse inelastic (M1+M3+M5) form factors. The calculation results were good with experimental data in all transfer momentum regions for all potential. The One-Body Density Matrix element values for this transition (M1, M3, and M5) calculated using zbme model space are shown in tables (3.19), (3.20), and (3.21) respectively.

Table (3.19): The calculated M1 transition OBDM element values for 5/2$^+$ ($E_x = 0.870\ MeV$) in $^{17}$O nucleus

| $^{17}$O | | M1 | |
|---|---|---|---|
| $j_i$ | $j_f$ | OBDM (ΔT=0) | OBDM (ΔT=1) |
| $1p_{1/2}$ | $1p_{1/2}$ | 0.00677 | -0.02241 |
| $1d_{5/2}$ | $1d_{5/2}$ | 0.99783 | 0.93012 |
| $2s_{1/2}$ | $2s_{5/2}$ | 0.00608 | -0.00343 |

Table (3.20): The calculated M3 transition OBDM element values for 5/2$^+$ ($E_x = 0.870\ MeV$) in $^{17}$O nucleus

| $^{17}$O | | M3 | |
|---|---|---|---|
| $j_i$ | $j_f$ | OBDM (ΔT=0) | OBDM (ΔT=1) |
| $1d_{5/2}$ | $1d_{5/2}$ | 0.97796 | 0.95020 |
| $1d_{5/2}$ | $2s_{1/2}$ | 0.00005 | -0.01566 |
| $2s_{1/2}$ | $1d_{5/2}$ | -0.00005 | -0.01566 |

Table (3.21): The calculated M5 transition OBDM element values for 5/2$^+$ ($E_x = 0.870\ MeV$) in $^{17}$O nucleus

| $^{17}$O | | M5 | |
|---|---|---|---|
| $j_i$ | $j_f$ | OBDM (ΔT=0) | OBDM (ΔT=1) |
| $1d_{5/2}$ | $1d_{5/2}$ | 0.97300 | 0.94847 |

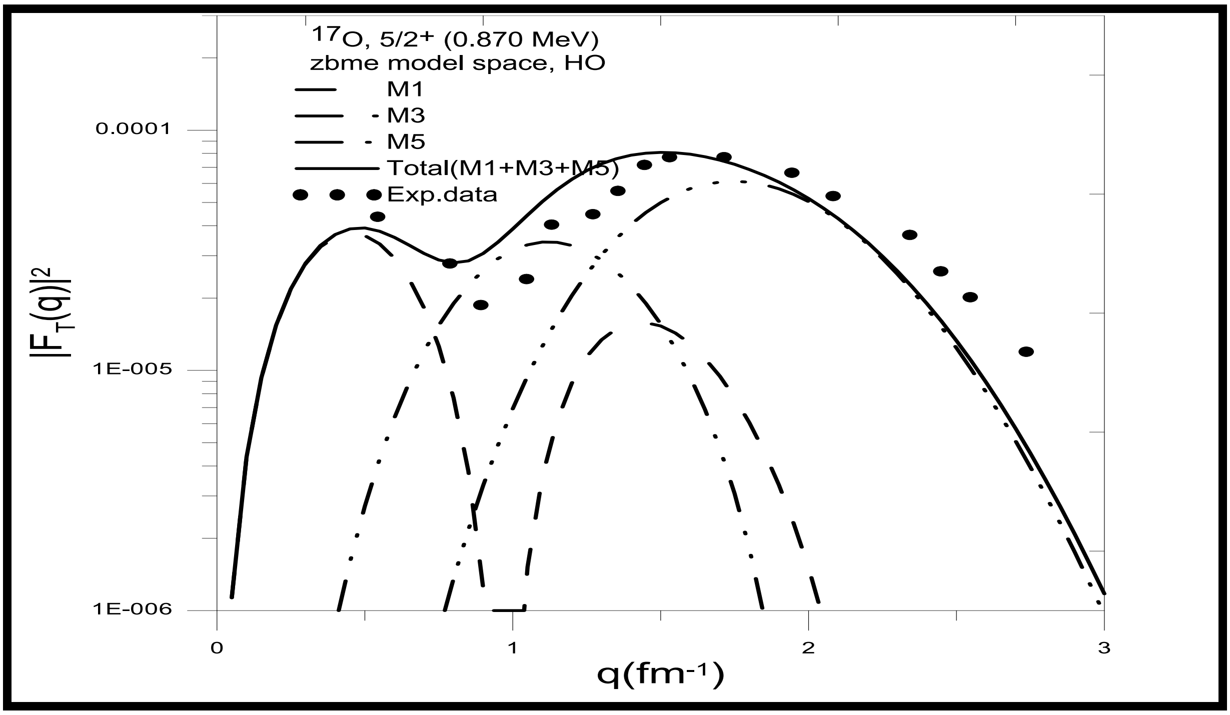


Fig. (3-50): The total transverse inelastic (M1+M3+M5) form factors for the transition $5/2^+$ (0.870 MeV) state calculated using HO potential for zbme model space. The experimental data are taken from reference [31]

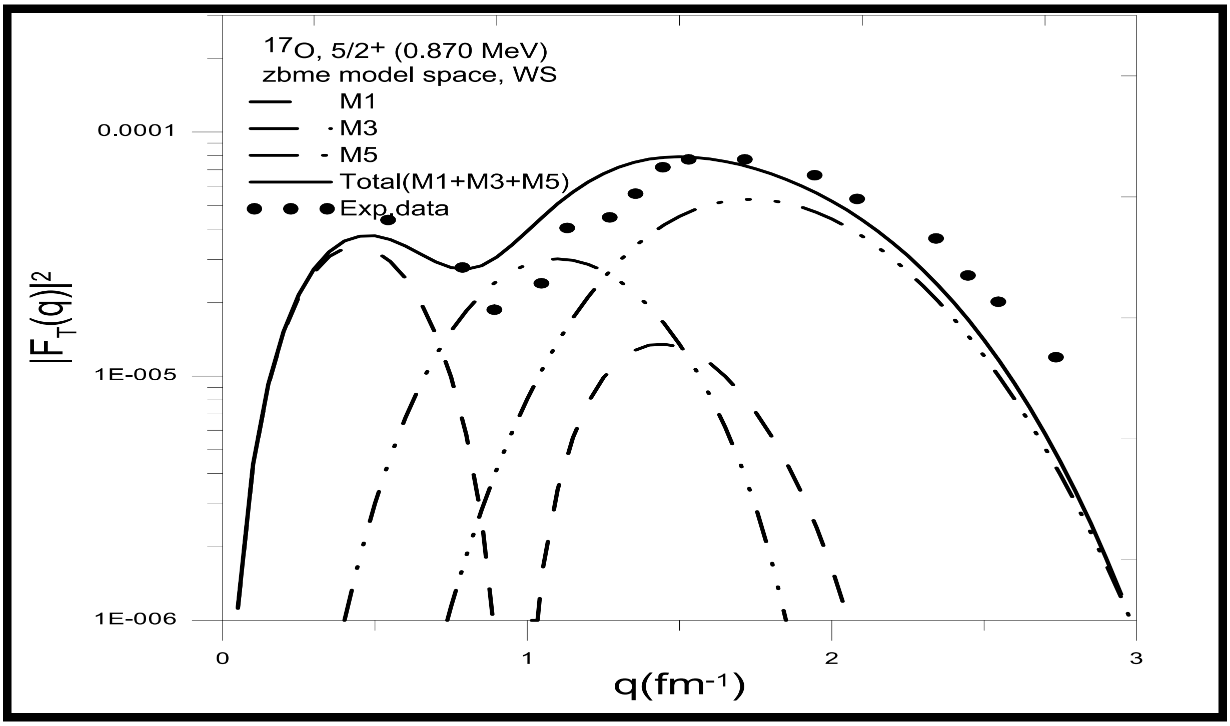


Fig. (3-51): The total transverse inelastic (M1+M3+M5) form factors in the transition $5/2^+$ (0.870 MeV) state calculated using WS potential for zbme model space. The experimental data are taken from reference [31]

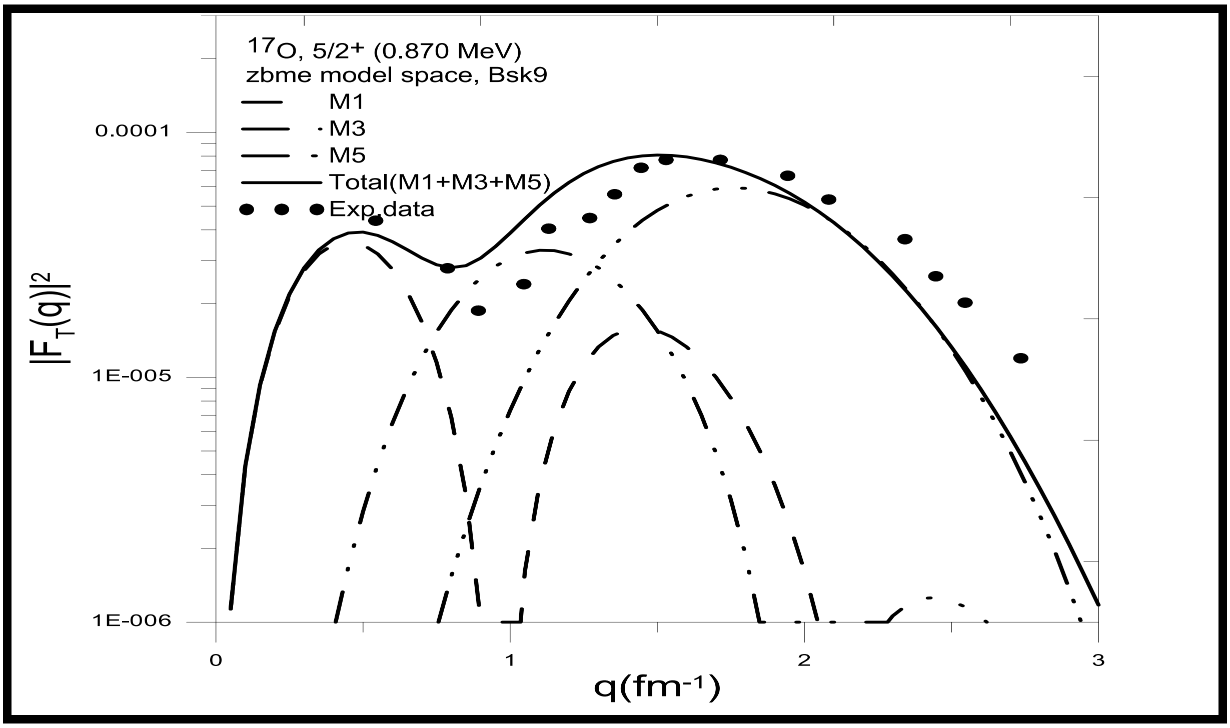


Fig. (3-52): The total transverse inelastic (M1+M3+M5) form factors in the transition $5/2^+$ (0.870 MeV) state calculated using Bsk9 potential for zbme model space. The experimental data are taken from reference [31]

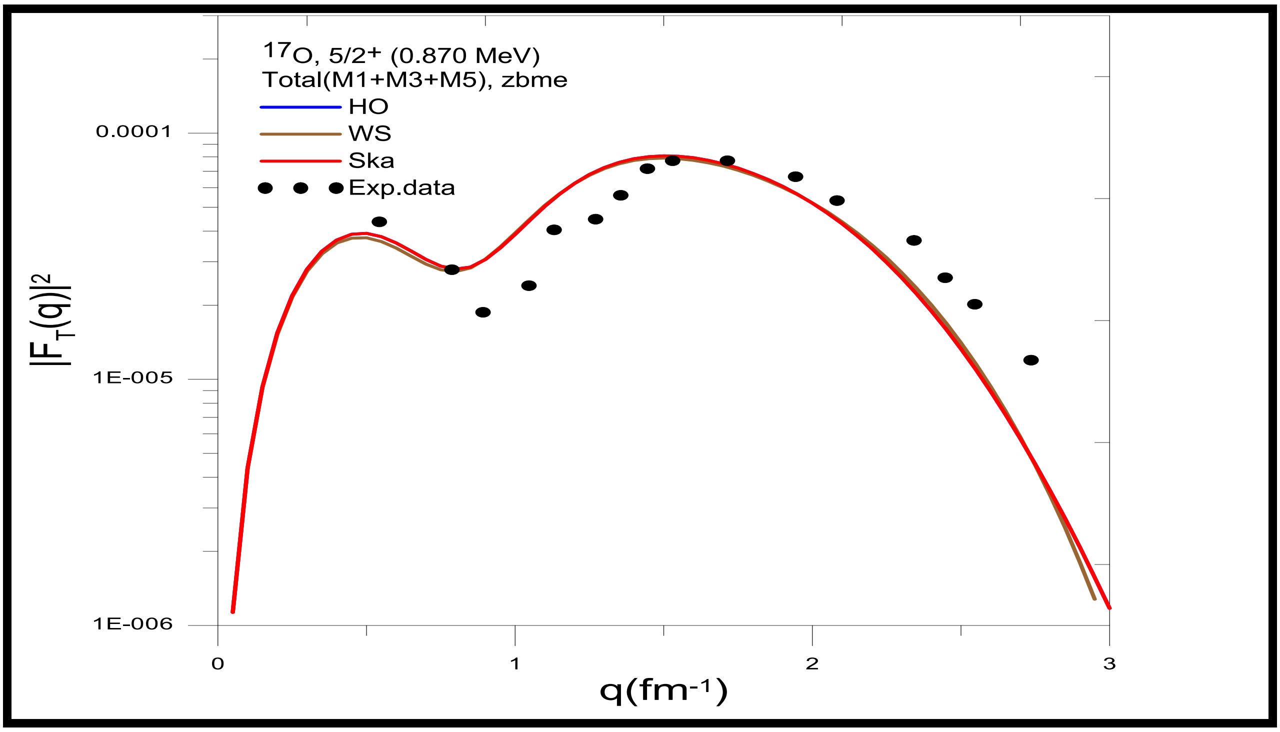


Fig. (3-53): The total transverse inelastic (M1+M3+M5) form factors in the transition $5/2^+$ (0.870 MeV) state calculated using zbme model space for different potentials. The experimental data are taken from reference [31].

## 3.5 Conclusions

In this work, we have described the nuclear properties of the $^{10}B$, $^{12}C$, and $^{17}O$ in the framework of the nuclear shell model with the psd, spsdpf models space with different potentials ( HO, WS, Skyrme).

1- $^{10}B$ nucleus

The calculated results without effective charge are in good agreement with experimental data, especially at higher momentum transfer values for the first ($1^+$ )and second (٢$^+$) transitions. While the third transition ($4^+$) state, gave good results with an effective charge (0.8, 0.4) for proton and neutron respectively. The transverse elastic form factors for M1, M3, and total (M1+M3) for the $3^+$ 0 calculated form factors with psd model space for all potentials (HO, WS, and Ska) have the same results. The calculated transverse inelastic (M3) form factor for the transition $0^+$ (1.74 MeV) state using p, psd, and spsdpf models space are in good agreement at first maximum then after that begins to deviate and show decline values at the second part. The transverse elastic form factor for M1 transition was calculated using different models (p, psd, and spsdpf) with default effective charge to yield an adequate description of the experimental data for all potentials ( HO, WS, and Ska). The Skyrme potential seems the best one to give a better description of the form factors with the psd model space.

2- $^{12}C$ nucleus

The calculation form factor with p-shell model space gives the best results for different potentials.

3- $^{17}O$ nucleus

The inelastic longitudinal Coulomb C2 form factor for the $1/2^+$ state of the $^{17}O$ at $E_x = 0.870\, MeV$ are calculated using zbme model space using different potentials (HO, WS, Ska, and Bsk9) with default effective charges are in good agreement with the experimental data in all regions of momentum transfer. While the transition $1/2^+$ (7.956 MeV) and $7/2^+$ $(7.576\, MeV)$ states with default effective charge give considerably overestimate the shape of the experimental data at $q \leq 1.8\, fm^{-1}$. The transition $5/2^+$ (8.402 MeV) state calculation results using the zbme model space with a default effective charge for this transition are in good agreement with experimental data at $q \geq 1.5\, fm^{-1}$, then that fall off slightly less rapidly of the all potentials. The inelastic longitudinal C0 and C2 form factors were calculated for the $5/2^+$ at 6.862 MeV state using (HO, WS, Ska, and Bsk9) potentials in good agreement and were able to produce the form factors that match the experimental data shape with high transfers momentum. The total longitudinal C2 and C4 form factors calculated for the $3/2^+$ at $E_x = 5.084\, MeV$ state using HO, WS, and Ska potentials at default effective charge, in general, are in agreement with the experimental data for all q dependence regions. The inelastic transverse (M3) form factors for the transition $1/2^+$ ($E_x = 0.870\, MeV$) the state was calculated using HO, WS, Ska, and Bsk9 potentials with default effective giving good agreement with the experimental data at lower values of momentum transfer than being after that underestimate the experimental data at higher values of momentum transfer. The total transverse inelastic (M3+ E2) form factors for the transition $1/2^+$ were calculated at $E_x = 0.870\, MeV$ using WS and Bsk9 potentials using of zbme model space with default effective charge agree well with experimental data at all momentum transfer regions. The form factor calculation for most results gives better agreement with experimental data using Skyrme (ska) potential.

## 3.6 Future works

1- Extension of the work presented in this thesis to be applied to the other nuclei in the sd-shell.

2- Adopting other interactions in the model space for these nuclei understudy to obtain better results for the transitions in which we did not obtain acceptable results.

# References

## References

[1] Haxel O, Jensen JHD, Suess HE. On the" magic numbers" in nuclear structure. Physical Review. 1949; 75 (11) :1766.

[2] Hoteling N.,” Structure of iron isotopes at the limits of the pf shell”, University of Maryland, College Park; 2008.

[3] Brussaard P, Glademans P.,” Shell-model Application in Nuclear Spectroscopy”, North-Holland Publishing Company, Amsterdam; 1977.

[4] Hoteling N, Walters W, Janssens R, Broda R, Carpenter M, Fornal B.,” Yrast structure of Fe 64”, Physical Review C. 2006;74(6):064313.

[5] Suprapti A. International Journal of Scientific and Research Publications (IJSRP)., "The Concept of Emic Knowledge of Bustaman in Surviving and Adapting as an Urban Kampong in Semarang, Indonesia", 2018; 8(9): 258–265.

[6] Dean D, Engeland T, Hjorth-Jensen M, Kartamyshev M, Osnes E.,” Effective interactions and the nuclear shell-model”, Progress in Particle and Nuclear Physics. 2004;53(2):419-500.

[7] Mayer MG.,” On closed shells in nuclei”, II. Physical Review. 1949; 75 (12): 1969.

[8] Adie Dawood Salman, “Theoretical study of the nuclear form factor of light nuclei by electron scattering including core-polarization effects up to second-order”, Ph. D. Thesis, University of Basrah (2005).

[9] Aubrecht G. A teachers guide to the nuclear science wall chart., “ Contemporary Physics Education Project”, 2003.

[10] Donnelly T, Walecka J. “Elastic magnetic electron scattering and nuclear moments”, Nuclear Physics A. 1973;201(1):81-106.

[11] Brown BA, Radhi R, Wildenthal BH.,” Electric quadrupole and hexadecupole nuclear excitations from the perspectives of electron scattering and modern shell-model theory”, Physics Reports. 1983;101(5):313-58.

[12] Lombard, P. Kossany and G. R. Bishop, Nuclear Physics, p. 59, 398 (1964).
[13] Lyman E, Hanson A, Scott M.," Scattering of 15.7MeV electrons by nuclei", Physical Review. 1951;84(4):626.
[14] Noor Thaer Tilab, MSc. Thesis., "Calculation of form factors for some p-shell nuclei with nħω excitation", University of Kerbala (2017).
[15] Flanz J, Hicks R, Lindgren R, Peterson G, Hotta A, Parker B, "Convection Currents and Spin Magnetization in E 2 Transitions of C12", Physical Review Letters. 1978;41(24):1642.
[16] Ansaldo E, Bergstrom J, Yen R, Caplan H., "Inelastic electron scattering from $^{10}B$", Nuclear Physics A. 1979; 322(2-3): p.237-52.
[17] M. V. Hynes, H. Miska, B. Norum, W. Bertozzi, S. Kowalski, F. N. Had, C. P. Sargent, T. Sasanuma, and W. Turchinetz., "Further explorations of Skyrme–Hartree–Fock–Bogoliubov mass formulas. IV: Neutron-matter constraint", 1979; 42(22).
[18] D. M. Manley, B. L. Berman, W. Bertozzi, T. N. Buti, J. M. Finn, F. W. Hersman, C. E. Hyde, M. V. Hynes, J. J. Kelly, M. A. Kovash, S. Kowalski, R.W. Lourie, B.Murdock, B. E. Norum, B. Pugh, and C. P. Sargent., "High-resolution inelastic electron scattering from 17 O", Phys. Rev C. 1987 (36), 1700.
[19] Peterson G., "Magnetic form-factors by 180° electron scattering", Phys Letters. 1962; 2.
[20] Amos K and Steward C., "Large basis space efFects in electron scattering form factors of light nuclei", Phys. Rev., C. 1990; 41(1) 336.
[21] Booten JG., "Electromagnetic properties of p-shell nuclei", 1992.
[22] Amaro JE, Co G, Lallena AM., "Meson-exchange currents in quasielastic electron scattering from 12C and 40Ca nuclei", Nuclear Physics A. 1994;578(3-4):365-96.

[23] Booten J, Van Hees A., “Magnetic electron scattering from p-shell nuclei”, Nuclear physics A. 1994;569(3):510-22.
[24] Karataglidis S, Halse P, Amos K., “Transverse electric form factors for electron scattering and violation of current conservation in nuclear models”, Physical Review C. 1995;51(5):2494.
[25] Cichocki A, Dubach J, Hicks R, Peterson GA, De Jager C, De Vries H., “Electron scattering from 10B”, Physical Review C. 1995;51(5):2406.
[26] Radhi R, Abdullah A, Dakhil Z, Adeeb N, “Core-polarization effects on C2 form factors of p-shell nuclei”Nuclear Physics A. 2001; 696 (3-4): 442-52.
[27] Zeina Abbass Salman MS. Thesis. University of Baghdad 2003.
[28] Majeed F. A and Radhi R. A., Phys Lett, 2006; 23(10), 2699.
[29] Khalid Salih Jassim. Ph.D., “Nucleon-nucleon realistic interactions in electron scattering with core-polarization”, University of Baghdad 2007.
[30] Radhi R, Dakhil Z, Manie N., “Microscopic calculations of quadrupole moments in Li and B isotopes”, The European Physical Journal A. (2014) 50 (7): p.1-9.
[31] Alzubadi AA, Radhi R, Manie NS., “Shell model and Hartree-Fock calculations of longitudinal and transverse electroexcitation of positive and negative parity states in O 17”, Physical Review C. 2018;97(2):024316.
[32] Salman AD, Tilab NT, Al-Ramahi SA, and Hossain I., “Core polarization effects up to 12 $\hbar\omega$ in 7Li and 10B nuclei”, International Journal of Modern Physics E. 2019;28(11):1950102.
[33] Brown B. A. and W. D. M. Rae, NuShell@MSU, MSU-NSCL report, 2007.
[34] Sheldon E., “Physics of Nuclei and Particles”, Academic Press; 1969.
[35] Dong Y, Junde H., “Nuclear datasheets for A= 52. Nuclear Data Sheets”, 2015;128:185-314.

[36] Adeeb NM., “Microscopic Calculations of Core-Polarization Effect on Inelastic Electron Scattering Form Factors for the Different Parity States in (14N)”, Journal of Physical Science and Application. 2012;2(9):392.

[38] Radhi R, Alzubadi AA, Rashed EM.,” Shell model calculations of inelastic electron scattering for positive and negative parity states in 19F”, Nuclear Physics A. 2016;947:12-25.

[39] Henry E, Kuhnert A, Becker J, Brinkman M, Wangt T, Cizewski J., “Lack of evidence for a superdeformed band in PB-192-comment”, Physical review C. 1994;49(5):2849-50.

[40] Washimi H, Taniuti T., “Propagation of ion-acoustic solitary waves of small amplitude”, Physical Review Letters. 1966;17(19):996.

[41] Glickman J, Bertozzi W, Buti T, Dixit S, Hersman F, Hyde-Wright C., “Electron scattering from Be9”, Physical Review C. 1991;43(4):1740.

[42] Radhi R, Salman E, “Collective E2 transitions in 18O”, Nuclear Physics A. 2008;806(1-4):179-90.

[43] Radhi R, Bouchebak A., “Microscopic calculations of C2 and C4 form factors in sd-shell nuclei”. Nuclear Physics A. 2003;716:87-99.

[44] Millener, D. I. Sober, H. Crannell, J. T. O’Brien, L. W. Fagg, S. Kowalski, C. F. Williamson, and L. Lapikás., “inelastic electron scattering from”.Physical Review, p.14 (1989).

[45] Van Vleck J., “On the Quantum Theory of the Specific Heat of Hydrogen Part I. Relation to the New Mechanics, B and Spectra, and Chemical Constants”., Physical Review. 1926;28(5):980.

[46] Vautherin D, Brink Dt., ”Hartree-Fock calculations with Skyrme's interaction”. I. Spherical nuclei. Physical Review C. 1972;5(3):626.

[47] Skyrme T.,” The effective nuclear potential. Nuclear Physics”. 1958;9(4):615-34.

[48] Vautherin D, Veneroni M and Brink D. “A Hartree-Fock calculation for the stability of super-heavy nuclei", Physics Letters B.1970;33(6):381-4.

[49] Köhler H., “Skyrme force and the mass formula”. Nuclear Physics A. 1976;258(2):301-16.

## الملخص

تمت دراسة عوامل التشكل لتشتت الإلكترون الكولومي لبعض الأنوية في القشرة p و sd بالإضافة إلى العديد من حالات عوامل التشكل المستعرضة. تم إجراء حسابات نموذج القشرة ذات الفضاء الواسع للعديد من النوى. لدراسة البنية وبعض الخصائص الفيزيائية لنوى البورن- ١٠ والكاربون- ٢ ١والأوكسجين- ١٧ باستخدام برنامج نيوشيل .(Nushell code) تضمنت حساب أنموذج القشرة ثلاثة من فضاء الأنموذج وهي p و psd و spsdpf مع تفاعلات ckpot و psdmwk و wbm ، على التوالي ، لنواتي البورون والكاربون وفضاء أنموذج zbme مع تفاعل rewile لنواة الأوكسجين. أن نتائج الحساب تضمينت تأثيرات الاستقطاب للقلب مع مساهمة شحنة الاستقطاب واختيار فضاء أنموذج مناسب أعطت نتائج أفضل لحساب عوامل التشكل المرنة وغيرالمرنة للحالة الدنيا المثارة لهذه النوى. في هذا العمل تم اعتماد جهود مختلفة لدالة موجة الجسيم المنفرد الشعاعية وهي كل من الجهد التوافقي (HO) وجهد وود- سكسون(WS) وجهد سكايرم(Ska) في حساباتنا لعوامل التشكل. تم إجراء العمليات الحسابية التي تمت مقارنتها بالبيانات التجريبية باستخدام مساحة نموذج spsdpf ذات الاساس الموسع والتي تتضمن المدارات 1s1/2، 1p3/2، 1p1/2، 1d5/2، 2s1/2، 1d3/2، 1f7/2، 2p3 / 2، 1f5 / 2، 2p1 / 2 ولكن تم اقتطاع الفضاء الى 2 ℏ لأن التوسيع إلى 4ℏ و 6ℏ لا يمكن أن يحسن النتائج بشكل كبير. في حين أن فضاء الأنموذج PSD الذي تضمن المدارات1p3/2، 1p1/2، 1d5/2، 2s1/2، 1d3/2 دون أي قيود تفرض على نيوكليونات التكافؤ خارج النواة أعطت نتائج مقبولة. كانت نتائج الحساب لكل من نوى البروم- ١٠ و الكاربون - ١٢ مع اعتماد مساحة نموذج PSD في توافق أفضل مع البيانات التجريبية مقارنة بالحسابات النظرية للعمل السابق التي استخدمت التوسعة spsdpf الى2 ℏ. اما بالنسبة لنواة الاوكسجين -١٧ فأن فضاءالأنموذج zbme المستخدم والذي تضمن المدارات 1p1/2، 1d5/2، 2s1/2، 1d3/2 بدون أي قيود أعطت توافقًا جيدًا مع البيانات التجريبية لجهد سكايرم (ska) مقارنة بالجهود الأخره كالمتذبذب التوافقي وود سكسون.

**جامعة كربلاء**

**كلية العلوم**

**قسم الفيزياء**


# دراسة الخصائص النووية لبعض الانوية الخفيفة باستخدام جهود مختلفة

رسالة مقدمة الى مجلس كلية العلوم / جامعة كربلاء
كجزء من متطلبات نيل درجة الماجستير في علوم الفيزياء


**كتبت بواسطة**

**بشائرحسن جواد**

**بكلوريوس جامعة كربلاء 2018**

باشراف

**أ.د. عدي داود سلمان**


**ايار ٢٠٢٢ م** **شوال ١٤٤٣ هـ**